A MULTISCALE MODEL OF LEUKOCYTE TRANSENDOTHELIAL MIGRATION DURING ATHEROGENESIS

by

Rita Bhui

APPROVED BY SUPERVISORY COMMITTEE:

Heather N. Hayenga, Chair

Stefano Leonardi

Lloyd Lumata

Robert Glosser

Jason D. Slinker

Dedicated to

My parents, Late Shri Gopal Chandra Bhui and Mrs. Anna Rani Bhui
for their love, blessing, and sacrifices

My brother Shri Pradip Kumar Bhui and sister Smt. Bina Pal
for their inspiration, support, and teachings

&

My husband Dr. Arup Polley
for his encouragement, motivation, and support

A MULTISCALE MODEL OF LEUKOCYTE TRANSENDOTHELIAL MIGRATION DURING ATHEROGENESIS

by

RITA BHUI, BS, MS

DISSERTATION

Presented to the Faculty of

The University of Texas at Dallas

in Partial Fulfillment

of the Requirements

for the Degree of

DOCTOR OF PHILOSOPHY IN

PHYSICS

THE UNIVERSITY OF TEXAS AT DALLAS

May 2018

ACKNOWLEDGMENTS

This dissertation would not have been possible without the love, support, and guidance of many people over the past few years. First, my sincere gratitude goes to my advisor, Dr. Heather N. Hayenga, for her motivation, patience, guidance, encouragement, and support during these past five years. I would also like to thank my committee members, Dr. Stefano Leonardi, Dr. Lloyd Lumata, Dr. Jason D. Slinker, and Dr. Robert Glosser, for their time and support. I express my gratitude for the valuable technical contributions and advices from Dr. Clark A. Meyer.

Thanks to my colleagues, Manasvini Ammanamanchi and Maziyar Keshavarzian for making the lab environment enjoyable and the stimulating discussions.

Finally, no person can be successful without the love and support of family. I am thankful to my loving husband Dr. Arup Polley for his patience, moral support, and continuous encouragement. My sweet thought goes to my son Amiyo Polley who makes my life full of joy. He was only a month old when I joined this group; at times we missed each other. Acknowledgement goes to my brother-in-law Dr. Anirban Polley for his encouragements and thoughtful ideas. I also acknowledge my parents-in-law Shri Anil Kumar Polley and Smt. Hira Polley for their love and support. I convey my gratitude to my brother-in-law Shri Asim Kumar Pal, my sister-in-law Smt. Minati Bhui, and my cousin Shri Madhav Chandra Bhui for their constant support, encouragement and love. I hold dear to my heart my nephew Priyanshu Pal, my nieces Adrija Bhui, Aditri Bhui and Priyanka Pal for always making me feel loved. There are not enough words to thank my elder sister, Smt. Bina Pal, who has been an abundant source of knowledge and guidance throughout my life. I will always be indebted to my brother Shri Pradip

Kumar Bhui for igniting the passion for knowledge since my childhood and always being the best teacher to me.

Finally, deepest gratitude is reserved for my parents, Late Shri Gopal Chandra Bhui and Mrs. Anna Rani Bhui, whose unconditional love, endless support, blessing and sacrifices are treasure of my life.

March 2018

A MULTISCALE MODEL OF LEUKOCYTE TRANSENDOTHELIAL MIGRATION DURING ATHEROGENESIS

Rita Bhui, PhD
The University of Texas at Dallas, 2018

Supervising Professor: Dr. Heather N. Hayenga

A vast amount of work has been dedicated to understanding the role hemodynamics and cytokines play in leukocyte adhesion, trans-endothelial migration (TEM) and subsequent accumulation of leukocyte-derived foam cells in the artery wall. However, a comprehensive mechanobiological model to capture these spatiotemporal events and predict the growth and remodeling of an atherosclerotic artery is still lacking. In this dissertation we present a multiscale model of leukocyte TEM and plaque evolution in the left anterior descending (LAD) coronary artery. The approach integrates cellular behaviors via agent-based modeling (ABM) and hemodynamic effects of pulsatile blood flow via computational fluid dynamics (CFD). We found that using fully developed steady blood flow does not result in a representative number of leukocyte TEM as compared to pulsatile flow, whereas passing wall shear stress (WSS) at peak systole of the pulsatile flow waveform does. Moreover, using the model, we found leukocyte TEM increases monotonically with decreases in luminal volume. Specifically, neutrophils are primary cell type entering the wall at the genesis of plaque evolution and again the lumen caliber is altered for the first time. At critical plaque shapes the WSS changes rapidly resulting in sudden

increases in leukocyte TEM, suggesting lumen volumes that will give rise to rapid plaque growth rates if left untreated. Overall, this multi-scale and multi-physics approach appropriately captures and integrates the spatiotemporal events occurring at the cellular level in order to predict leukocyte transmigration and plaque evolution.

TABLE OF CONTENTS

LIST OF FIGURES

LIST OF TABLES

CHAPTER 1

INTRODUCTION: DISSERTATION LAYOUT

Coronary artery disease (CAD) is the leading cause of death in advanced countries. The most common cause of CAD is atherosclerosis [22]. Atherosclerosis is a local inflammatory disease characterized by recruitment of leukocytes into the arterial wall. Through a sequence of events the arterial wall develops an atherosclerotic plaque, comprising of leukocyte-derived foam cells, lipids, calcium and other constituents [23]. In the event an atherosclerotic plaque ruptures, it may block blood flow completely, which typically results in a life-threating heart attack or stroke.

The endothelium comprises the inner lining of the artery, and thus is in direct contact with flowing blood. Hence, the endothelium is constantly exposed to the mechanical forces exerted by blood. The frictional force per unit area of the vessel wall, called wall shear stress (WSS), is a critical factor in maintaining endothelial function and leukocyte adhesion on the endothelial cell (EC) surface. It is well known that the low and oscillating WSS is associated with the early stage of atherosclerosis as it favors the leukocyte adhesion to the endothelium. Thus, arterial bifurcated regions are prone for plaque development.

The recruitment steps involved in the leukocyte transmigration cascade (i.e., capture, rolling, firm adhesion and transmigration) are well established [24-26]; however, a computational framework which can capture and predict the effects of these events is lacking. Clinically hemodynamics has been used to predict areas of plaque progression [27-30] or the need for treatment (e.g., Fractional Flow Reserve). Experimentally, the dynamics relating WSS, endothelial cell activation and leukocyte trans-endothelial migration (TEM) have been quantified [31-33] However, a computational model incorporating the interdependency of leukocyte TEM, plaque

growth and WSS with time is lacking. This motivated the need to build a predictive model of leukocyte TEM and the consequential progression of plaque in order to deepen our understanding of the pathophysiology of atherogenesis.

Thus the overall goal of this dissertation is to create a novel predictive model of leukocyte TEM by incorporating pathophysiological dependencies on changes to the mechanical (hemodynamics) by computational fluid dynamics (CFD) and biological (leukocyte TEM, chemotaxis, outward remodeling of the artery, monocyte to foam cell differentiation, cell activation, and protein diffusion) environment by agent based model (ABM) to determine the evolution of an atherosclerotic plaque. Eventually, such a model will be able to predict growth and remodeling of patient-specific human plaques and be fundamental to treatment planning and optimization. This dissertation is broken down into seven chapters.

Chapter 2 provides a background of leukocyte transmigration. The vascular events involved in leukocyte TEM and the influential factors are qualitatively described in this section.

In Chapter 3, we performed a CFD simulation of a bifurcated channel and investigated the change of hemodynamics as function of inlet flow rate, bifurcation angle and width of the channel. Previous computational and *in vitro* studies have suggested that arterial bifurcations are susceptible locations for formation of atherosclerotic plaques [34-36]. Indeed our results support why plaque most often occurs near the aortic bifurcation. Specifically, Dr. Schmidtke's group at UTD experimentally investigated neutrophil adhesion at bifurcations using microfluidic channels. We then performed CFD simulations to mimic the experimental setup. It was found that the regions where neutrophils adhere in the experiment corresponds with the low WSS regions.

In Chapter 4, we developed an agent based model which captures the growth and remodeling as a result of leukocyte transmigration. First, we identified the primary factors affecting leukocyte adhesion and TEM. Next a series of equations (called "rules") capturing leukocyte adhesion as function of the identified key factors were developed and implemented into the ABM. The rules were derived from previous literature studies that were sometimes inconsistent or limited in their findings. Therefore, a rule scoring metric was used to verify each rule [37]. Altogether, our ABM included diffusion of key biological proteins and cytokines, leukocyte adhesion and transmigration, and chemotactic driven leukocyte migration into and within the artery wall. Lastly, we coupled and verified the ABM with CFD to model the effect of hemodynamics on leukocyte adhesion.

In Chapter 5, we proposed a computationally effective way to capture the pulsatile nature of blood flow in the CFD-ABM. Since, blood flow through an artery is pulsatile in nature, the WSS and therefore rate of leukocyte TEM varies with time. We hypothesized that using average WSS is not physiological because it does not capture the effect of low WSS as well as high WSS in TEM. To test this hypothesis, we used an ABM to compare the total leukocyte transmigration during time averaged and instantaneous flow in a stenotic coronary artery. Specifically, WSS was determined using direct numerical simulations (DNS) performed using in-house code by Dr. Leonardi's group. The WSS computed from DNS was then coupled with our ABM of leukocyte transmigration. The adhesion rate computed from mean flow field generally under predicts the leukocyte transmigration compared to the actual rate of adhesion as the instantaneous flow field can be quite different from the mean flow. This analysis emphasizes the importance of the instantaneous flow conditions in evaluating the leukocyte rate of adhesion. As an alternative, we

found that passing WSS profile at peak systole of the pulsatile flow waveform gives same leukocyte adhesion as when using instantaneous flow. Towards the end of the chapter, we show simulated results of the coupled CFD-ABM. We found that leukocyte TEM increases monotonically with decrease of plaque volume and the type of leukocytes entering the plaque depend on the stage of plaque growth. Finally, we found that at critical plaque shapes the WSS changes rapidly resulting in sudden increases in leukocyte TEM. These results suggest specific plaque shapes will give rise to rapid plaque growth rates if left untreated.

In Chapter 6, we made the model more physiological by adding more mechanistic rules in regards to leukocytes adhesion and the atheroprotective nature of high density lipoprotein (HDL). That is, previously the probability any given leukocyte would enter the artery wall was only dependent on WSS and cytokine concentration. In this chapter, we expand on these functions to include WSS, cholesterol, and cytokine induced upregulation of adhesion molecules (AM) and selectins. AM and selectins are receptors on the endothelial cells that bind to integrins on leukocytes from the blood and facilitate transmigration into the artery wall. Specifically, we added the effects of different factors such as cytokine concentration, oxidized low-density lipoprotein (ox-LDL), tri-glyceride rich lipoprotein (TGRL), and WSS have on Intercellular adhesion molecule-1 (ICAM-1), vascular adhesion molecule-1 (VCAM-1), and endothelial selectin (E-selectin). In this way, leukocyte adhesion depends on the cell type and concentration of AMs and selectins on the endothelium. Moreover, the effects of lipoproteins within the artery wall on cell differentiation were also added to the ABM. Specifically, macrophages consume both LDL and ox-LDL and form lipid laden foam cell. HDL on the other hand reduces the concentration of AMs

as well as the effect of oxidized LDL (ox-LDL) and thus slower down the progression of atherosclerosis.

In the last part of this dissertation (Chapter 7), our future work is proposed. Future work includes incorporating longitudinal patient data from intravascular ultrasound-virtual histology (IVUS-VH) into our ABM, and compare the simulated progression of plaque growth to the follow-up patient data set. We present preliminary results in processing patient specific virtual histology (VH) data, using MatLab, to get the composition and morphology of artery. We then used that data to setup our ABM. We will then run simulations and compare the growth and remodeling with 6 months follow up patient data.

CHAPTER 2

BACKGROUND AND SIGNIFICANCE

Normal Artery

The main conduits for blood flow include arteries, arterioles, capillaries, venules, and veins. Arteries (except pulmonary and umbilical artery) are the blood vessels that deliver oxygen-rich blood from the heart to the tissues of the body. Arteries consist of three layers. An inner layer (tunica intima) is composed of single layer of endothelial cells. It forms an interface between circulating blood in the lumen and the rest of the vessel wall. A middle layer (tunica media) is primarily comprised of circumferentially arranged smooth muscle cells and elastic fibers (**Figure 2.1**). The outer layer (tunica adventitia) is comprised primarily of fibroblasts, vasa-vasorum. The dimension of an artery and the thickness of each layer vary depending on the

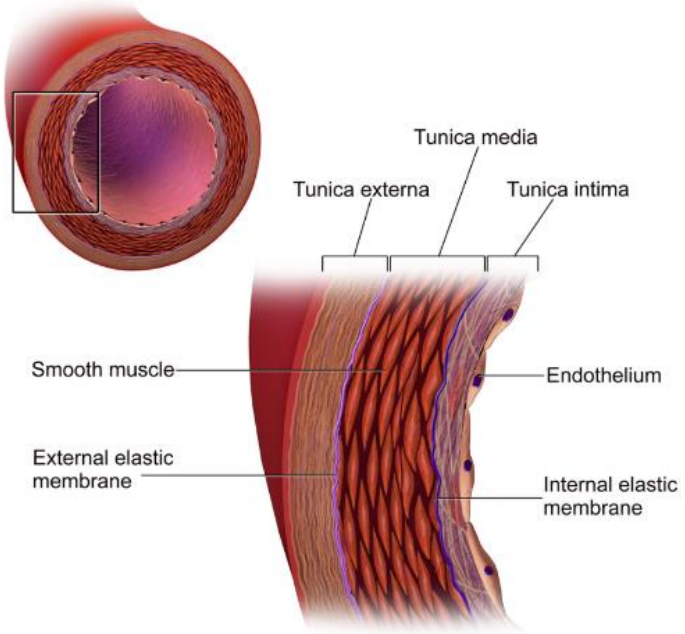

Figure 2.1. Cartoon of an arterial cross-section illustrating its three layers, and the majority cell type in each layer: Source: Blausen.com staff (2014). "Medical gallery of Blausen Medical 2014". WikiJournal of Medicine 1 (2). DOI:10.15347/wjm/2014.010. ISSN 2002-4436.

type of artery, and obviously on species. For the human coronary artery, the average thickness of the intima is 80 μm, media is 200 μm,[38, 39] and adventitia is 300- 500 um [39] . The internal space, through which blood flows, is called lumen. The average lumen diameter is 3600±1400 um, where the size range is due to tapering [39].

Atherosclerosis

Atherosclerosis is an inflammatory disease. It originates from leukocytes entering the artery wall and forming what is called an atheroma or plaque inside the artery wall. Over time, plaque grows larger and blocks blood flow through lumen (**Figure 2.2**). In the event an atherosclerotic plaque ruptures, it may block blood flow completely, which typically results in a life-threating stroke or myocardial infarction. Indeed, the less stenotic plaques may be more vulnerable to rupture due to their underlying structure. According to a metastudy approximately

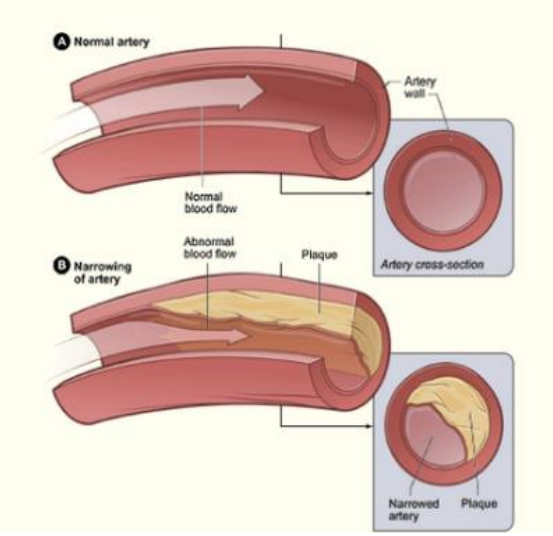

Figure 2.2. Longitudinal and transverse cross section of a normal and stenosed artery: A) Normal artery with normal blood flow. B) Blood flow through an artery with plaque. Source: "Atherosclerosis." *National Heart Lung and Blood Institute*, U.S. Department of Health and Human Services, www.nhlbi.nih.gov/health-topics/atherosclerosis.

85% of acute myocardial infarctions arose from lesions with degrees of stenosis less than 60% on an antecedent angiogram.[40]

Factors affecting inflammation or atherogenesis

It was largely believed that the accumulation of cholesterol, in particular low density lipoprotein (LDL) in the artery wall, initiates atherosclerosis; however, it is much more than that. Despite changes in lifestyle and the use of new pharmacologic approaches to lower plasma cholesterol concentrations, cardiovascular disease continues to be the principal cause of death in advance countries [22]. However, the known key factors responsible for atherogenesis are as follows:

Leukocyte adhesion and TEM: Leukocytes, also called white blood cells (WBC), are the cells of the immune system that are involved in defending the body against both infectious disease and foreign invaders. Five different and diverse types of leukocytes exist: Neutrophil, eosinophil,

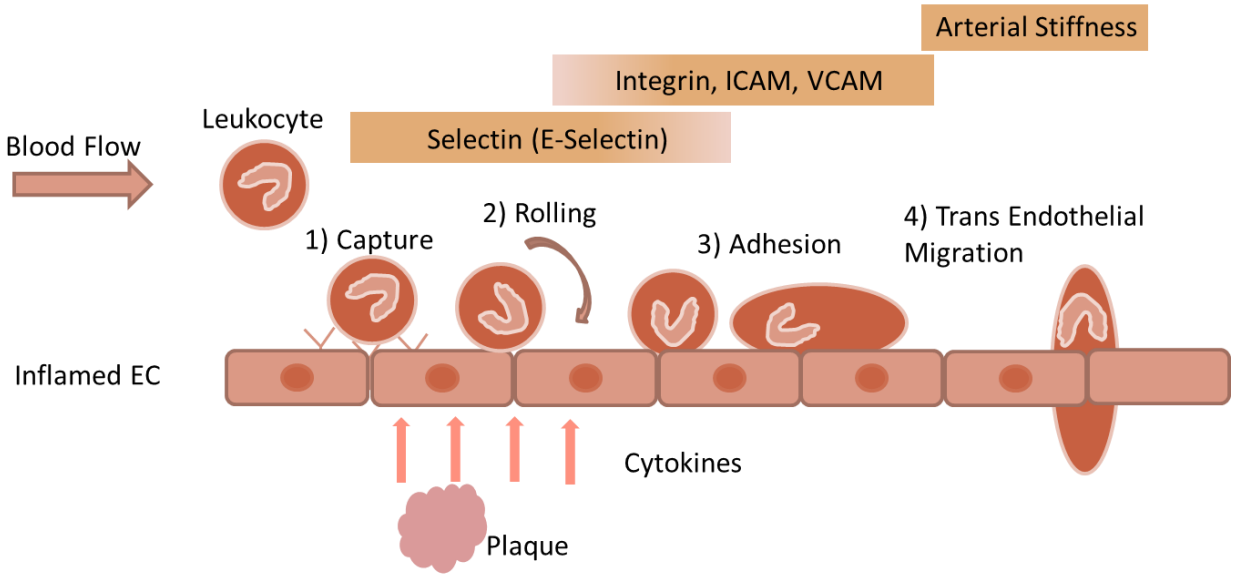

Figure 2.3 Different steps of leukocyte TEM and associated selectins and integrins: Leukocyte TEM is a multistep process. Capture and rolling are mediated by selectins whereas adhesion is integrin dependent. Finally, leukocytes transmigrate through wall depending on stiffness of the artery wall.

basophil, lymphocyte and monocytes (which become macrophages when residing in tissue). Leukocyte adhesion to, and transmigration through, the endothelium of blood vessels is an essential event in inflammation and the pathogenesis of atherosclerosis. It is a well-known multistep process. **Figure 2.3** shows all the steps of leukocyte adhesion and transmigration.

Cytokines, WSS and cholesterol mainly activate the endothelium through outside-in signaling leading to expression of selectins and integrins on the endothelial surface. Capture or tethering represents the first contact of leukocytes with the endothelium cells. When a leukocyte in the blood stream moves close enough to be in contact with endothelium it gets captured (i.e., weak selectin bonds are formed between the leukocyte and endothelial cell). Once leukocytes are captured, they slow down and begin to roll along the inner surface of the vessel wall. Rolling is mediated by selectins (L-selectin, P-selectin and E-selectin). The low-affinity, selectin-dependent interaction is then transformed into a high-affinity, integrin-mediated firm adhesion. The firm arrest of leukocytes to endothelial cells is mediated by interactions between leukocyte integrins, such as VLA-4 (α4β1), α4β7-integrin, Mac-1 (αMβ2) and LFA-1 (αLβ2), and their endothelial counter-receptors of the immunoglobulin superfamily, such as the vascular cell adhesion molecule-1 (VCAM-1), and intercellular adhesion molecules (ICAM). VCAM-1 interacts with VLA-4, and ICAM-1 binds to β2-integrins (including LFA-1 and Mac-1).

After firm adhesion, leukocytes move slowly over the endothelial cell surface, a process called crawling or locomotion, until they reach an area appropriate spot for transmigration. TEM (also designated as diapedesis or extravasation) may take place at the intercellular junctions or through the endothelial cell. The average time taken for this process (from capture to TEM) depends on the type of leukocyte. Not considering the effects of flow, a neutrophil typically

takes around 10 minutes to transmigrate after it gets captured to the endothelium [17], whereas a monocyte takes approximately 20 minutes [16].

Hypercholesterolemia and modified lipoproteins: Mass transport of LDL from the lumen into the arterial wall is also an important factor contributing to atherogenesis [41]. Once in the wall, LDL is oxidized, and this oxidized form of LDL (ox-LDL) is consumed by monocyte derived macrophages forming foam cell (Table 4.2, rules 19 and 21) [42]. High-density lipoprotein (HDL) on the other hand, has a protective role towards atherogenesis by inhibiting oxidation of LDL.

Hemodynamics: The nature of blood flow is considered an important factor for atherosclerosis. Specific arterial sites, such as branches, bifurcations and curvatures cause characteristic alterations in the flow of blood including decreased WSS and increased turbulence. At these low WSS regions (WSS< 0.3Pa), the bond strength between cells and endothelium is weak and the leukocytes stay attached and thus the leukocyte adherence and migration increases [43].

Vascular remodeling

An important concept for vascular remodeling, termed Glagov's phenomenon, is that arteries remodel to maintain constant flow despite increases in atherosclerotic lesion mass. In 1987, Glagov et al. reported the pivotal finding that atherosclerotic arteries initially remodel outward in attempt to preserve the luminal blood flow i.e. the external diameter increased while the lumen area of atherosclerotic human coronaries remained constant until the percent of plaque area exceeded 40% of the luminal area.

All these factors and events, mentioned above, were implemented in the agent-based-model (ABM) (see chapter 4). However, before creating an ABM, we need to know how WSS

affects leukocyte adhesion in the case of different flow rates, and artery geometries (straight and bifurcated). This is explained in Chapter 3.

CHAPTER 3

EFFECT OF WSS ON LEUKOCYTE ADHESION AT ARTERY BIFURCATION

Overview

Previous computational and in vitro studies have suggested that arterial bifurcations are susceptible locations for formation of atherosclerotic plaques. In this chapter we use experimental microfluidic cell channels and computational fluid dynamics (CFD) to identify how the angle of the daughter branches and their width affects not only the WSS profile but also leukocyte adhesion. Experimentally, a previous master's student in Dr. Schmidtke's group investigated cell adhesion at bifurcations. We then performed computational simulations to mimic the experimental setup and compared hemodynamic calculations with experimental results quantitatively. Low WSS regions (WSS $\leq$ 0.3Pa) were considered as regions where leukocytes could adhere. In this way, we showed that the area of leukocyte adhesion increases with decrease of inlet flow rate. For a bifurcated chamber with asymmetric daughter channels, the larger channel has more adhesion than that of smaller channel. Conversely, if both daughter channels are the same width then the adhesion is the same for both. We also found when the bifurcation angle is >60°, leukocyte adhesion does not change much (< 0.5%) with increases in angle degree. Likewise, when the bifurcation angle increases from 30° to 60° the change in amount of neutrophil adhesion is small; that is the stagnate zone increases by 6%, 8% and 15% when the inlet flow rate is 25 dyne/cm^2, 50 dyne/cm^2 and 100 dyne/cm^2 respectively. Together, these results suggest modulating the angle of bifurcation of daughter vessels does not change how many neutrophils will adhere as much as modulating the flow rate.

Introduction

Atherosclerosis is a cardiovascular disease characterized by the accumulation of lipoprotein, cholesterol and cellular products in the vascular wall [44, 45]. As mentioned previously, WSS, along with lot of other significant factors, affects cell adhesion and atherosclerotic plaque formation. Previous studies have observed that atherosclerotic plaques typically originate in regions of the vascular system that are characterized by recirculating flow [46], or abnormally low or high shear stress [47-49]. In-vitro studies, performed with sudden expansion flow chambers, have shown the effects of unsteady shear stress on endothelial cells [50, 51] and leukocytes [52, 53]. Although these studies demonstrate the factors affecting cell adhesion in regions of unsteady shear, only a few studies have investigated the direct effects of shear stress on adhesion at bifurcations.

Previous computational [54-57] and in vitro [58-61] studies have suggested that the apexes of bifurcations are susceptible to points of stagnation. That is at the tip of the apex the velocity and WSS are low (stagnant), therefore leukocytes are likely to roll and adhere at the apex. However, these in vitro studies investigated only flow patterns (WSS, velocity) rather than cell adhesion patterns, i.e. they did not show leukocyte adhesion or correlate how the fluid dynamics affect adhesion for a bifurcated chamber. Recently, microfluidic chambers with significantly smaller dimensions have been used to model leukocyte adhesion [62-65] as well as the complex geometrical structures found in the vascular system, such as bifurcated chambers [66-68]. However, they all used low WSS ($\leq$ 2 dynes/cm^2). Herein we investigate flow patterns and neutrophil adhesion in a bifurcated channel, with the WSS ranging from 1-100 dyne/cm^2.

Prabhakarpandian et al. showed that biotinylated microspheres in avidin coated microvascular networks tended to adhere more at bifurcation apex sites than in linear channel sections [69]. However, they only used shear stresses in the range of 0.1 – 2.5 dynes/cm^2. Urschel et al. also reported increased monocyte adhesion to endothelial cell layers cultured in bifurcations but only on the outer channel walls and at shear stresses less than 10 dynes/cm^2 [70]. They did not report whether adhesion was observed at the bifurcation apex.

In this chapter we performed CFD analysis for a bifurcated microfluidic chamber using inlet WSS ranging from 1-100 dynes/cm^2 and investigated the WSS distribution near the apex The regions of low WSS (< 0.3Pa) were then compared with the experiment of neutrophil adhesion in the bifurcated microfluidic chamber.

Experimental Methods

Dr. Schmidtke's group at UT Dallas used bifurcated microfluidic chambers to investigate neutrophil adhesion at the bifurcation apex. The chambers consist of a single inlet channel that forks into two symmetric daughter channels, which then converge downstream into a single exit (**Figure 3.1**). Devices are fabricated with different bifurcation angles.

Figure 3.1. Experimental devices: Neutrophil adhesion was measured using microfluidic chambers with bifurcation angles of 30, 60, 90 and 120º (left to right).

Cell suspensions of isolated neutrophils (10^6 cells/mL) are perfused through P-selectin (3.0 μg/mL incubated 3 hrs) coated chambers at a constant inlet channel wall shear stresses (τ_w) ranging from 1-100 dyne/cm^2 for 2 minutes. Here, flow rate, which gives a constant inlet channel WSS, was determined according to the relation $\tau_w = 6\mu Q/H^2W$, where μ is the dynamic viscosity of the fluid, Q is volumetric flow rate at the inlet and H and W are the height and width of the inlet channel respectively. A fresh chamber was used each time the shear stress was changed. Neutrophil adhesion was observed both in the inlet channel and at the bifurcation apex.

Experimental Results

Adhesion depends on geometry (angle of bifurcation, and cross-sectional dimension of channel), shear stress, and time. There is significant adherence at the apex.

Simulation Methods

A commercial software package (COMSOL) was used to simulate flow through bifurcated microfluidic chambers. COMSOL is based on finite element analysis (FEA) method, which solves non-linear partial differential Navier-Stokes equations. Recreating the experimental conditions, we calculated the wall shear stress (WSS) distribution and compared the stagnant zone (WSS ≤ 0.3 Pa) under different experimental conditions. WSS below 0.3 Pa is consider stagnant because the adhesion bond strength of the neutrophils surpasses the detachment shear force, as a result the cells should stay attached. Thus the stagnant zone was correlated to regions of neutrophil adhesion.

Geometry

Geometry is created based on parameterized dimensions (**Figure 3.2**). Length, width and height of inlet, daughter channels and bifurcation angle are taken from the experimental values (Table

3.1). Radius of curvature of the microfluidic chamber was determined using microscopic analysis.

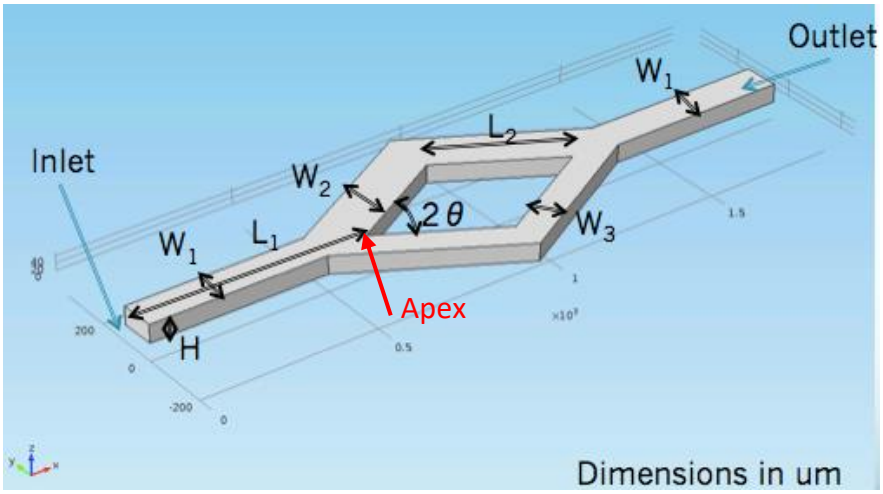

Figure 3.2 Geometry and parameters used for COMSOL simulation: The parameters used for simulation are same as experiment.

Table 3.1 List of parameters used in COMSOL simulation

Geometry Parameters	L_1 (µm)	L_2 (µm)	W_1 (µm)	W_2 (µm)	W_3 (µm)	H (µm)	Bifurcation angle(^{0})	Radius of curvature (µm)
	8000	5600	1000	1000	1000	100	30 60 90 120	290 487 600 785
Fluid Properties	ρ (Kg/m^3) 1000			µ (Pa-s) 1000			ν (m^2/s) 3.3x10	
Inlet Shear Stress (dyne/cm^2)	1, 5, 25, 50, 100							

Properties of flow

The flow was considered as steady, laminar, and incompressible with rigid walls and no slip conditions (according to experiment). A constant pressure boundary at the outlet and a steady, uniform flow at the inlet were introduced according to the following equation.

$$Q = \tau * \frac{H^2 W}{6\mu} \quad (1)$$

Where, Q is volumetric flow rate, τ is shear (experimental value) at inlet, H and W are respective height and width of the channel and μ is the viscosity (10^3 Pa-s). The gravity effect was ignored as the microchannel was horizontal for all experiments, and the height only 100 µm.

The governing Navier-Stokes equations for a Newtonian incompressible fluid are:

$$\rho \nabla . u = 0 \quad (2)$$

$$\frac{\partial u}{\partial t} + (u.\nabla)u = -\frac{1}{\rho}\nabla \mathrm{p} + \nu \nabla^2 \mathrm{u} \quad (3)$$

Here u is the velocity vector, p is the pressure, ρ is the density (1000 Kg/m^3), ν is the kinematic viscosity (3.3x10^{-6} m^2/s) and t is the time.

Measurement of stagnant zone

Figure 3.3 shows the reference stagnant zone (dark shade), whose dimension is close to the experimental region of measurement of cell adhesion. After each simulation in COMSOL the shear stress, inside and surrounding the above mentioned polygon (light shade), was exported to a grid. The shear stress file was then imported to MATLAB and the interpolated shear stress was calculated. The mesh size in MATLAB is 1µm x 1µm.

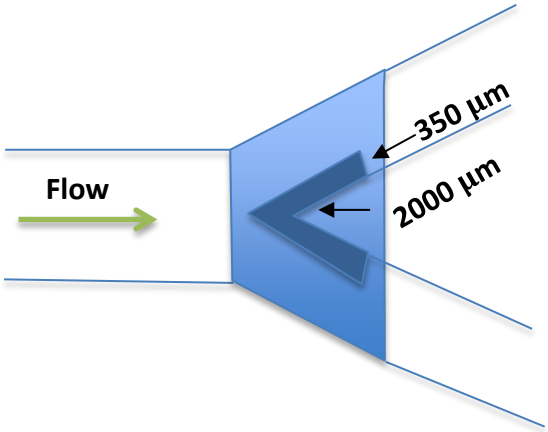

Figure 3.3 Illustration of the zones used for experimental and computational analysis: The WSS from the lightly shaded polygon zone was exported for post-processing. However, only the darkly shaded zone was used for experimental and computational analysis

Simulation Results

Results were obtained for velocity, shear stress distribution inside the artery and finally compared the stagnant zone (region with WSS≤ 0.3 Pa), obtained in the experiment with low wall shear stress region near apex.

Velocity

Figure 3.4 shows velocity distribution in the middle plane (z = 50 µm) of the chambers with the inlet flow rate equivalent to 100 dyne/cm^2. The direction of flow is from left to right, and the subplots are with different bifurcation angles. Overall, the velocity profile did not change much with change in bifurcation angle.

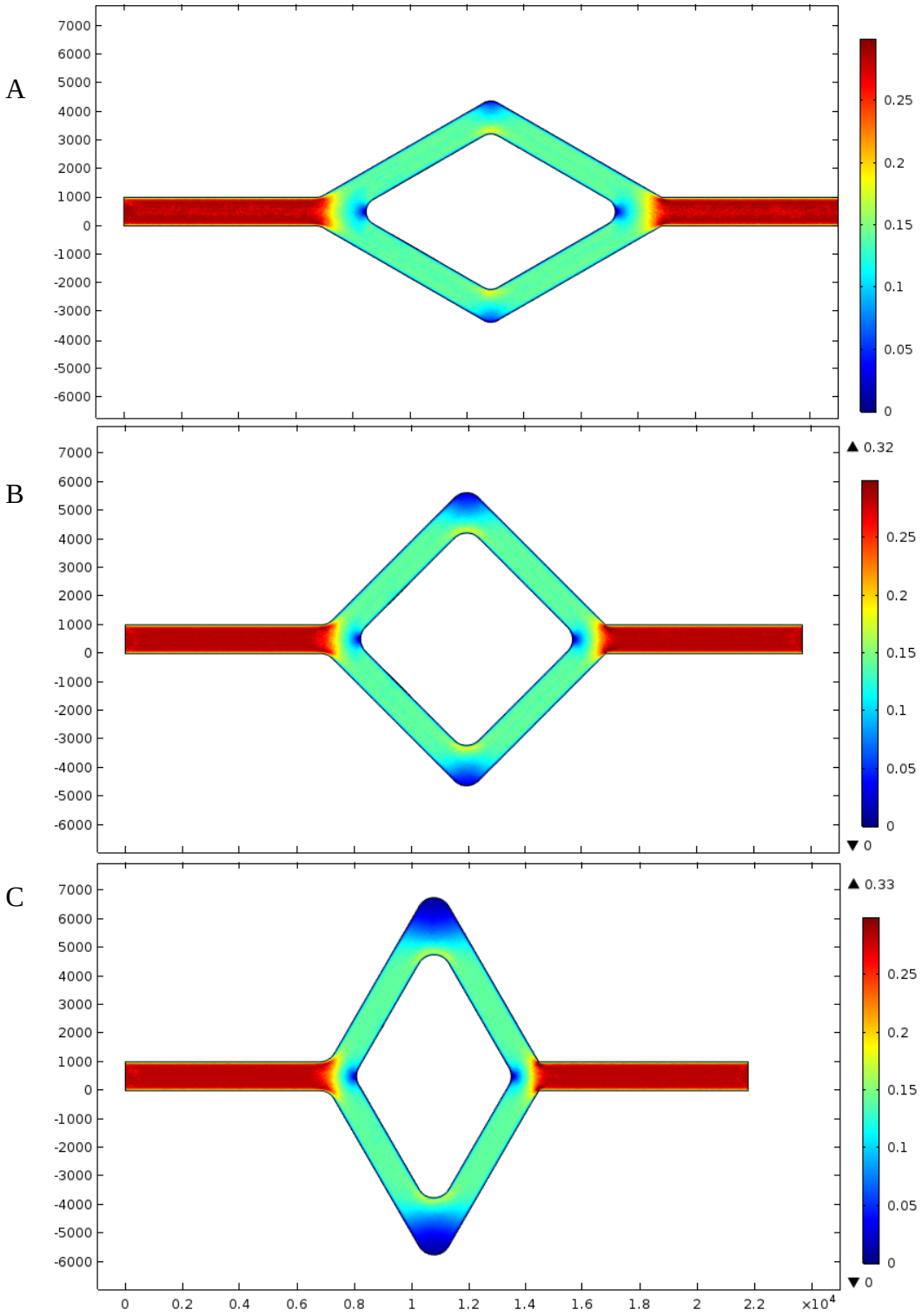

Figure 3.4 Velocity from COMSOL simulation: The color plot represents the velocity of the middle plane (at z = 50µm) at (A) 60^0, (B) 90^0 and (C) 120^0 bifurcation angle. W1, W2 and W3 (see **Figure 3.2**) are 1000µm each and H is 100µm. The color bar represents the magnitude of velocity (m/s). The velocity reduces (close to zero) at apex

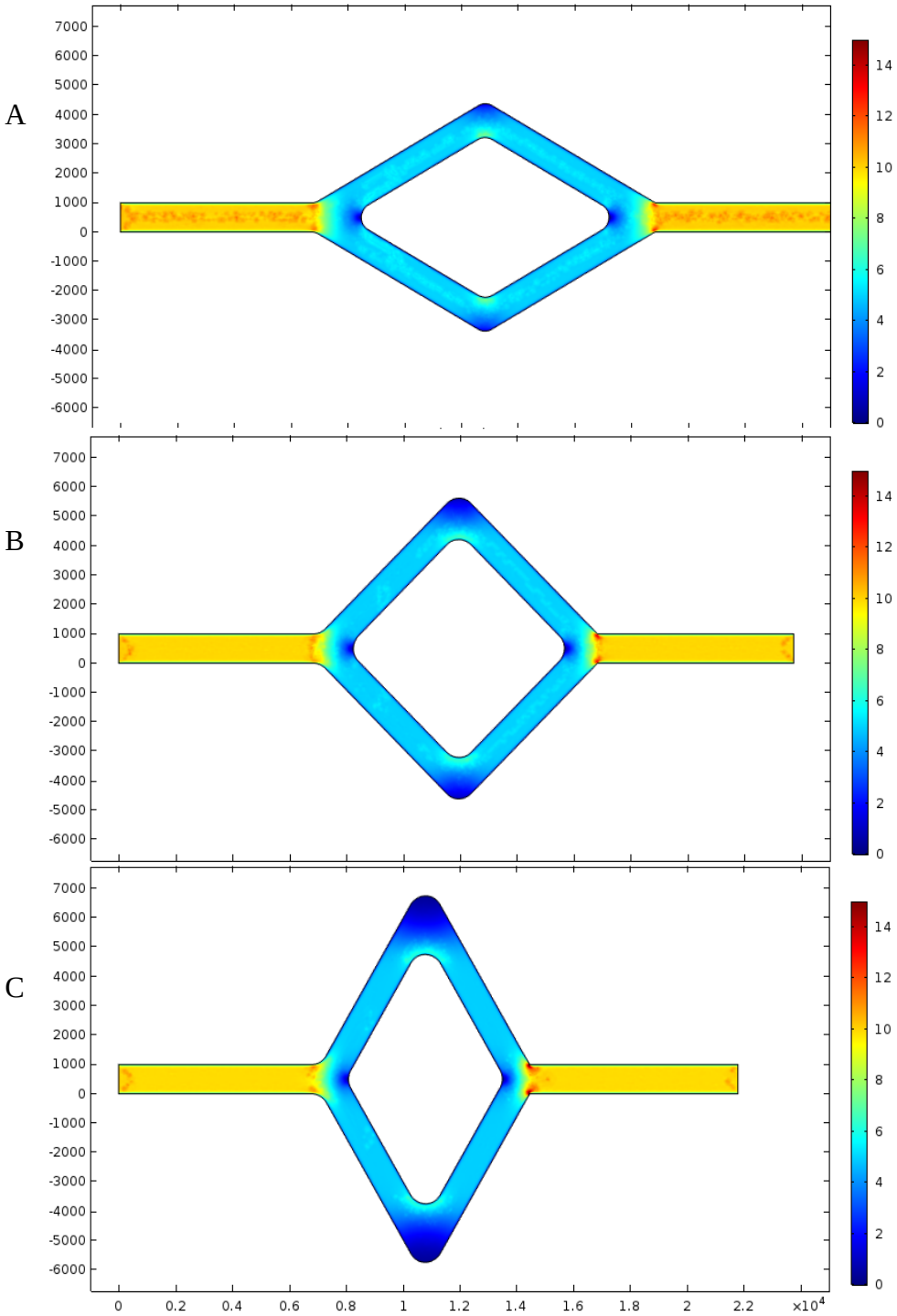

Figure 3.5 WSS from COMSOL simulation: The color plot represents the WSS distribution on the lower plane (at z = 0μm) at (A) 60^0, (B) 90^0 and (C) 120^0 bifurcation angle. W1, W2 and W3 (see **Figure 3.2**) are 1000μm each and H is 100μm. The color bar represents the magnitude of WSS (Pa). The WSS reduces (close to zero) at apex.

Wall Shear Stress

Figure 3.5 shows WSS distribution on the lower plane (z = 0 μm) of the chambers with inlet flow rate equivalent to 100 dyne/cm^2. As shown above, the flow is traveling from left to right and the plots are with bifurcation angles of 60, 90, and 120 degrees. The inlet dimension (W x H) is 1000 x 100 μm whereas the daughter channel widths are 1000 μm each. Like the velocity profile, WSS also did not change much with different angles.

Correlating simulation results with experimental results

I. *Neutrophil adhesion on device with the small channel cross sectional dimension:*

Experimentally neutrophils were perfused at flow rate equivalent to τ_w = 100 dyne/cm^2 through the device with small inlet channel cross-sectional dimensions (100 um x 50 um, W x H) and investigated neutrophil adhesion on daughter channels downstream. The daughter channels were either asymmetric (channel of different width, 130 μm and 80 μm) or symmetric. The asymmetric microchannel leads to asymmetric adhesion in daughter channels (**Figure 3.6** A)

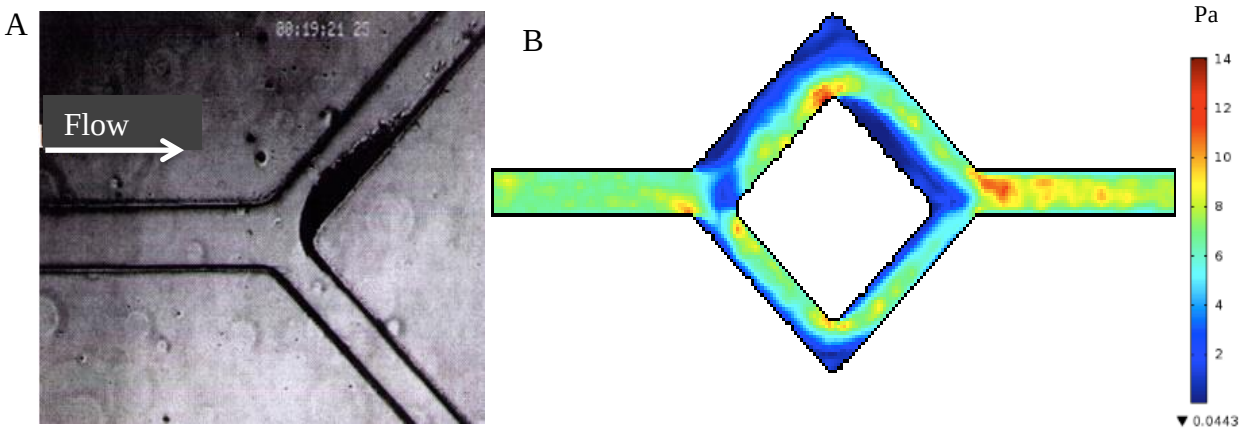

Figure 3.6 Asymmetric adhesion at daughter channels: (A) (experiment): neutrophil aggregation occurred preferentially in the larger of the two daughter channels after 20 minutes of perfusion at 100 dynes/cm^2 (B) Simulation result showing asymmetric region of low WSS representing asymmetric adhesion.

with the larger channel having more neutrophil adhesion than smaller channel. Hemodynamic simulations were performed for the device using the above dimensions. **Figure 3.6** B shows wall shear stress distribution along the bottom surface inside the chamber. At the inlet of the larger daughter channel there is a lower region of shear, which corresponds to where the neutrophils aggregated in the experiments.

The same experiment as mentioned above but with symmetric daughter channels was performed. In this case, neutrophil buildup occurred symmetrically in both the daughter channels. **Figure 3.7** B shows shear stress distribution. Note, the flow is moving from right to left now. In this condition, the low WSS (i.e., < 2 dyne/cm^2) is equally distributed along the apex of bifurcation of each daughter channel, consistent with where the neutrophils aggregate.

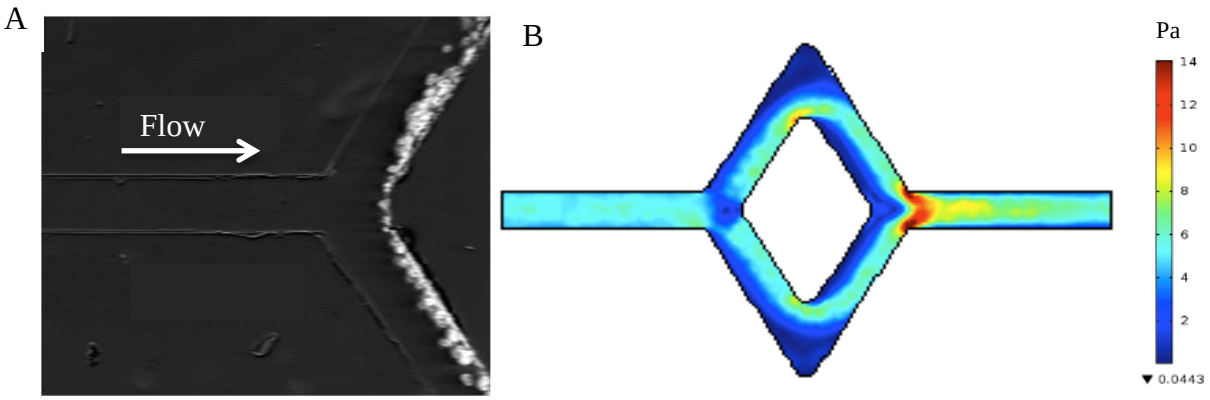

Figure 3.7 Same adhesion at daughter channels: (A) (experiment): The buildup of neutrophil aggregates downstream of the bifurcation after 20 minutes of perfusion at 100 dynes/cm^2. The aggregate buildup occurred simultaneously and symmetrically in both daughter channels. (B) Simulation result showing symmetric region of low WSS representing symmetric adhesion

II. Neutrophil accumulation in the low WSS stagnant zone:

To quantify the relationship between channel geometry, and low WSS zones we define regions with low WSS (≤ 0.3Pa) as stagnant zones. **Figure 3.8** shows the color plot of WSS distribution, flow streamlines, and velocity vectors of fluid inside the microfluidic channels. It is obvious that

the WSS and the velocity vectors at the apex of bifurcation are very small, this suggests why neutrophils adhere at the apex. The stagnant zone decreases with increase of inlet velocity (from left to right), whereas remains almost same with increase of angle (from top to down).

We then quantified the stagnant area (WSS < 0.3 Pa), which was measured as described in **Figure 3.3** (darkly shaded zone).The stagnant area decreased as the inlet WSS increased (**Figure**

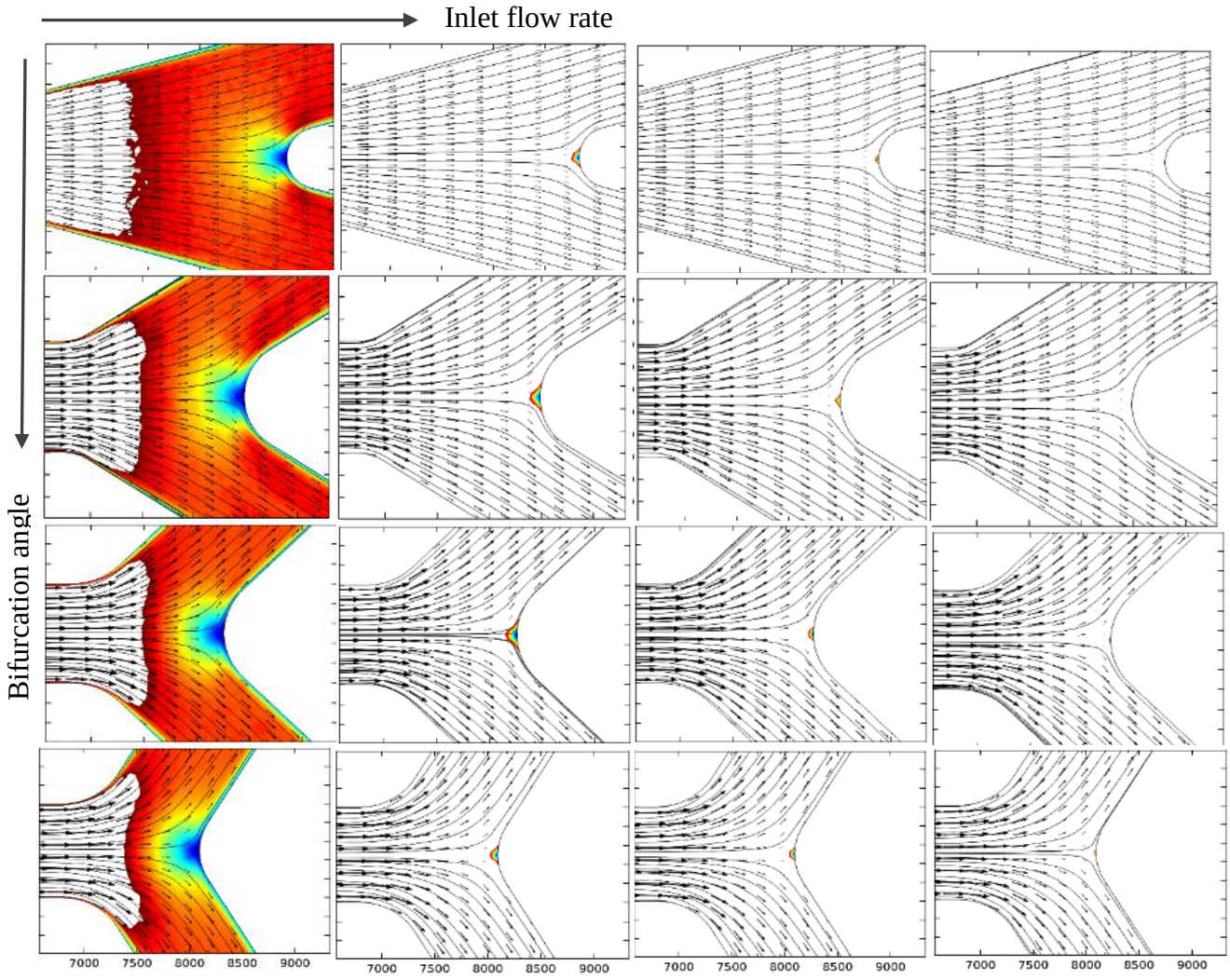

Figure 3.8 COMSOL plot of stagnant zone (zone with wall shear stress ≤ 0.3Pa) with inlet flow and bifurcation angle. From left to right, the plots are with inlet flow 5, 25, 50 and 100 dyne/cm^2 resp. From top to bottom, the plots are for 30^0, 60^0, 90^0 and 120^0 resp. The lines represent streamline flow and arrows represent the velocity vector. From all the figures it is clear that the velocity reduces near apex

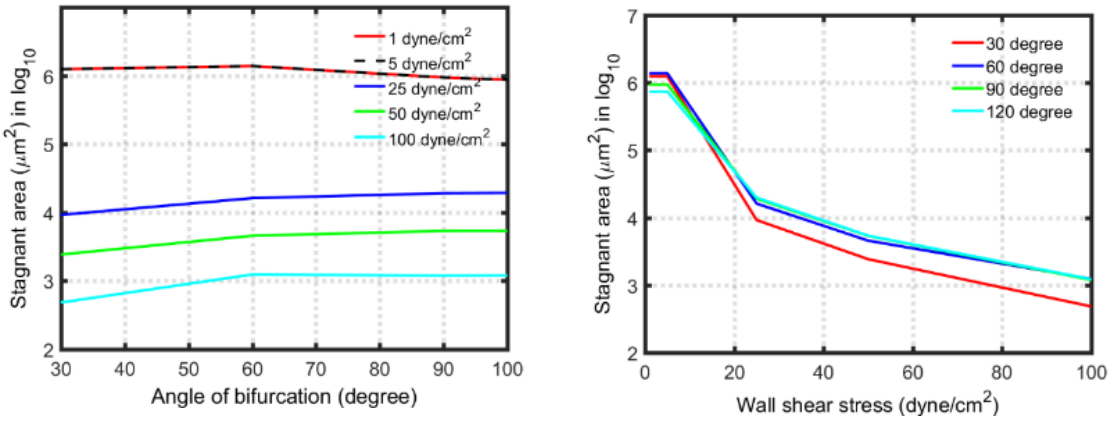

Figure 3.9 Variation of stagnant zone (zone with wall shear stress ≤ 0.3Pa) with inlet flow and bifurcation angle: A) Stagnant zone remains almost constant with bifurcation angle B) Stagnant zone decreases with increase of inlet flow rate.

3.9 A). **Figure 3.9** B shows, regardless of the angle of bifurcation, as the inlet WSS increases the stagnant area decreases. This is especially true for inlet WSS values between 5 and 25 dynes/cm^2.

Discussion:

In this chapter we used computational fluid dynamics to compare how WSS at the apex of a bifurcated flow chamber correlates to neutrophil adhesion kinetics. Our computational results show that WSS significantly reduces near apex which results in a stagnant zone and of cells accumulation. This is in agreement with previous in-vitro studies [54-57] which show low WSS is responsible for increased leukocyte adhesion. We also observed (**Figure 3.9**) that the stagnant area (region with WSS ≤ 0.3Pa) significantly increases with decreases in inlet flow rate. However, the stagnant area did not change much with changes in the bifurcation angle. These results suggest, when the adhesion molecules are not a factor, inlet flow rate influences leukocyte adhesion more than the size of the bifurcation angle. These results are significant in that they

provide a better understanding of leukocyte adhesion at bifurcations and will aid in the development of in vitro models of atherosclerosis.

CHAPTER 4

HEMODYNAMICLY COUPLED AGENT BASED MODEL OF LEUKOCYTE TRANSMIGRATION

Overview

In this chapter we present the setup of the multiscale model of leukocyte transendothelial migration (TEM) and plaque evolution in the left anterior descending (LAD) coronary artery. The approach integrates cellular behaviors via agent-based modeling (ABM) and hemodynamic effects via computational fluid dynamics (CFD). ABM considers biological events such as diffusion, protein-protein interactions, cell-cell interactions, cell migration, cell apoptosis, and differentiation, whereas CFD considers the hemodynamics. Hence, this computational model incorporates the interdependency of leukocyte TEM, plaque growth and influence of WSS with time.

ABM Design

Agent-based modeling is a class of computational modeling that predicts the evolution of a dynamical system by simulating the behavior of autonomous cellular components, called "agents." The agents follow behavioral "rules" that control their responses to changes in their environmental or internal properties. This dynamic system allows for complex phenomenon to emerge from the interaction of simple rule-based behaviors of agents. As illustrated in **Figure 4.1**, the system resides in a regularized 3D environment, commonly implemented as a grid. The grid spaces are called "patches" in the ABM and within each patch, agents, extracellular matrix (ECM) and soluble factors can reside.

System description

The 3D model of leukocyte TEM is developed in an open source ABM software, NetLogo 3D 5.3.1. The entire 3D space is segmented into cubical patches of edge length 100 μm. **Figure 4.1** illustrates an arterial cross-section and all the agents included in this ABM. The modeled artery is allowed to spatiotemporally evolve after each time tick, which represents a 1-hour interval. The initial conditions and parameters are given in Table 4.1.

Development of Rules for ABM

To computationally model leukocyte adhesion and TEM into the arterial wall, we need to first identify the factors affecting migration quantitatively, and then make a series of

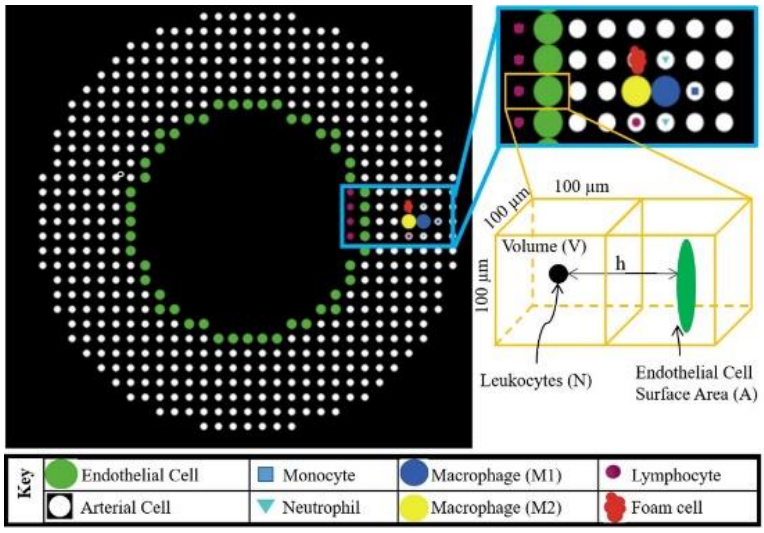

Figure 4.1 Schematic illustrating the spatial distribution of each type of cell (i.e. agent) in the ABM. The bottom right schematic represents a luminal and artery wall patch where N is the number of leukocyte agents residing in this luminal patch. Among all leukocytes (N), M is the number that adheres to the endothelial cell surface area (A). V is the patch volume and h is 100μm or the distance between the patch centroids. All these parameters are used to find leukocyte adhesion probability (see equation 2).

Table 4.1. Initial ABM Parameters

Parameters	**Value**	**References**
Patch size (μm x μm x μm)	100x100x100	
One tick	One hour	
Lumen radius (μm)	1800	[71]
Artery length (μm)	6000	
Coronary artery wall thickness (Media + Adventitia) (μm)	600	[39, 72]
Initial plaque	15 leukocytes	
Leukocyte concentration in blood	$7x10^9$/liter	[73]
Neutrophil concentration in blood	62% of leukocytes	*
Monocyte concentration in blood	5.3% of leukocytes	*
Lymphocyte concentration in blood	30% of leukocytes	*
LDL concentration in blood	Normal: 956 ng/μl	[74]
Diffusion coefficient of cytokines	$3x10^{11}$ m^2/s	[75]
Diffusion coefficient of LDL	$2.5x10^{11}$ m^2/s	[76]
Healthy WSS (Pa)	1.4	[30]
Stiffness of artery wall (kPa)	Normal:3	[16]
Diameter of neutrophils & lymphocytes (μm)	12	[77]
Diameter of monocytes (μm)	24	
Diameter of foam cell (μm)	25	

*Assigned values; patient specific

mathematical/procedural relations, called rules, and lastly program these rules into an ABM. The model of leukocyte TEM and atherogenesis considers the following biological events and the corresponding factors.

1. Endothelial activation

Cell adhesion molecules (CAMs) are proteins located in the surface membrane of endothelial cells and are involved in binding with other cells or with the extracellular matrix (ECM) in the process called cell adhesion. In essence, cell adhesion molecules help cells stick to each other and to their surroundings. Cytokine is a small protein released by leukocytes. Research has shown that several pro-inflammatory cytokines, including Tumor Necrosis Factor-α (TNF- α) and Interleukin-1β (IL-1 β), increase the expression of many CAMs and thus increase the adhesiveness between leukocytes, in the blood, and the endothelium. Whereas other cytokines are anti-inflammatory, such as IL-10, and inhibit the production of pro-inflammatory cytokines. The effect of anti-inflammatory cytokines results in a net reduction of CAMs and thus less leukocyte adhesion.

2. Adhesion of leukocytes

The probability of leukocyte adhesion (p) to the endothelium depends on endothelial cell activation via cytokine concentration, WSS and the concentration of leukocytes in the blood. Thus, in our ABM, the rules of adhesion are of the form:

$$\frac{R_i}{\rho_i t} = \frac{f_i(\alpha)}{t_{exp}} \qquad (1)$$

Where index *i* represents the type of leukocyte, either lymphocyte, monocyte or neutrophil. R_i/t is number of leukocytes of type *i* that adhere per unit surface area (leukocytes/mm^2) per time. ρ_i is the density of leukocytes of type *i* in the blood (leukocytes/mm^3). t_{exp} is time duration of the experiment, and *f(α)* are experimentally derived functions, where *α* represents WSS, TNF-α and IL-1β (see Table 4.2, rules 1-9), which are specific to each type of leukocyte. f(α) is derived from the published literature by first plotting R_i/ρ_i versus α and using matlab regression

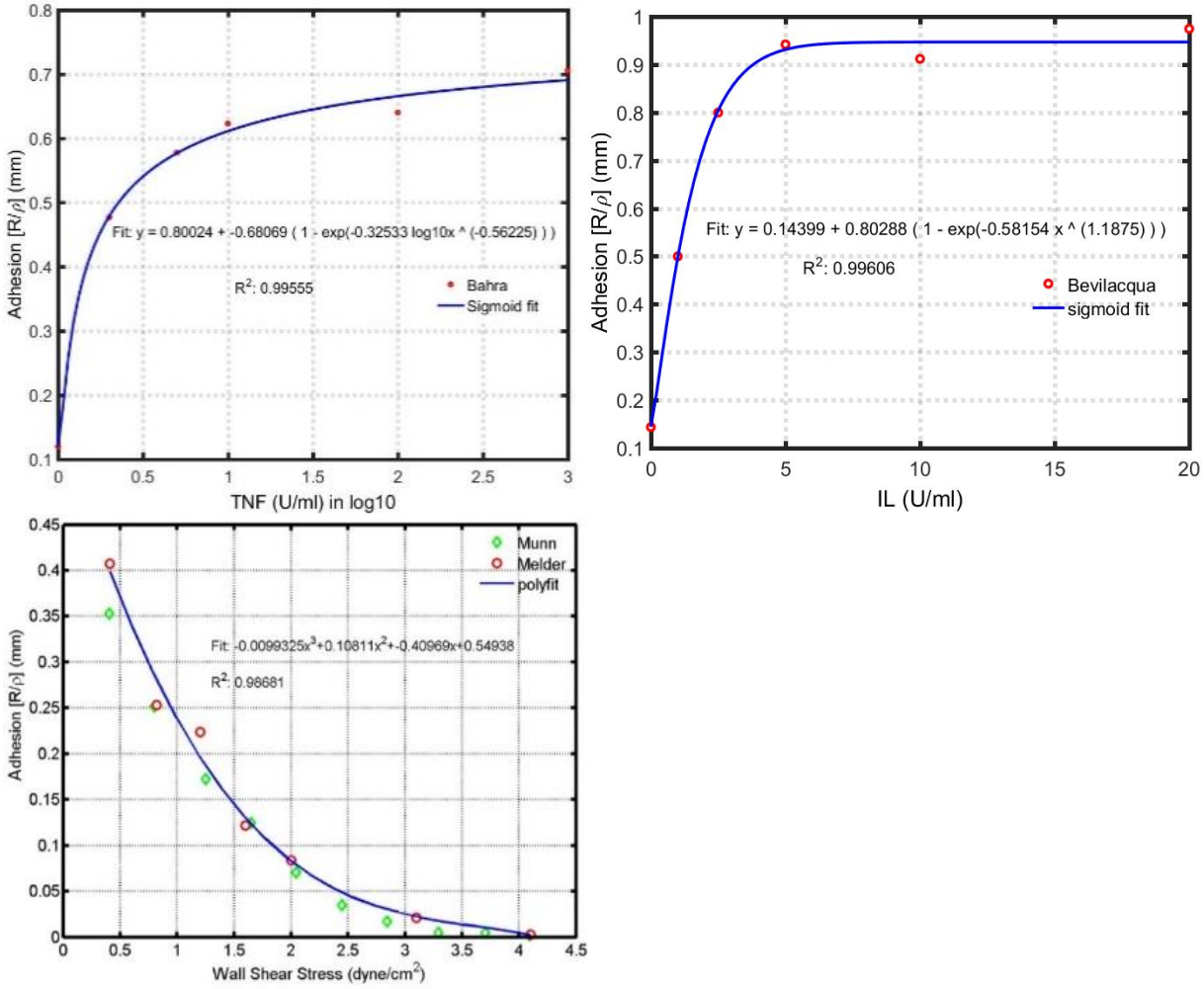

Figure 4.2 Leukocyte adhesion with cytokines and WSS. The top left represents the neutrophil adhesion as a function of TNF-α. Red dot represent the data from literature [9-12] and the line plot represent the fit of the data. Top right is the monocyte adhesion with IL-1β and the bottom represent lymphocyte adhesion with WSS.

algorithms to determine the best fit equation to resent the data (as shown in **Figure 4.2**). E.g. Bahra et al. [9] studied lymphocyte adherence as a function of TNF-α concentration. Lymphocyte cells (10^6 cells/ ml) were perfused over human umbilical vein endothelial cell (HUVEC) which had been grown on micro slides of glass, and cultured with varying concentrations of TNF-α (1-1000 U/ml) for 4h, and observed the adhesion rate. The data are plotted and the best fit function of these data determined. It has been found that the best fit function for leukocyte adhesion based on endothelial activation by cytokines (TNF, IL-1) are sigmoid functions (rule 1,2,4,5,7,8), whereas the best fit functions for leukocyte adhesion dependent on WSS (rule 3,6,9) are polynomial of order two or more.

Now, using the model, the probability of adhesion (p) can be computed for each leukocyte type. **Figure 4.1** illustrates a luminal and adjacent artery patch containing leukocytes and ECs, respectively. N is the total number of leukocytes present in the luminal patch of volume, V (mm^3). Among N, M is number of leukocytes that adhere to the endothelium of surface area, A (mm^2). Hence according to law of large numbers (LLN: It holds when the same experiment is done a large number of times and gives long-term results for the average of some random events. It states that for statistical application, as the number of experiments increase, the average of the results gets increasingly close to the hypothetical mean), the probability of adherence (p) is M/ N. Since, volume V=Ah, where h is the patch length (mm), the following relation can be derived to compute the probability of leukocyte adhesion by type, p_i.

$$\frac{R_i}{\rho_i t} = \frac{M_i/A}{N_i/V}\frac{1}{t} = \left(\frac{M_i}{N_i}\right)\left(\frac{V}{A}\right)\frac{1}{t} = \frac{\mathrm{p}_i h}{t}$$

Recalling, $\frac{R_i}{\rho_i t} = \frac{f_i(\alpha)}{t_{exp}}$

$$\therefore p_i = \frac{f_i(\alpha)}{h} \frac{t}{t_{exp}} \quad (2)$$

3. Leukocyte TEM and chemotaxis

Once the leukocytes adhere to the endothelium, they then have the potential to transmigrate through the endothelium, depending on the arterial stiffness. Arterial stiffness increases the leukocyte transmigration through EC surface. Stroka et al.[17] and Hayenga et al. [16] investigated neutrophil, monocyte transmigrations respectively vs. arterial stiffness through TNF-α activated (25 ng/ml for 24 hours) EC surface (**Figure 4.3**)

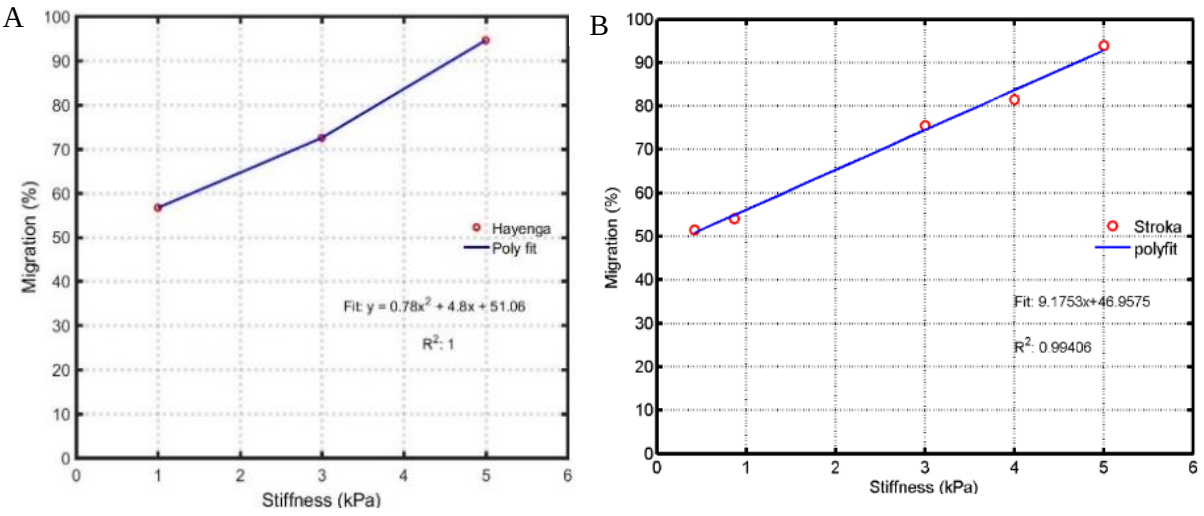

Figure 4.3 Leukocyte transmigration with arterial stiffness: (A) Lymphocyte and monocyte transmigration increases with subendothelial matrix stiffness. If the stiffness is > 5 kPa, 91% of adhered mononuclear leukoctyes transmigrate. (B) Neutrophil transmigration also increases with stiffness. 95% of neutrophils undergo transmigration for artery with stiffness > 5 kPa. Source data from [16, 17].

Upon entering the artery wall, leukocyte migration is guided by chemotaxis, i.e., directed cell movement towards higher concentrations of chemoattractant. Since our goal is to model leukocyte TEM and plaque evolution as a function of hemodynamics, the wall composition is considered uniform throughout, with no distinction between media and adventitia. Specifically,

60% of the arterial wall is considered fixed and composed of ECM, namely collagen and elastin, and the remaining 40% is composed of cells and soluble factors [78-80]. Consequently, 40% of each patch of that makes up the artery wall is available for leukocytes, macrophages and foam cells.

Once the leukocytes adhere to the artery wall they first determine which neighboring patch has space available. Secondly, of those patches with available space which one has the highest concentration of pro-inflammatory cytokines, and finally the leukocyte moves towards that patch based on its migration speed. This process repeats, within a tick and at each following tick, until the leukocyte finds the patch with space and the highest concentration of cytokines as compared to neighboring patches. **Figure 4.4** illustrates the chemotactic process using a 2D ABM.

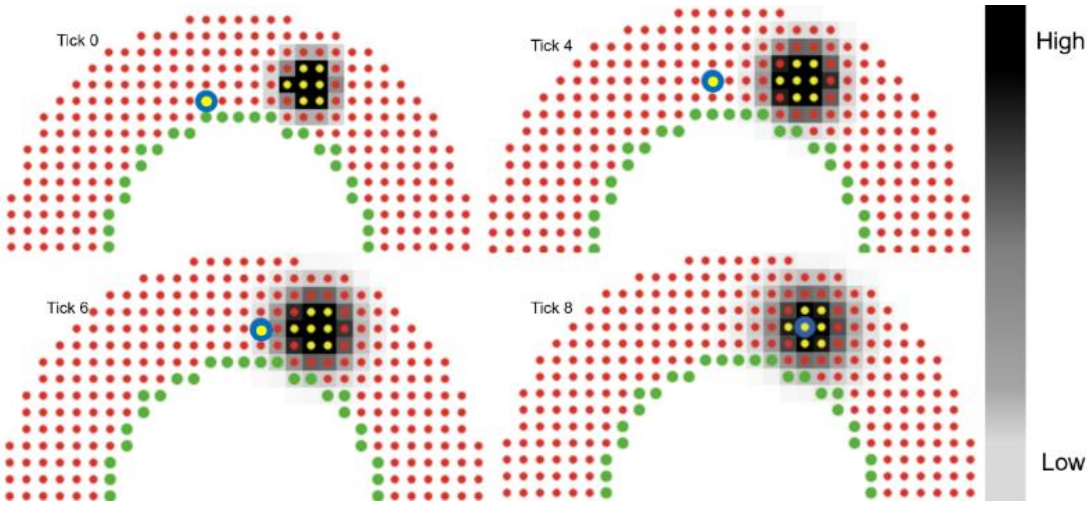

Figure 4.4 Protein diffusion and leukocyte chemotaxis. 2D example of leukocyte (yellow circle with blue outline) migration. Color bar represents the cytokine concentration gradient (black (highest) to white (lowest) via gray). Yellow agents produce the cytokines. At tick 0 the leukocyte is 5 patches away from the source. Cytokines diffuse at each tick following Fick's law. At tick 4, the leukocyte moves to its topmost neighboring patch, since that patch has the highest cytokine concentration and space available. In next ticks, the leukocyte surveys it's neighboring patches and moves to the one with space available and the highest concentration. At tick 8, it has reached the patch with the highest concentration (darkest). Each tick represents 1 hr.

4. Transport of cytokines and low density lipoproteins (LDLs)

At each time step cytokines, generated from leukocytes in the wall, diffuse through space (i.e. patches) in the artery wall according to Fick's law [75]. Fick's law (equation 3) states that the flux (solute) goes from higher concentration regions to the lower concentration region. The magnitude depends on concentration gradient as well as the diffusion constants of the solute. Fick's law in one dimension is as follow:

$$J = -D\frac{\partial \phi}{\partial x} \qquad (3)$$

Here J is the diffusion flux, measured as amount of substance per unit area per unit time, D is the diffusion coefficient or diffusivity and $\frac{\partial \phi}{\partial x}$ is the concentration gradient with position.

We assume at the lumen and outer wall, the cytokine concentration is zero due to convection (from luminal blood flow). In this model we consider two pro-inflammatory, TNF-α and IL-1β, and an anti-inflammatory cytokine, IL-10. At each time point, the total cytokine amount present

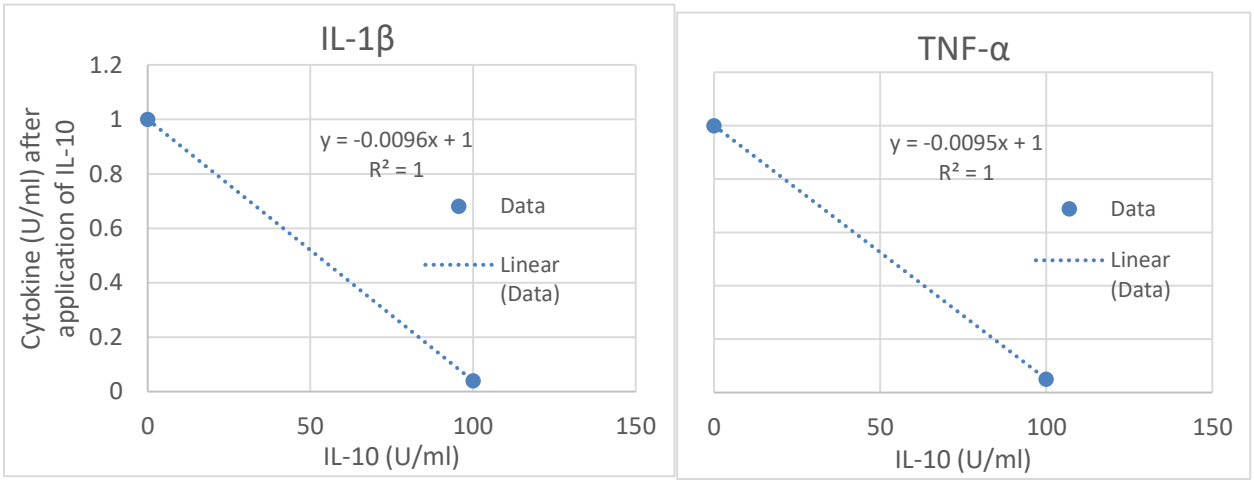

Figure 4.5 Removal of proinflammatory cytokine by IL-10: IL-10 inhibit the release of IL-1β (A) and TNF-α (B) from leukocytes [4, 5]

in a patch is the amount of cytokine present from previous ticks, plus the amount produced from all the leukocytes present in that patch, plus or minus the amount diffused into or from the patch, minus the cytokines removed according to IL-10 (**Figure 4.5**) interactions (see Table 4.2, rules 22 and 23).

Mass transport of LDL from lumen into the arterial wall is also an important factor for atherogenesis [81]. The majority of LDL transport occurs through leaky cell-cell junctions (> 90%) and the remainder through endocytosis [82]. The occurrence of leaky junctions is governed largely by blood flow, hence WSS is considered a potent factor in LDL transport. Deng et al. presented a numerical analysis of mass transport of LDL within a physiological range of WSS. They used steady laminar flow of blood (considered homogeneous, incompressible and Newtonian) with fully developed velocity profile through a straight uniform cylinder. Depending on inlet flow rate, the WSS through the cylinder changes and thus the LDL transport. Hence, we

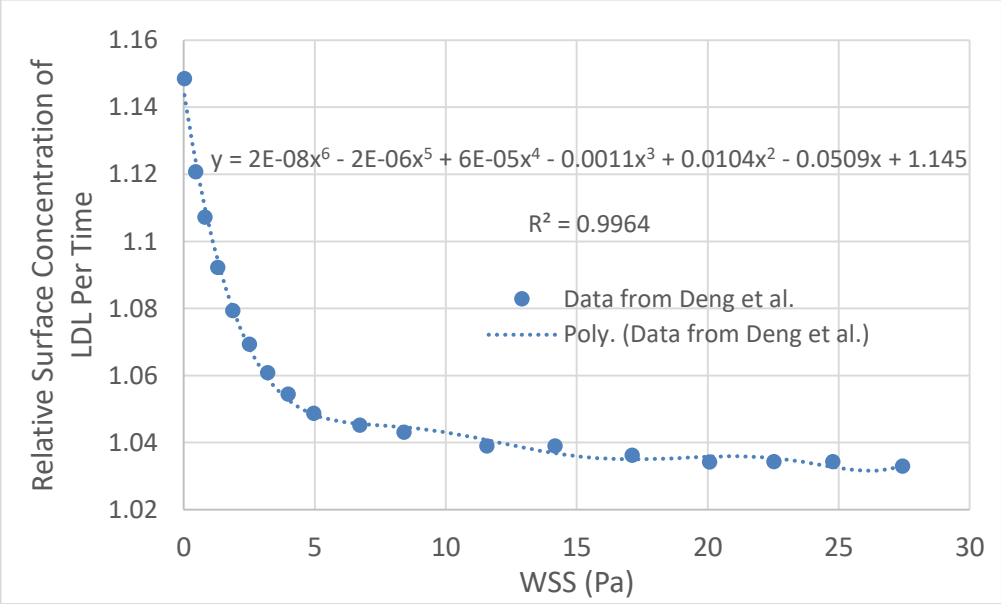

Figure 4.6 Dependence of LDL accumulation into endothelium on WSS: Data was taken from Deng et al.[20] LDL accumulation decreases with increase of WSS. Data was measured as relative concentration of LDL (ratio of concentration of LDL in the wall and in the lumen).

can found LDL transport as function of WSS from their numerical data (**Figure 4.6**). LDL then diffuses spatiotemporally according to Fick's law. LDL is oxidized in the arterial wall and this oxidized form of LDL (ox-LDL) is consumed by monocyte derived macrophages forming foam cell (Table 4.2, rules 19 and 21) [83].

5. Plaque growth and artery remodeling:

In 1987 Glagov et al. reported the pivotal finding that atherosclerotic arteries initially remodel outward in attempt to preserve the luminal blood flow. Glagov and colleagues found that the external diameter increased while the lumen area of atherosclerotic human coronaries remained constant, until the percent of plaque area exceeded 40% of the luminal area at that specific axial-plane [84]. To determine when inward growth would occur, at each time tick in the ABM, the plaque area to lumen area along the axial length (in segmented intervals of one patch) of the artery is compared. If the plaque area is greater than 40% of the lumen area then that axial segment of the plaque starts growing inside the lumen in addition to outward growth (see Table 4.2, rule 16). **Figure 4.7** shows a 3D model of arterial remodeling following Glagov phenomenon. Plaque area is considered as number of patches with macrophages, leukocytes and foam cells, whereas lumen area is considered as number of patches in the lumen of the corresponding axial plane. Although, the mechanisms for this compensatory remodeling effect are still being established [85], the Glagov phenomenon informs growth and remodeling (G&R) in our ABM of plaque evolution. In these cases in which the mechanisms to observed phenomenon, such as Glagov remodeling, and LDL oxidation rate (rules 16, 18 and 19), are less

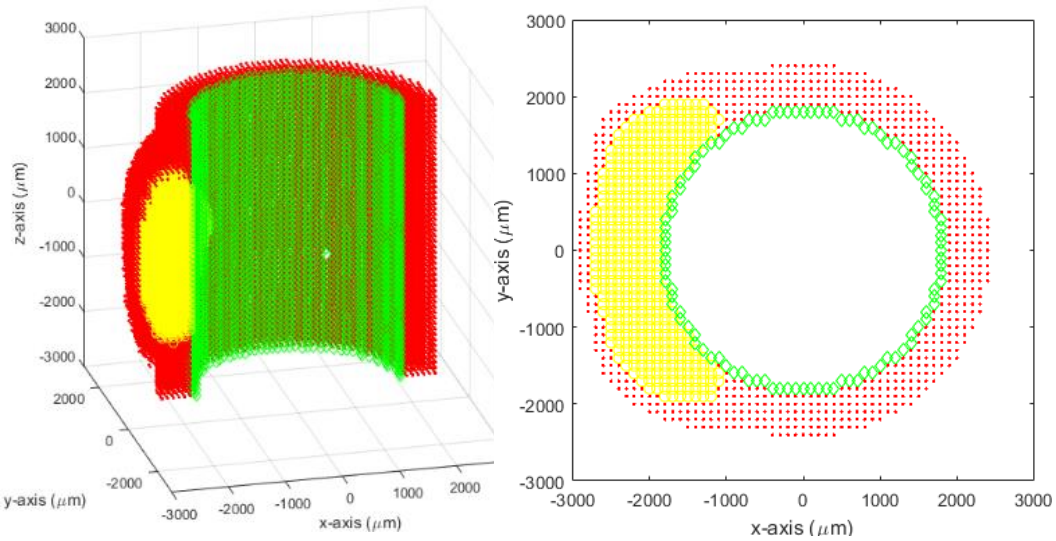

Figure 4.7 Glagov remodeling. Longitudinal (left) and corresponding transverse (right) views of an evolving artery where ECs, ACs and leukocytes are represented by green, red and yellow respectively. Initially the artery is impregnated with 15 leukocytes. At 6 months the plaque area is 40% of the lumen area and will start growing inside lumen according to Glagov's phenomenon.

known the phenomenon was simply hard-coded in the model. However, when the mechanisms become more know they can easily be replaced by rules that are more mechanistic.

All rules quantifying the influence of primary factors on leukocyte adhesion, TEM and plaque progression are derived from the published literature and are listed in Table 4.2.

Table 4.2. List of rules used in the ABM (reprinted with permission from [86]).

No.	Behavior	ABM Rule	Ref.
1.	Dependence of neutrophil adhesion on TNF-α	$\frac{R}{\rho t} = \frac{1}{180}[0.80 - 0.68(1 - exp(-0.33(log_{10}x)^{-0.56}))]; \mathrm{x} > 1$ $= \frac{1}{180}[0.0996x]; \mathrm{x} \leq 1$ $x: TNF\alpha[U/ml]\,;\ R[\#/mm^2]; \rho[\#/mm^3];\ t[sec]$	[9]
2.	Dependence of neutrophil adhesion on IL-1	$\frac{R}{\rho t} = \frac{1}{900}[0.10 + 0.19(1 - exp(-28.29x^{1.46}))]$ $x: IL1\beta[U/ml]\,;\ R[\#/mm^2]; \rho[\#/mm^3]; t[sec]$	[87]

3.	Dependence of neutrophil adhesion on WSS	$\frac{R}{\rho t} = \begin{cases} \frac{1}{300}[0.26x^2 - 0.8x + 0.63]; 0 < x < 1.2 \\ 0; x > 1.2 \end{cases}$ $x: WSS[Pa]\ ;\ R[\#/mm^2]; \rho[\#/mm^3]; t[sec]$	[88]
4.	Dependence of monocyte adhesion on TNF-α	$\frac{R}{\rho t} = \frac{1}{180}\big[0.80 - 0.68\big(1 - exp(-0.33(log_{10}x)^{-0.56})\big)\big]; \text{x} > 1$ $= \frac{1}{180}[0.0996x]; \text{x} \leq 1$ $x: TNF\alpha[U/ml];\ R[\#/mm^2]; \rho[\#/mm^3]; t[sec]$	[9]
5.	Dependence of monocyte adhesion on IL-1	$\frac{R}{\rho t} = \frac{1}{600}[0.14 + 0.80\big(1 - exp(-0.58x^{1.19})\big)]$ $x: IL1\beta[U/ml];;\ \ R[\#/mm^2]; \rho[\#/mm^3]; t[sec]$	[10]
6.	Dependence of monocyte adhesion on WSS	$\frac{R}{\rho t} = \begin{cases} \frac{1}{600}[-0.3295x^3 + 1.4x^2 - 1.8x + 0.79]; 0 < x \\ 0; x > 1.0 \end{cases}$ $x: WSS[Pa];\ \ R[\#/mm^2]; \rho[\#/mm^3]; t[sec]$	[89]
7.	Dependence of lymphocyte adhesion on TNF-α	$\frac{R}{\rho t} = \frac{1}{180}\big[0.80 - 0.68\big(1 - exp(-0.33(log_{10}x)^{-0.56})\big)\big]; \text{x} > 1$ $= \frac{1}{180}[0.0996x]; \text{x} \leq 1$ $x: TNF\alpha[U/ml];\ \ R[\#/mm^2]; \rho[\#/mm^3]; t[sec]$	[9]
8.	Dependence of lymphocyte adhesion on IL-1	$\frac{R}{\rho t} = \frac{1}{900}[0.10 + 0.19\big(1 - exp(-28.29x^{1.46})\big)]$ $x: IL1\beta[U/ml]\ ;\ \ R[\#/mm^2]; \rho[\#/mm^3]; t[sec]$	[87]
9.	Dependence of lymphocyte adhesion on WSS	$\frac{R}{\rho t} = \begin{cases} \frac{1}{25}[-9.93x^3 + 11x^2 - 4.1x + 0.55]; 0.04 < x < \\ 0; x > 0.41 \end{cases}$ $x: WSS[Pa];\ R[\#/mm^2]; \rho[\#/mm^3]; t[sec]$	[11, 12]
10.	Dependence of monocyte TEM on stiffness	$\%\ TEM = \begin{cases} 0.78x^2 + 4.8x + 51.06\ ; 1 < x < 5 \\ 95\ ; x > 5 \end{cases}$ $x: stiffness[kPa]$	[16]

11.	Dependence of lymphocyte TEM on stiffness	$\%\,TEM = \begin{cases} 0.78x^2 + 4.8x + 51.06\,;\, 1 < x < 5 \\ 95\,;\, x > 5 \end{cases}$ $x: stiffness[kPa]$	[16]
12.	Dependence of neutrophil TEM on stiffness	$\%\,TEM = \begin{cases} 9.18x + 46.96\,;\, 0.42 < x < 5 \\ 91\,;\, x > 5 \end{cases}$ $x: stiffness[kPa]$	[17]
13.	TNF-α production	$5x10^{-6}$ U/ml/1h/neutrophil; $6.7x10^{-4}$ U/ml/1h/monocyte	[82]
14.	IL-1 production	$5x10^{-7}$ U/ml/1h/neutrophil; $5x10^{-5}$ U/ml/1h/monocyte	[82]
15.	IL-10 production	$3.75x10^{-5}$ U/ml/1h/lymphocyte	[90]
16.	Dependence of directional plaque growth on plaque to lumen area ratio at each z-plane	Plaque area < 40% lumen area = plaque grows outward Plaque area ≥ 40% lumen area = 65% inward and 35% outward	[84]
17.	Dependence of wall concentration of LDL, C_w, on WSS	$\frac{C_w}{t} = C_0(2e^{-8}x^6 - 2e^{-6}x^5 + 6e^{-5}x^4 - 1.1e^{-3}x^3 + 1.04e^{-2}x^3 - 0.05x + 1.15)$ $x: WSS[Pa]; C_0 =$ $LDL\ concentration\ in\ lumen[ng/\mu l]; t = 1h$	[20]
18.	LDL infiltration through wall	70% of C_w	[20]
19.	LDL oxidation (OxLDL) rate	1.2 % /1h of total LDL concentration;	[74]
20.	Macrophage type ratio	M1(pro-inflammatory): M2(anti-inflammatory) = 2:1	[83, 91-93]
21.	Foam cell formation	If oxLDL > 100 μg/ml, macrophage becomes foam cell	[94]
22.	Removal of IL1β by IL-10	$\frac{IL1\beta}{t} = (-0.0096x + 1) \times IL1\beta$ $x: IL10[U/ml]; t = 1h$	[4]
23.	Removal of TNFα by IL-10	$\frac{TNF\alpha}{t} = (-0.0095x + 1) \times TNF\alpha$ $x: IL10[U/ml]; t = 1h$	[5]
24.	Lifespan of leukocytes in wall	Neutrophils: 3 days, Monocytes: 7 days, Lymphocytes: 7 days	

= number of leukocytes

Rule confidence

Since a model is only as good as its rules, and each rule is derived from different sources we used a rule scoring metric to gain confidence in each rule, as previously described [37]. Briefly, each rule is independently evaluated for 1) universal acceptance by different published literature sources, 2) physiological accuracy of the articles methods, 3) similarity of the conditions in the article to those being simulated in our ABM, and 4) precision of the data measurements. Table 4.3 is an example of rule scoring from three blinded researchers. If the average score for a given rule is under 5 it is deemed less reliable. Thus we either rederived the rule (e.g., formulating the rule from one of the articles making a contradictory but more prevalent claim) or generalized the correlation if limited data exists.

Table 4.3 An example of rule scoring

Rule	Monocyte adhesion on IL-1β		
article	Bevilacqua et al.		
1. Article agreement (3)	5	5	5
2. Phsiological methods (in-vitro, sound environment)	4	4	2
3a. Same species (human)	10	10	10
3b. Same organ (coronary artery)	5	5	5
3c. Same cell type (endothelial cell)	10	10	10
3d. Same in vivo state	0	0	0
3. Similarity metric total:	6.25	6.25	6.25
4a. Numerical	10	10	10

4b. Measured directly	10	10	10
4c. Many data points (6-10)	4	4	4
4. Data type total:	8	8	8
Average confidence	5.8125	5.8125	5.3125
Compose score by	Res. 1	Res. 2	Res. 3

Computational fluid dynamics (CFD)

Wall shear stress (WSS) in a coronary artery is known to play a significant role in the early atherogenosis. CFD allows for efficient and accurate computations of hemodynamic features of both normal and abnormal situations in the cardiovascular system. CFD is different from medical imaging visualization. Medical imaging techniques such as coronary angiography or computed tomography angiography, only the degree of lumen changes such as stenosis or occlusion can be assessed. In contrast, CFD analysis enables us to calculate the hemodynamic changes (WSS) in the coronary artery, and based on the values predict where the plaque may grow. Specifically, low WSS is an early indicator of plaque growth; thus, to some extent, CFD allows early detection of coronary artery disease and helps to understand the progression of plaques, which has great impact to clinical treatment.

As the plaque grows inward (according to Glagov phenomenon) the change in luminal geometry alters the blood flow. Therefore, CFD analysis is used to investigate the hemodynamic effect of the plaque burden in the left coronary artery. This investigation gives spatiotemporal information about WSS, which in turn is used to predict the leukocyte transmigration. A commercial CFD package COMSOL (5.2a) is used for the hemodynamic calculations.

Conditions of the CFD model

- *Blood:* Density and dynamic viscosity of blood are 1060 kg/m^3 and 3.5e-3 Pa-s respectively. Blood is considered homogeneous, incompressible and Newtonian. Johnston et al. showed that for transient blood flow in arteries the use of Newtonian model is reasonable [95]. Moreover, Chaichana et al. conducted a study investigating WSS at stenotic locations using either Newtonian or non-Newtonian flow and concluded that the WSS was not significantly different [96]. Therefore, although blood behaves more as non-Newtonian, for simplicity and given the minimal error introduced we considered blood as non-Newtonian.
- *Flow and boundary conditions:* Laminar pulsatile blood flow (**Figure 4.8**) with a cardiac period of 0.8 sec is introduced at inlet [19]. Nosovitsky et al. validated the assumption of laminar flow in stenotic arteries is appropriate [97]. They compared laminar flow model and turbulence model for two representative stenosis level (25% or 75%) and showed that the velocity vector and WSS profile are same for both the models. They concluded that the effect

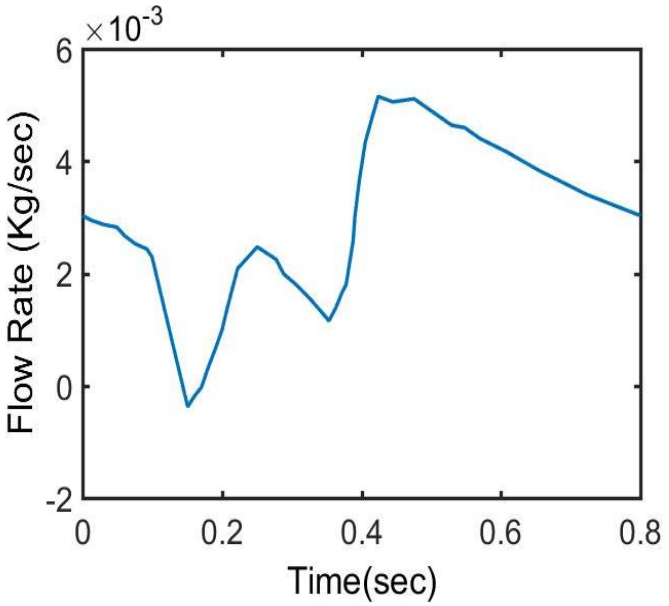

Figure 4.8 Coronary blood flow rate profile: Pulsatile flow rate with a period 0.8s is used for CFD analysis. The flow rate was taken from [19]

of turbulence is very small and can be neglected. The wall is considered rigid and cylindrical. Differences of WSS between compliant and rigid wall models depend on several factors (e.g., degree of compliance, geometry, curvature, and stenosis severity). Coronary arteries with mild stenosis, exhibit a change in diameter < 2% over a cardiac cycle and peak WSS differences between compliant and rigid wall models is < 10% [98]. In arteries with severe stenosis the difference is around 30-40% [99]. Therefore, a rigid wall assumption was a close approximation for the case of early atherosclerosis studied herein. No slip at wall and constant pressure at the outlet are used.

Coupled CFD-ABM model

Leukocyte accumulation and leukocyte derived foam cells form plaque inside the wall. Plaque grows over time and eventually blocks the blood flow depending on the severity of plaque. Since the hemodynamics change when plaque enters lumen, the rate of leukocyte transmigration also changes. Hence a coupling between ABM and CFD is necessary for a self-consistent leukocyte transmigration model. **Figure 4.9** shows the flow chart of the integrated model.

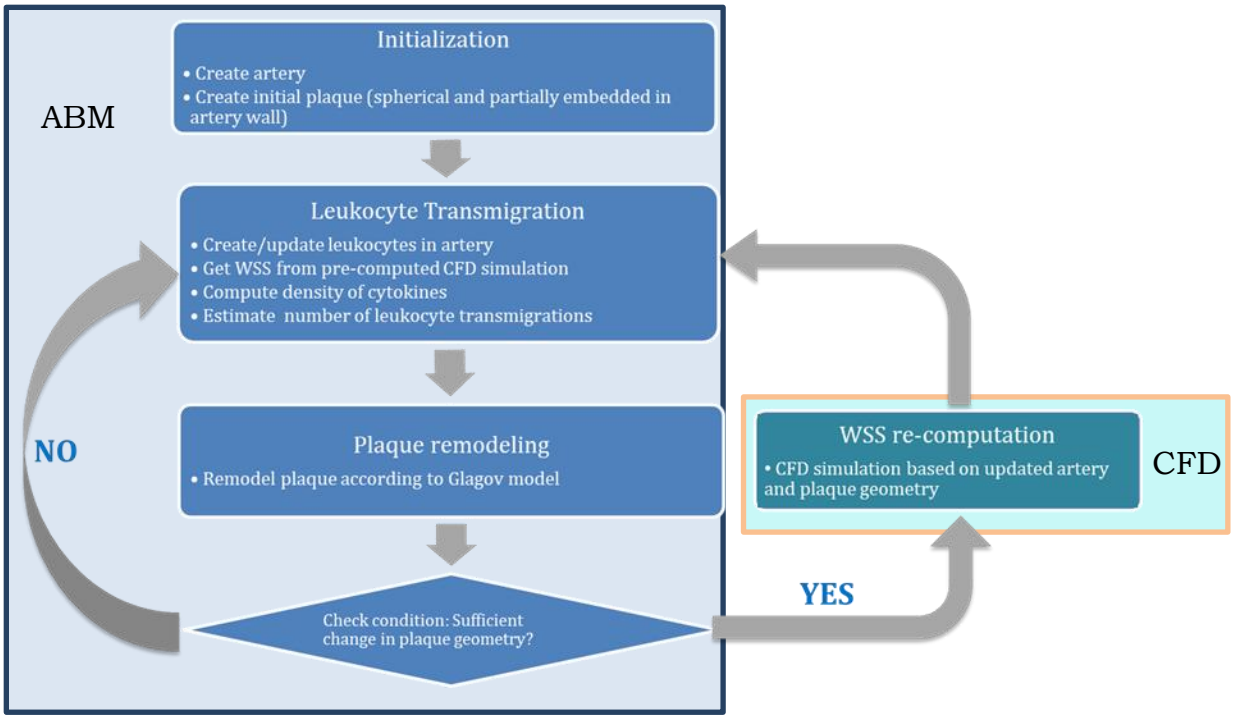

Figure 4.9 Flow chart of the handshaking between two modeling tools: After setting up the artery with a small plaque embedded in the wall and leukocytes in the lumen, leukocytes transmigrated according to rules, described before at each tick. The plaque area was then calculated for each segment and compared with corresponding lumen area. The artery then remodels following Glagov phenomenon. Once the plaque enters lumen, CFD simulation was done and updated ABM with new WSS.

Transferring geometry from ABM to CFD

The luminal surface of the artery, according to ABM, is passed to COMSOL. Specifically, a text file containing the position of each EC, at the centroid of cubical patches, is first passed to MATLAB (R2016a). A MATLAB routine then reconstructs the inner layer by sorting all the x and y points in the azimuthal direction for each z-plane and smooths the shape by first taking the average of two consecutive x, y points in the azimuthal direction and then applying the built-in smooth function in MATLAB (**Figure 4.10**), and finally creates a surface mesh stereolithographic (STL) file. The STL file is then imported in COMSOL.

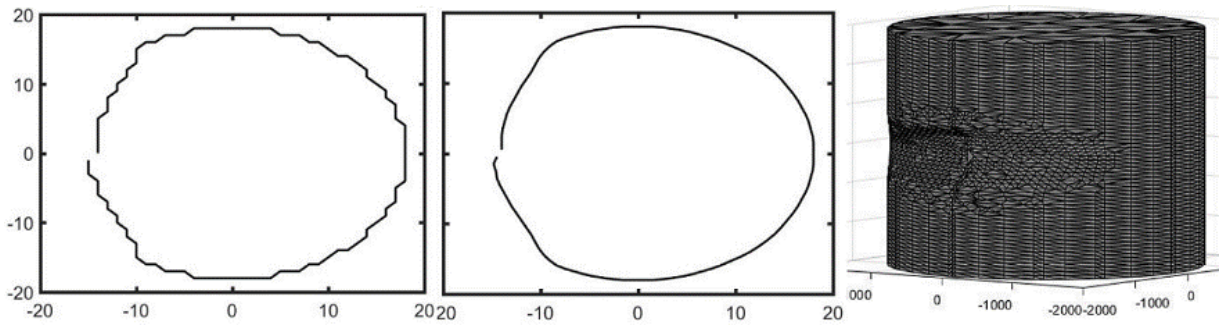

Figure 4.10 Inner layer data from ABM: Left: Cross section of the lumen. Since agents in ABM are at centroid of patches, the inner layer is a saw-toothed line. Middle: Smooth surface of the inner layer. Right: STL file generated in MATLAB

Transferring WSS from CFD to ABM

As before, the WSS of the artery also should be formatted to be usable in the AMB model. A text file is created containing the WSS distribution throughout the whole inner surface points of the artery with appropriate resolution. A matlab function is then used to interpolate the WSS at the specific X, Y, and Z centroid patch locations determined previously. This WSS information is then imported into the ABM.

Confidence of the model

Verifying model stability

To assess homeostatic stability the ABM was run under normal conditions (healthy blood flow with normal WSS i.e. 1.4 Pa and no endothelial activation) for a week. There is not any leukocyte adhesion or TEM, as expected (**Figure 4.11**A). In reality, your blood pressure may temporarily fall, for example when sleeping. These temporary spikes should not lead to atherosclerosis. To check this, we simulated temporary spikes of low WSS (35% lower than normal) at every 10 hour for a week. These spikes did not affect leukocyte TEM or lead to plaque development (**Figure 4.11** B).

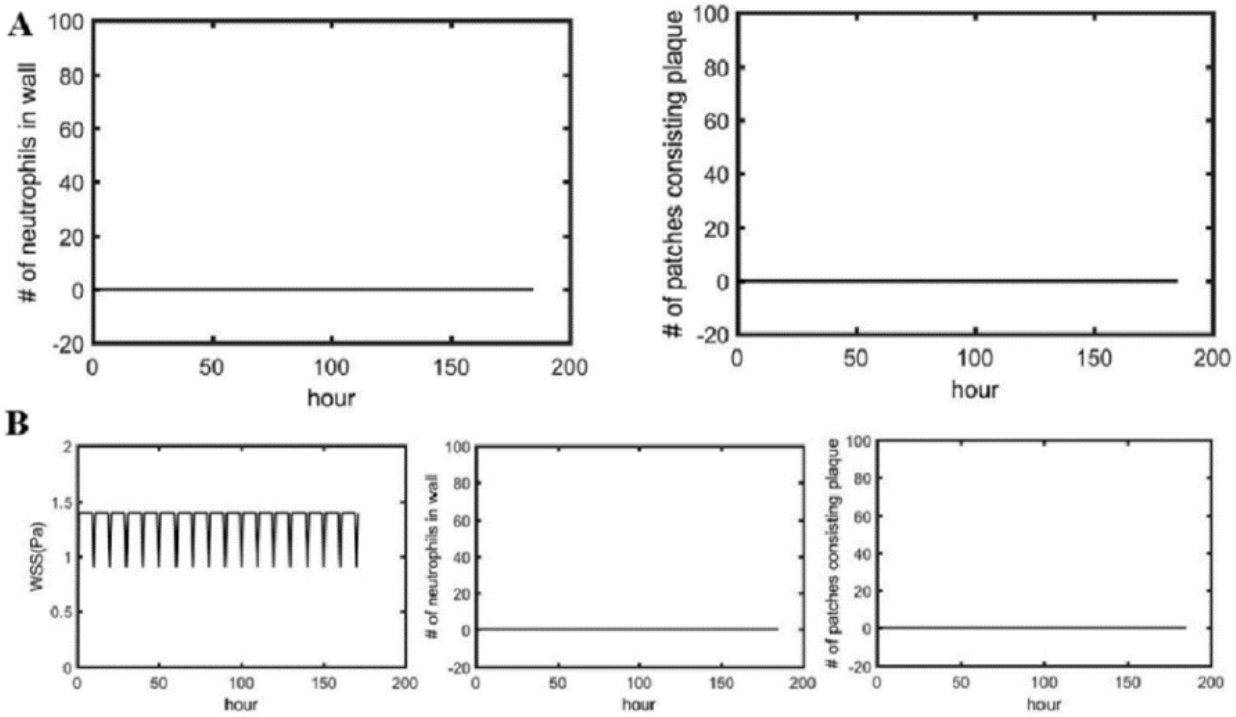

Figure 4.11 ABM ensures homeostatic and stability under temporary spikes: (A) the model is run with normal WSS (1.4 Pa) and inactivated endothelium. As expected no transmigration (left) as well as no plaque growth (right) is overserved. (B) An example result of the model under temporary spike of WSS. WSS is lowered to 0.9 Pa (left) periodically at each 10 hour. The artery adapts this temporary change of WSS resulting no transmigration (middle) and hence no plaque growth (right).

Verification of spatial WSS distribution and leukocyte TEM are correct

Leukocyte TEM and WSS are inversely proportional. To confirm we observe what we expect/programed, we plotted WSS (from CFD) with the spatial positions of leukocyte TEM at the lowest flow rate (33% of cardiac cycle) and the highest flow rate (6% of cardiac cycle). As expected, transmigration was highest and distributed over the plaque evenly under low flow conditions. Conversely, under higher flow conditions the WSS was high and the level of transmigration was low. **Figure 4.12** illustrates the WSS distribution over a stenosis with overlaid transmigration positions (red dots), as obtained from the ABM.

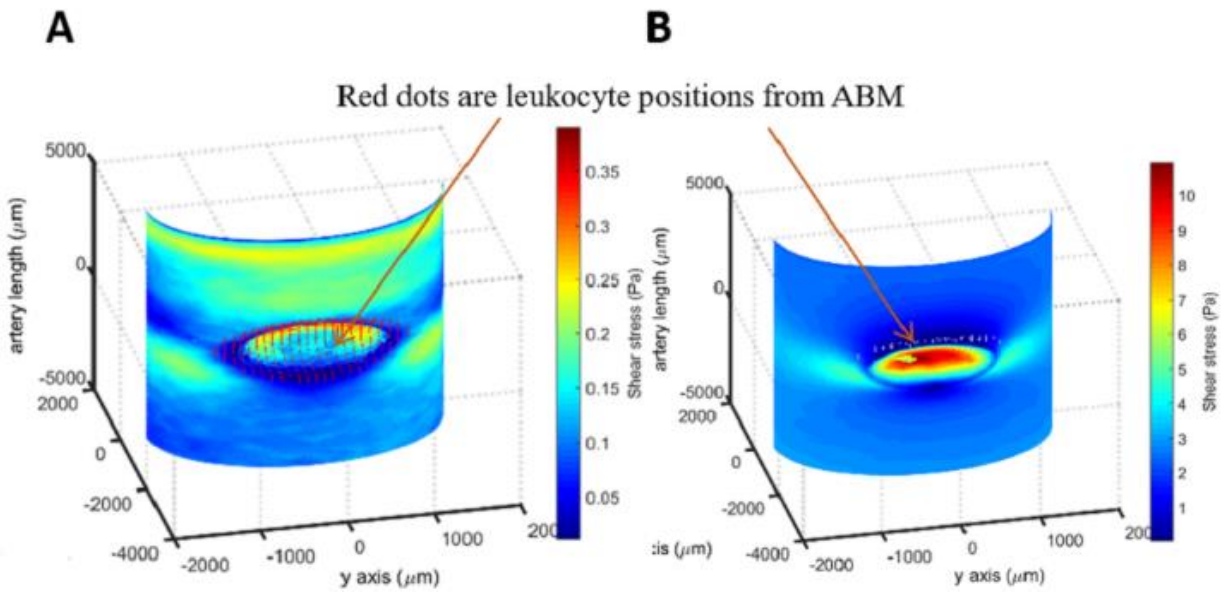

Figure 4.12 Comparing WSS and transmigration position: Contour plots represent overlaid WSS (from CFD) and transmigration positions (form ABM). The endothelium is activated only adjacent to the plaque. A) At 33% of cardiac cycle the blood flow is very small (Fig. 3.10A) and so the WSS is also very small throughout whole artery. Hence leukocyte (generated only near plaque) transmigration occurs from almost everywhere (red dots). B) Likewise at 6% of cardiac cycle blood flow is very high and so the WSS. Hence few leukocytes transmigrated. Note color scale magnitude is different for A) and B).

Discussion

In this chapter we presented a coupled ABM-CFD model. ABM considers biological events such as diffusion, endothelium activation, cell adhesion, TEM, chemotactic driven migration, cell apoptosis, differentiation and foam cell formation. We identified the primary factors affecting leukocyte adhesion and plaque progression and defined a set of rules to program into ABM. ABM captures compensatory arterial growth and remodeling following Glagov's phenomenon. Once the plaque starts growing into the lumen, the inner geometry at each endothelial cell was passed to COMSOL to preform CFD analysis. CFD updates and passes the

spatial WSS values into the rules of ABM controling leukocyte TEM.We have shown that the ABM and CFD are able to successfully handshake information. This integrated model shows stability under homeostasis and temporary spike conditions. Verification of the model handshaking was completed by observing the positions of leukocyte adhesion positions under low and high flow. Indeed the areas of low WSS correlated with leukocyte adhesion.

Obviously, leukocyte transmigration is dependent on the flow rate of blood (**Figure 4.8**); due to the pulsatility of blood, within one cardiac the likelihood of leukocyte transmigration varies. However, updating WSS at each fraction of cardiac cycle requires a lot of handshaking between two models and making this option a challenge as it would take years to simulate the complete model of atherosclerosis. In the next chapter we will introduce an effective way of including the pulsatile nature of blood flow in the model.

CHAPTER 5

EFFECTIVE CONSIDERATION OF PULSITILE HEMODYNAMICS AND ATHEROGENESIS MODEL

Overview

Since blood flow is pulsatile in nature, WSS, the rate of leukocyte adhesion, and trans-endothelial migration change throughout the cardiac cycle. Using direct numerical simulation (DNS) techniques to model pulsatile flow of incompressible and Newtonian blood through an artery (performed by Dr. Leonardi's group), we found that leukocyte adhesion from either mean flow or instantaneous flow give significantly different results. On further investigation, we found that passing WSS at peak systole results in a representative number of leukocyte TEM compare to pulsatile flow whereas using fully developed steady blood flow does not. Moreover, using the model, we have found leukocyte TEM increases monotonically with decreases in luminal volume. At some plaque shapes the WSS changes rapidly resulting in sudden increases in leukocyte TEM. Moreover, the model was able to capture which leukocyte types are predominate at different phases of plaque growth; specifically neutrophils are predominate in the beginning and when the plaque starts blocking blood flow. Together these results give us insight, at a cellular level as to the evolution of atherosclerotic plaque growth.

Introduction:

Blood flow through artery is pulsatile in nature and so the WSS. Since leukocyte adhesion depends on WSS, the adhesion also changes with time over a cardiac cycle. Therefore, one may wonder, how can the pulsatility of the blood flow be captured in the ABM? One way of answering this question is to simulate the events exactly the way it is happening, that means

updating the WSS at every fraction of cardiac cycle (0.8s) for example 0.01s. However, to simulate a very long process like atherogenesis, which occurs over the span of years, in increments of 0.01s time steps is not feasible (with our current processor speeds). A compromise will be to use a constant WSS corresponding to average flow rate but that would not be physiological, as it would not capture low WSS, which is mainly responsible for transmigration.

To confirm the time-dependent nature pulsatile flow has on leukocyte adhesion, Dr. Leonardi's group implemented a direct numerical simulation (DNS) of pulsatile flow for an incompressible, Newtonian blood flow model. WSS computed from the DNS was coupled with a leukocyte transmigration model and compared the total value of leukocyte transmigration with time-averaged and instantaneous flow. It was found that the leukocyte transmigration from mean flow and instantaneous flow are significantly different. Therefore, an appropriate time interval at which WSS would be passed from CFD to ABM is needed in order to emulate pulsatile flow.

Method:

Comparing effect of average flow rate and instantaneous flow rate on leukocyte transmigration (DNS)

Numerical Method

DNS is a simulation in CFD in which the Navier-Stokes equations are numerically solved. The flow in stenotic coronary artery was investigated using DNS. The in-house DNS code was developed by Dr. Leonardi's group. The Navier-Stokes equations for a Newtonian incompressible fluid are assumed as the governing equations.

$$\nabla . u = 0 \qquad (1)$$

$$\frac{\partial u}{\partial t} + (u . \nabla)u = -\frac{1}{\rho}\nabla p + \vartheta \nabla^2 u \qquad (2)$$

Here, u is the velocity vector, p the pressure, ρ= 1060 kg/m^3, ν = 3.3 x 10^{-6} m^2 /s is the blood density and is the blood kinematic viscosity and t is time. The incoming velocity profile is assumed to be axisymmetric and parabolic.

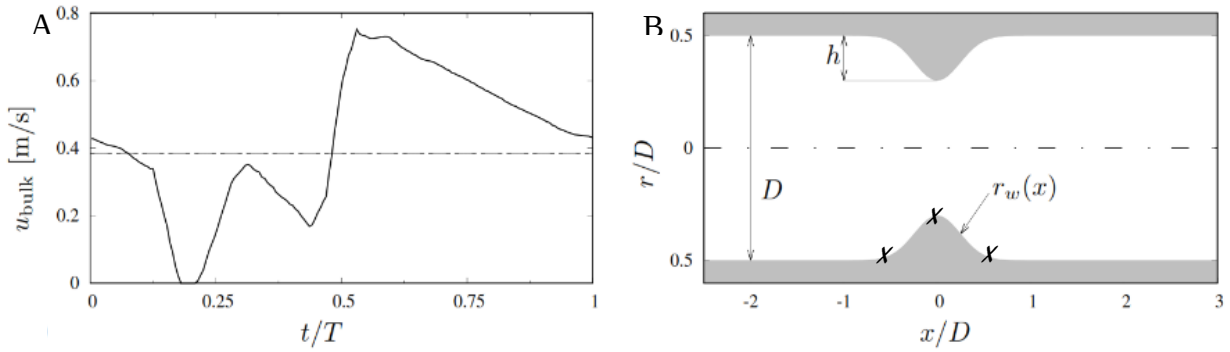

Figure 5.1 Flow rate and geometry used for DNS: (A) solid line represents the instantaneous bulk velocity and dashed line represent mean velocity (u_{mean} = 0.384 m/s) (B) Geometry of stenosis, used in DNS. 'X' are the positions (at MLA, 1.615 mm upstream and 1.615 mm downstream from MLA) where the velocities are compared with COMSOL.

The artery was considered as a rigid circular cylinder of diameter D = 2.9 mm (**Figure 5.1**). Height of the stenosis is h, x is the streamwise distance from minimum lumen area (MLA) and r is the radial distance.

Verification of the in-house code by COMSOL

Previously, the code was extensively validated in cases of flow over rough surfaces (Orlandi et al, 2006; Burattini et al., 2008). Herein, to validate the code further the same simulations were performed using a commercial software, COMSOL. Simulations with COMSOL are two-dimensional and axisymmetric to save computational time. On the other hand, the use of our in-house code runs fasters, and allows us to calculate the WSS and transmigration instantaneously. The results from the fully three-dimensional Direct Numerical Simulation (DNS), averaged along the azimuthal direction ϑ, are consistent with COMSOL and to reproduce

the overall effect of the stenosis. In fact, because of the regular geometry of the configuration in this study, the flow properties are homogeneous in the azimuthal direction. In the following sections u = u(x, r, t) indicates such azimuthally-averaged velocity, and is simply referred to as the "instantaneous" velocity. The mean velocity is obtained from the time-average of u over the cardiac cycle and is denoted as u(x, r). An analogous notation is applied to the other variables.

Leukocyte adhesion at different instant of cardiac cycle

Previously, we quantified leukocyte adhesion as a function of WSS (Table 4.2, rule3, 6, 9). Using the instantaneous WSS, predicted from in-house code, neutrophil adhesion was computed at four instants during cardiac cycle. The mean rate of adhesion, using time-averaged flow over the complete period of cardiac cycle was also computed and compared with that of instantaneous flow.

Determination of the optimal timescale to pass WSS into the ABM

To determine the actual leukocyte transmigration over one cardiac cycle, WSS was computed using pulsatile flow over two spherical plaques (one of radius 1.0 mm and other 1.5 mm) and saved at each 0.01 sec interval for each lumen patch location. The average number of leukocyte TEM over one full cardiac cycle can then be determined. Then we identified a representative time point, within the cardiac cycle, which would give us the same number of leukocyte transmigration as if we used instantaneous flow profiles. This value is compared to steady flow, and used to determine the appropriate flow rate that will generate approximately the same total leukocyte transmigration over a cardiac cycle. Future simulations pass the WSS calculated at this time point within the cardiac cycle.

Determining rate of leukocyte TEM

To quickly grow a large plaque in order to determine how many leukocytes enter the artery wall as a function of WSS and plaque shape, we have used an accelerated G&R version of ABM. This accelerated version of the ABM considers only 4%, instead of 40%, of the patch is available for leukocytes. This will accelerate the growth rate because the patches will fill up faster requiring the generation of new patches. Now, after a change in internal geometry, i.e. change in number of luminal patches, the ABM was paused, CFD is performed with the current geometry, and WSS was updated into ABM and ABM restarted. This method was used starting with three spherical plaques of different severity, small (0-5% stenosis), medium (5-20% stenosis) and big (20-35% stenosis) and the leukocyte transmigration was measured as a function of only WSS (i.e. cytokine concentration was held constant at 25 ng/mL of TNFα).

Results

Results from DNS

Comsol results are in good agreement with the results from DNS

Figure 5.2 compares the results of the DNS with velocity profiles obtained using the commercial software COMSOL. The profiles were sampled at four equally spaced instants of the cardiac cycle 1.615 mm upstream the MLA (**Figure 5.2**, top), at the MLA (**Figure 5.2**, middle), and 1.615 mm downstream the MLA (**Figure 5.2**, bottom). A quantitative measure of the difference between the two CFD solvers is provided in Table 5.1.

The normalized mean square error (NMSE) is defined as:

$$NMSE(x,t) = \frac{< (u_{COMSOL} - u_{DNS})^2 >_r}{< u_{COMSOL} >_r . < u_{DNS} >_r}$$

Where $<.>_r$ indicates an average along the radial direction.

Table 5.1 Statistical measured of the difference between COMSOL and the present DNS

X[mm]	NMSE[%]				Average NMSE[%]
	t/T = 0	t/T = 1/4	t/T = 1/2	t/T = 3/4	
-1.615	0.096	1.522	1.432	0.046	0.663
0	0.020	1.710	0.918	0.020	0.453
1.615	0.043	3.344	1.683	0.074	0.851

Overall, the agreement was quite good. The maximum NMSE between the two simulations is about 3% downstream the MLA at t = T/4; otherwise the error is lower than 2%. Note that the error is relative to the instantaneous mean velocity in the lumen. At t = T/4 the incoming flow rate is near the minimum (**Figure 5.2**) and the instantaneous mean velocity is quite low.

In absolute terms, the maximum NMSE corresponds to a difference of 0.07 m/s between COMSOL and in-house code (Table 5.1). The absolute maximum difference is about 0.2 m/s downstream the MLA at t = T/2 (**Figure 5.2**, bottom, c).

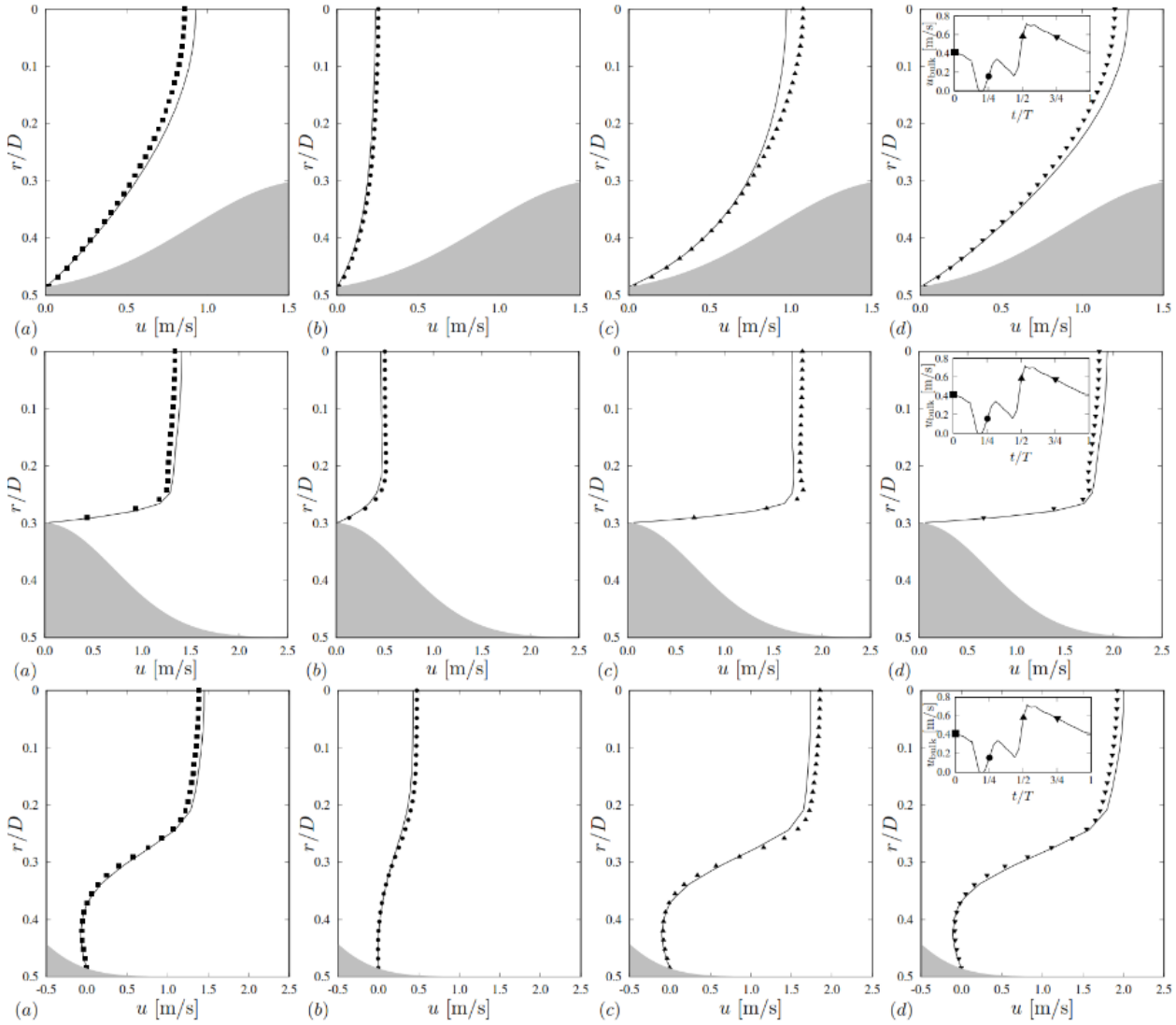

Figure 5.2 Comparison of velocity profiles, simulated using DNS and COMSOL, at different instant of cardiac cycle: From top to bottom: velocity profiles at 1.615 mm upstream from MLA, at MLA and 1.615 mm downstream from MLA at different instant during the cardiac cycle: ((a) t/T = 0; (b) t/T = 1/4; (c) t/T = 1/2; (d) t/T = 3/4). Line represents the COMSOL simulation, and symbols represent in-house code calculations.

Leukocyte adhesion depends on instantaneous flow of cardiac cycle

The instantaneous flow over a cardiac cycle has a significant influence on leukocyte adhesion. **Figure 5.3** shows that the rate of adhesion computed from the mean stress (shown as a solid black line) is considerably different from leukocyte adhesion computed from instantaneous

WSS. Hence, there is a need to find the time interval of cardiac cycle to pass WSS from CFD to ABM.

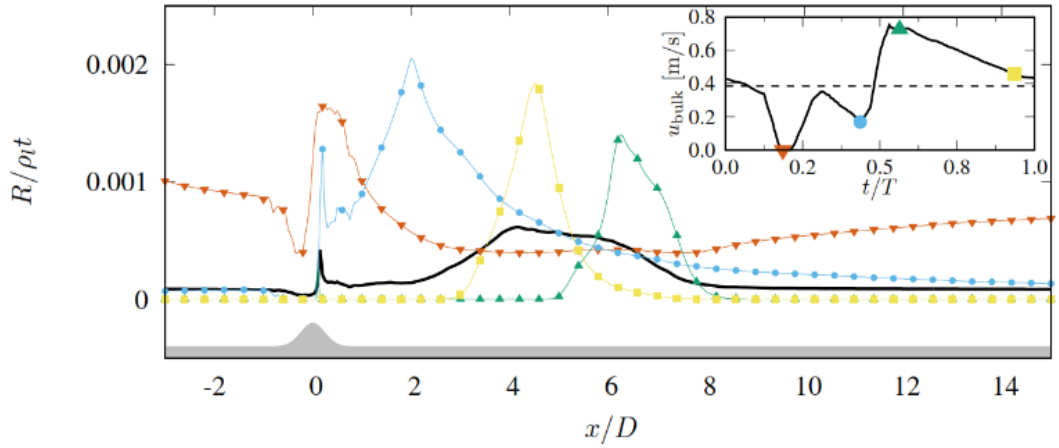

Figure 5.3 Comparing rate of neutrophil adhesion with instantaneous WSS and average WSS: Line plot represents the rate of neutrophil adhesion with time averaged WSS value and symbol represent rate of neutrophil adhesion at different instant of cardiac cycle: at t/T = 0, at t/T = ¼, at t/T = ½ and at t/T = ¾

Capturing instantaneous WSS effects in the ABM

We observed that over an entire cardiac cycle, the average number of leukocytes undergoing TEM per hour was 16 in an artery with a spherical plaque of radius of 1mm or 26 for a 1.5mm plaque (**Figure 5.4** B, C). These numbers correspond to the flow rate at the peak coronary flow during systole, i.e., between the opening and closing of the aortic valve. In contrast, with an input of mean steady flow, an average of only 7 leukocytes transmigrated into the wall after 1 hour. Thus, a steady flow profile was inadequate in capturing the full effect of leukocyte transmigration. However, a judicious choice from the pulsatile flow case can provide a computationally tractable alternative. This simplifying assumption for handshaking between the

ABM and CFD generated approximately the same total leukocyte transmigration as if we include the complete pulsatile flow history.

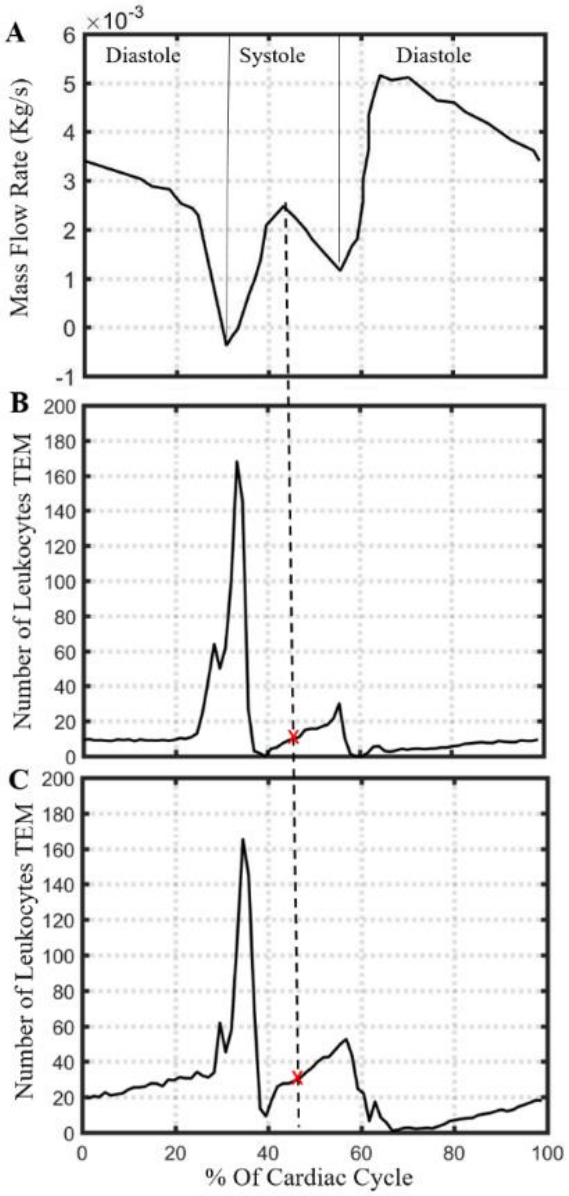

Figure 5.4 Representative cardiac cycle to pass spatial WSS profile into ABM: (A) Coronary blood flow rate profile used in CFD according to [19]. Number of leukocytes undergoing TEM in 1 hour using instantaneous pulsatile flow over a spherical plaque with radius (B) 1.0 mm or (C) 1.5 mm. The average number leukocyte TEM per hour, over one cardiac cycle, is 16 for (B) and 26 for (C). The WSS profile at peak flow during systole corresponds to these average TEM values, as indicated by the dashed line and red '*x*' marks

Rate of leukocyte TEM for accelerated model

Leukocyte transmigration was found during the G&R process of the accelerated model with spherical plaques (see methods). Using these accelerated models, we observed leukocyte TEM over a given change in luminal volume. After a change in luminal patches of around 80, 35 and 10 for small (**Figure 5.5** A), medium (**Figure 5.5** B) and big plaques (**Figure 5.5** C) respectively, the number of leukocytes transmigrating changes significantly. Overall, the rate of leukocyte transmigration increased with increase in stenotic severity.

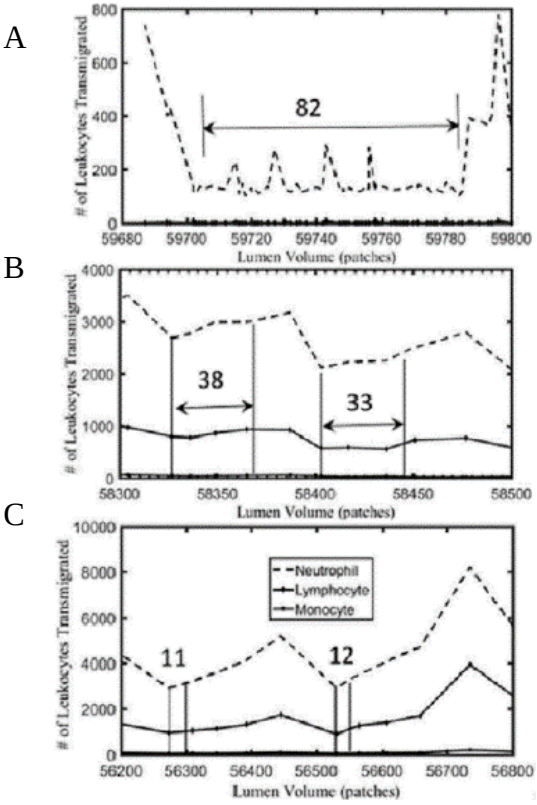

Figure 5.5 Frequency of updating WSS: WSS was updated at each change of geometry (lumen patch) and corresponding leukocyte TEM is obtained from ABM. It is found that for small (A), medium (B) and big (C) spherical plaques, up to change of lumen patches of 80, 35, 10, respectively. TEM is almost constant. Hence, WSS update is necessary after change of 80, 35, and 10, respectively.

Leukocyte TEM increases with the level of stenosis

To confirm the rate of leukocyte TEM pattern, found using spherical plaques, we updated the WSS at each change in luminal patch in a non-accelerated model where TEM is a function of WSS as well as endothelial activation. Leukocyte TEM increased monotonically as the plaque

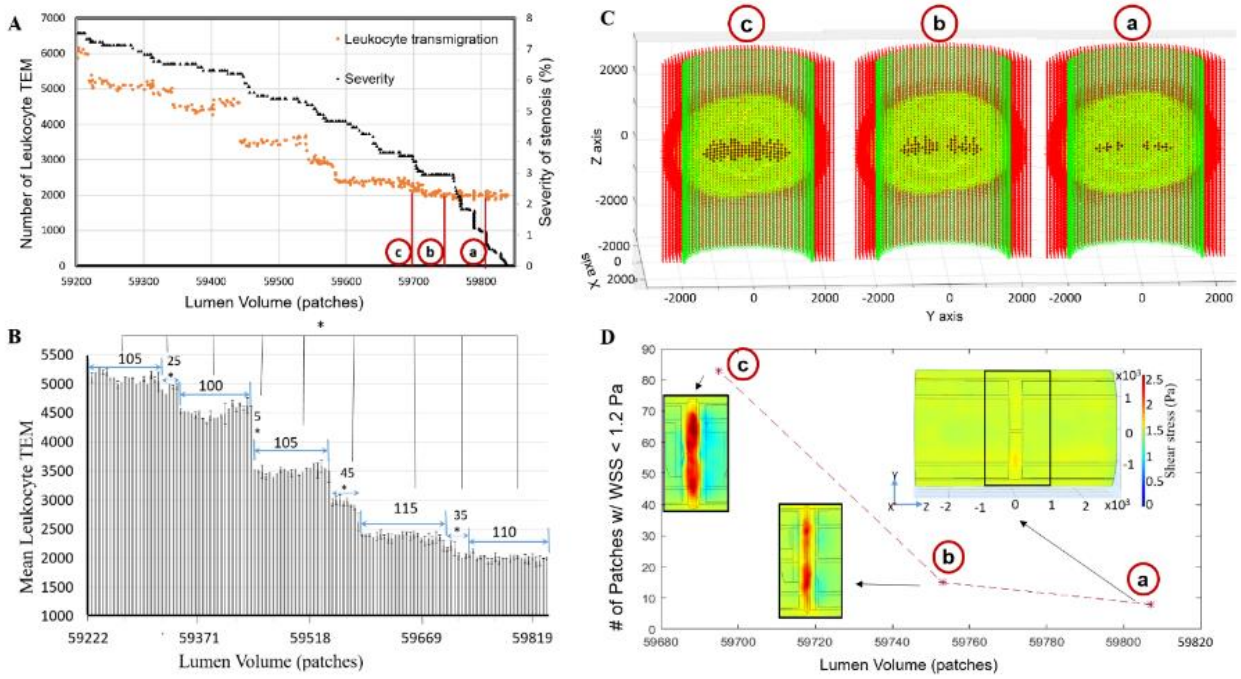

Figure 5.6 When the degree of stenosis was below 8%, the level of leukocyte TEM was constant over an average change in lumen volume of 107±5 patches, followed by a rapid increase in TEM over the next 28±17 patches: (A) Scatter plot displaying leukocyte TEM and severity of stenosis as a function of luminal volume (patches). (B) Bar plot indicating the change in lumen volume after which a significant increase in leukocyte TEM was observed. (Mean ± SD, *p < 0.05). (C) Longitudinal cross sections of the ABM at 'a', 'b', and 'c' points from 5A, illustrating where the initial inward growth occurred. ACs, ECs, and leukocytes in the plaque are indicated in red, green and yellow, respectively. Black represents the new ECs added in the lumen. Inlet flow is at the bottom of each subfigure. (D) Subplot showing the number of patches (from ABM) with WSS < 1.2 Pa at specific plaque shapes (i.e., lumen volumes) corresponding to 'a', 'b', and 'c' points from 5A. Overlaid color contour plots of the WSS (from CFD) over the plaque at each point. The number of patches of low WSS (blue region) are almost constant (13 and 15 respectively) corresponding to nearly constant TEM. Then, the number of patches having low WSS increases (83) as does TEM. Inlet flow is at the left of each subfigure in (D).

grew into the lumen over time (**Figure 5.6** A). Initially, we created spherical plaques, varying in severity of stenosis, into an accelerated version of the ABM and monitored leukocyte TEM and plaque growth. Interestingly, we observed the rate of leukocyte TEM was not constant as the plaque grows, that only a few leukocytes transmigrated followed by a significant increase in leukocyte TEM. These increases occurred after luminal changes of 80, 35 and 10 patches (lumen volume corresponds to number of patches in the lumen) when the severity of stenosis was between 0-5%, 5-20%, and 20-35%, respectively (**Figure 5.5**). When plaque severity was below 8%, our non-accelerated ABM predicted significant increases in leukocyte TEM after growing by 100 to 115 (average ± standard deviation 107 ± 5, n = 5) patches into the lumen (**Figure 5.6**, $p < 0.05$). Together, these results corroborated that during initial plaque growth (i.e., level of stenosis < 8%) the plaque will grow inside of the lumen by at least 80 patches or 0.08 mm^3 before a significant increase in leukocyte TEM was observed. **Figure 5.6** B illustrates between two constant zones (few leukocytes performing TEM) there was a "transition zone" of about 28 patches where the rate of TEM increases significantly. Next we used the ABM to better understand what spatiotemporal conditions lead to these transition zones.

Variations in WSS has a greater influence on leukocyte TEM, as compared to cytokines. **Figure 5.6** C, D highlight two representative plaques undergoing similar levels of leukocyte transmigration (points a and b) and one representative plaque experiencing significantly higher rates of leukocyte TEM (point c). At these three time points, the endothelial patches with the highest cytokine concentration (1.6 ± 0.06 ng/ml TNF, 0.18 ± 0.01 ng/ml IL-1) were near the minimal luminal area (MLA) or maximum stenosis. WSS was also the highest (> 2 Pa) at the maximum stenosis and lowest (< 1.2 Pa) in the distal and proximal zones. However, leukocyte

adhesion due to low WSS was almost 10 times higher than due to the highest cytokine concentration. Hence, most of the leukocyte TEM occurred in the distal zone of the plaque where the WSS was favorable for TEM (i.e. < 1.2 Pa, **Figure 5.6** D). For example, when the lumen volume was 59807, 59753 and 59695 the number of endothelial patches with favorable low WSS were 8, 15 and 83 respectively. Hence, leukocyte TEM was nearly constant with a luminal geometry of the first two points, after which TEM increased significantly (transition zone) (**Figure 5.6** D). More leukocytes entering the artery wall caused the plaque to grow or expand inwardly. Figure 5C illustrates the locations where the plaque start to protrude into the lumen during the constant zone (points a and b) and at the higher TEM zone (point c).

Model of atherogenesis reveals spatiotemporal growth and remodeling

Figure 5.7 illustrates the ABMs ability to capture growth and remodeling of the LAD coronary after an initial insult of 15 leukocytes placed in the middle of the arterial wall (**Figure 5.7** A). Cytokines generated by these leukocytes activated local endothelial cells leading to leukocyte adherence and TEM. Once in the wall, the leukocytes migrate, differentiate, undergo apoptosis, phagocytosis and synthesize proteins based their behavior rules and environmental conditions. The sum of these events resulted in outward arterial remodeling until the plaque area was 40% of lumen area (**Figure 5.7** B). As expected, acutely neutrophils were the predominate leukocyte cell type in the wall (**Figure 5.8**). After 60 days of growth monocytes and monocyte-derived cells became the majority. Once the plaque started growing predominately inward, at select z-planes (**Figure 5.7** B), altered blood flow gave rise to lower WSS in the distal regions as compared to the maximal lumen stenosis (**Figure 4.12**). Interestingly, the ratio of neutrophils

within the plaque began to increase again (**Figure 5.8**). After about a month of inward growth the ratio of lymphocytes within the artery increased. Together, once the plaque starts to stenosis the lumen volume, the increase in leukocyte adhesion results in accelerated plaque growth (**Figure 5.7** C).

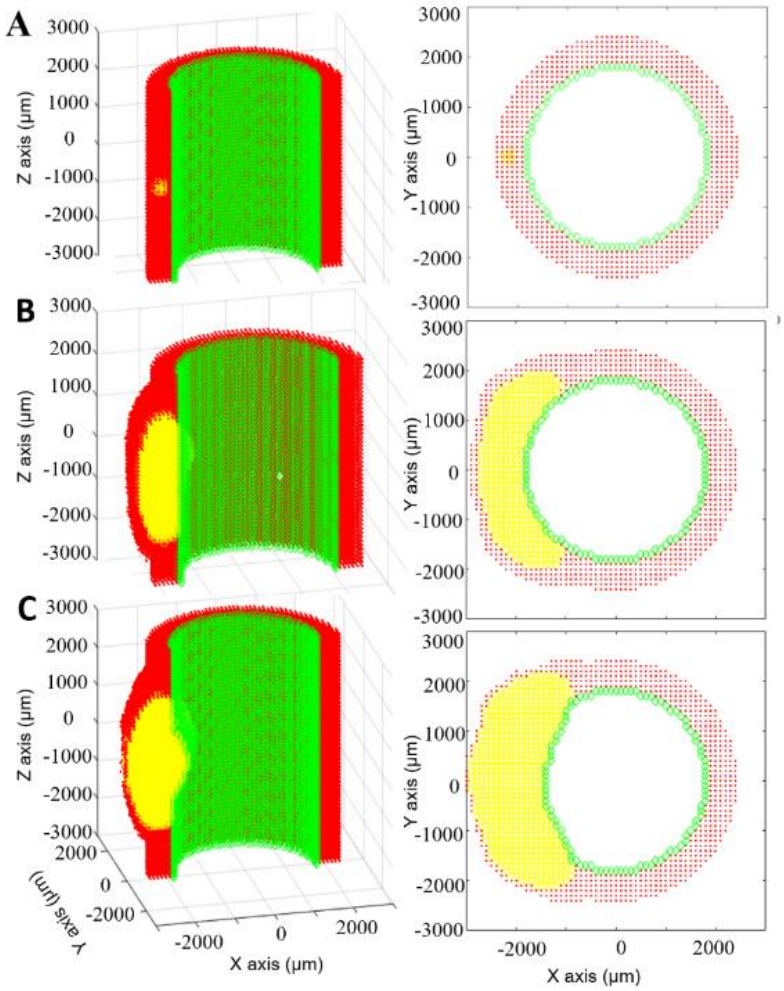

Figure 5.7 Eccentric plaque growth and remodeling prediction: Longitudinal (left) and corresponding transverse (right) views of an evolving artery where ECs, ACs and leukocytes are represented by green, red and yellow respectively. A) Initially the artery is impregnated with 15 leukocytes. B) At 6 months the plaque area is 40% of the lumen area and will start growing inside lumen according to Glagov's phenomenon. C) At 7 months the plaque has grown inward and outward, changing the luminal geometry.

Model sensitivity and stochasticity

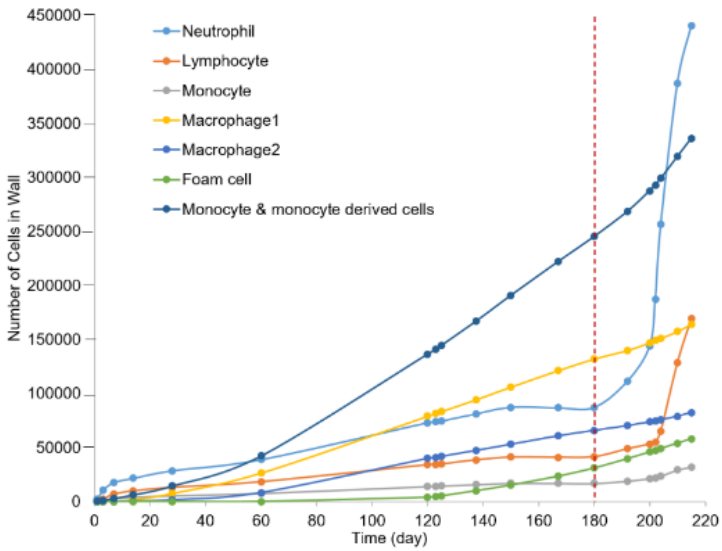

Figure 5.8 Different types of leukocytes present in the plaque as it evolves: Before the plaque reduces the caliber of the lumen, as indicated by the vertical dashed red line, TEM is only due to endothelial activation by cytokines. Initially neutrophils constitute the majority of the plaque volume, followed by monocytes and monocyte-derived cells and then neutrophils again. When the plaque starts growing inside the lumen (vertical dashed line) leukocyte TEM is largely influenced by blood flow. With time the severity of stenosis increases and so does the region of low WSS. Therefore, the rate of leukocyte TEM is greater for all cells. Among these cells, the concentration of neutrophils (62%) in blood is higher than monocytes and lymphocytes (5.3% and 30% respectively). Also neutrophils adhere on the EC surface with WSS < 1.2 Pa whereas the monocytes and lymphocytes adhere with WSS < 1 Pa and < 0.4 Pa respectively. Thus there is a rapid increase of neutrophils immediately after 6 months whereas the rate for lymphocyte increases after several days when the plaque is bigger and WSS < 0.4 Pa.

Neutrophil adhesion is more dependent on IL-1β than TNF-α. According to Bahra et al. [9] and Breviario et al. [87] when the concentrations of IL-1β and TNF-α are low (< 1 U/mL), neutrophil adhesions is primarily due to IL-1β, whereas if the concentrations of both are high (> 1 U/mL) the reverse is true (**Figure 5.9** B). From the model we found that the highest concentration of either IL-1β or TNF-α in an endothelial patch over a 50 day simulation is below

0.04 U/mL (**Figure 5.9** A). That is the probability of neutrophil adhesion due to the maximal concentration of IL-1β in an endothelial patch is 24.7%, whereas the probability of adhesion due to the maximal concentration of TNF-α is only 0.3%. Indeed, even after 7 months the maximum value of IL-1β and TNF- α concentration on an endothelial patch are 0.006 U/ml and 0.07 U/ml, respectively; this means the probability of adhesion is still influenced more by IL-1β than TNF-α (25.3% and 0.8%, respectively). Similarly, the probability of adhesion of monocytes and lymphocytes (according to rules 4, 5, 7, 8) is greater for the predicted endothelial concentrations of IL-1β than for the predicted endothelial concentrations of TNF- α (data not shown).

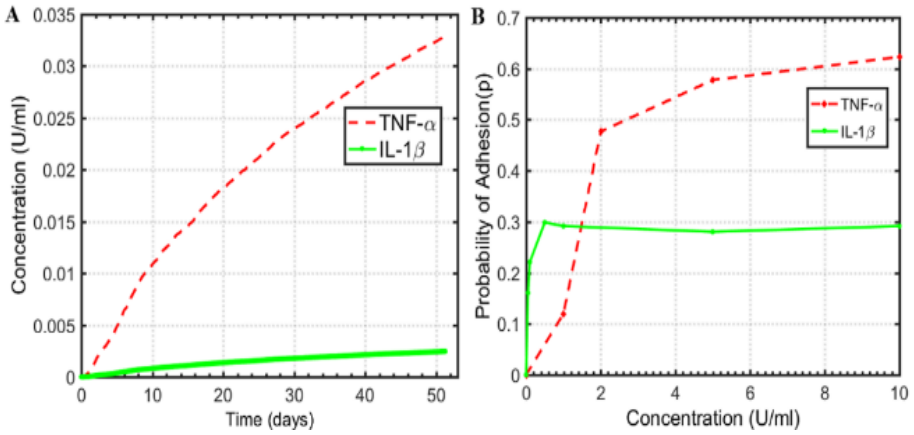

Figure 5.9 ABM-CFD model is more sensitivity to IL-1β than TNF-α: A) Represents the highest concentration of IL-1β or TNF-α in an EC patch over a 50 day ABM-CFD simulation. The concentration is < 0.04U/ml during the entire simulation. B) Shows the ABM rules for probability of neutrophil adhesion as a function of TNF-α and IL-1β concentration. Therefore, over a 50 day simulation, neutrophil adhesion is primarily due to IL-1β.

Prior to stenosis, the model exhibits little run-to-run variation. To determine the stochasticity of the model, we repeated the simulation three times. **Figure 5.10** shows average number (from three simulations) of different cell types in the wall and the shaded region shows the standard deviations.

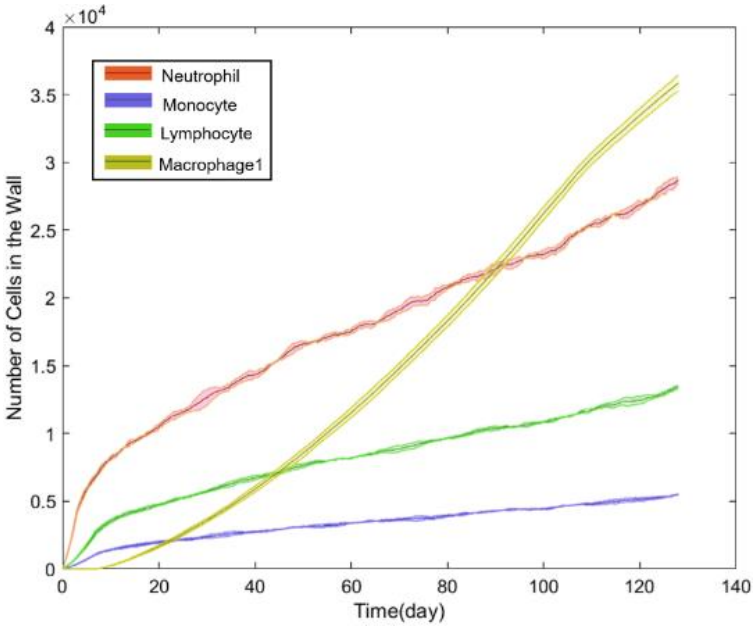

Figure 5.10 ABM-CFD model exhibits minimal stochasticity in regards to the predicted number of cells in the wall with time: The figure represents the average number of each leukocyte in the artery wall over a 130 day simulation. Shaded areas represent the standard deviation from three repetitions. The standard deviation is never above 220 in all cases. Indicating minimal stochasticity in the model despite having probabilistic functions.

Tissue-level validation of the model with an experimental study

Predicted plaque area with time was compared to that observed in a pig model of atherogenesis. Pigs are good experimental models for atherosclerosis since the coronary hemodynamics and atherosclerotic lesion morphology in the pig heart closely resembles those seen in the human heart [100-102]. Pelosi et al. [103] studied atherogenesis in the coronary of pigs at 0, 2, and 4 months of high cholesterol diet. They measured mean lesion area of 4-5 cross sections, each separated by 0.5 mm. The ABM initially mimicked the conditions of the experimental pig model in regards to wall composition, blood hematocrit and 30% increase in LDL at day 0. The model simulated 4 months, and the mean lesion area was determined using 5

cross sections, 0.5 mm apart and centered about the middle of the plaque. The results (**Figure 5.11**) were similar to the plaque growth seen in the pigs. Thus, simulated results corroborated the experimental porcine model at the tissue-level.

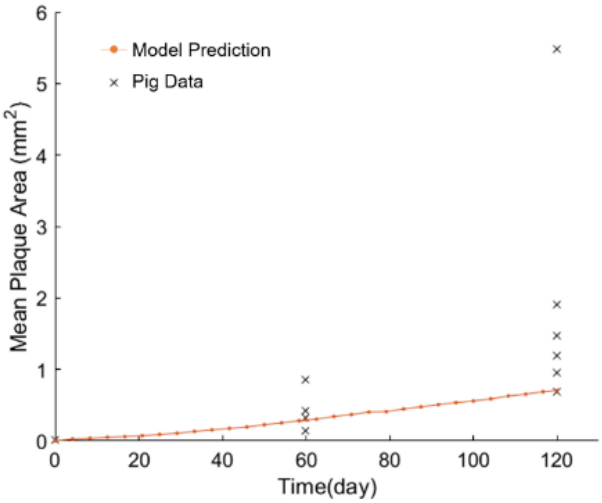

Figure 5.11 ABM-CFD predictions corroborate an experimental porcine model of atherogenesis: 'x' represents mean plaque area from individual pigs, fed high cholesterol diet. '.-'represents predicted plaque area as a result of a 30% increase in LDLs.

Discussion

Herein we present a novel way to predict leukocyte TEM and overall G&R of a LAD coronary artery during atherogenesis. We developed an ABM to capture the spatiotemporal effects of hemodynamics on leukocyte adhesion, transmigration and plaque formation. Previously, a 2D ABM was employed to study vascular remodeling due to a focal stenosis (via ligation) in a rabbit vein graft model [104]. In the study, the exerimental model and their 2D ABM predicted significant intimal thickening, mostly via smooth muscle cell proliferation and extracellular matrix production, in low WSS zones distal to the stenosis. Likewise, our 3D ABM predicted increased wall thickening in low WSS zones. Yet the increased thickness was due to an increase in extremal mass (i.e. leukocyte infiltration) rather than cell proliferation. Moreover, we

present an ABM-CFD modeling approach that accounts for instantaneous fluctuations in WSS throughout the cardiac cycle, as well as updates the WSS after significant changes in geometry, as opposed to updating the WSS at an arbitrary frequency. In the next generation of the presented ABM-CFD model we plan to add new rules related to behaviors of residual artery wall cells and ECM properties to tease out the influence they have on plaque development. Recently, Olivares et al. used ABM to parametrically identify oxLDL, out of other parameters such as cell migration, statins and auto-antibodies, as the most influential factor in macrophage to foam cell transition during early atherosclerosis [105]. However, being chiefly a parametric study, they did not include important interconnected events such as hemodynamic regulation of LDL, leukocyte TEM, chemotactic-guided cell migration, cytokine synthesis by the various leukocytes that invade the artery wall (i.e., lymphocyte, monocyte, leukocyte, macrophage (M1, M2) and foam cell), or cytokine induced endothelial activation. The ABM presented herein introduces an original way to capture these complex interconnected events. ABM is a promising tool to understand how spatiotemporal changes influence plaque progression and how complex and integrated processes give rise to emergent phenomenon.

Our mechanobiolical ABM builds on, and is in agreement with, previous multi-level modeling attempts to capture hemodynamically inspired inflammation and atherogenesis. In 2007, Bailey et al. used a 2D ABM of mouse to capture WSS- and chemokine/cytokine-induced monocyte adhesion to ECs of microvessels [106]. Similar to our results they found monocyte adhesion to the endothelium increases under low WSS and decreases once the WSS crosses the maximum threshold to withstand leukocyte adhesion. In 2012, Filipovic et al. used finite element modeling and a series of reaction-diffusion equations to look at LDL transport into the lumen

and growth of an advanced stenosis. Recently in 2016, this group expanded on these studies by developing a multi-level numerical model capable of capturing WSS-induced monocyte TEM and predicting areas particularly susceptible to plaque growth [107]. Similarly, we also report a positive correlation between low WSS regions and LDL accumulation and plaque growth. The model developed herein is unique and novel in comparison to the above mentioned models in that it includes multiple types of leukocytes, not just monocytes, it has continuous and/or stochastic rules rather than discrete and deterministic rules, cell migration is based on chemotaxis rather than convection-diffusion, and it allows the plaque to evolve non-symmetrically while observing tissue-level Glagov phenomenon rather than axisymmetric steady state simulations. Collectively these added features predict monotonic plaque growth with periodic increases in leukocyte TEM.

As expected, leukocytes entered the arterial wall and migrated towards the center of the plaque according to chemotaxis. When the plaque was > 40% of the lumen area it started growing inward (i.e. towards the lumen). Interestingly, new luminal patches were first added near the center of the plaque but laterally from the centerline (see **Figure 5.6** C, (a)). We used the model to determine the mechanisms behind this phenomenon. First, we observed that most of the endothelium near plaque constituents is activated; second, and leukocytes entering the wall from the edges or "shoulder" regions of the plaque migrate to the center. Third, because the plaque has advanced within the artery wall, the first location the leukocytes find with space still available and the highest cytokine is just off the centerline. Therefore, these lateral regions exceed 40% of the luminal area before the centerline does and are the first to protrude into the luminal space. Once several luminal patches have been added as to form a layer over these

lateral regions, leukocyte TEM occurs at a more rapid rate (**Figure 5.6** C, (c)). At this point of time, inward growth starts occurring in the centerline of the artery because of their patches having a WSS < 1.2 Pa (blue regions in **Figure 5.6** D). As a result, the model predicts a "transition zone" where an increase in the rate of leukocyte TEM is observed. After ~28 luminal patches are added, the number of leukocytes performing TEM levels; this is because luminal patches are mostly added to the lateral regions again. These results corroborate with the general idea that the height of the stenosis appreciably influences the low WSS zones [108]. Herein we use our ABM to provide insight as to how the integration of hemodynamics, TEM, chemotaxis, and remodeling phenomenon influence plaque shapes.

Clinically, hemodynamics has been used to predict areas of plaque progression [30, 109]. Stone et al. used coronary angiography and intravascular ultrasound (IVUS) to reconstruct the artery and calculate WSS from 374 CAD patients (2.7 coronary arteries per patient) at baseline and 6-10 months later [109]. They found that regions with low WSS (< 1 Pa) distal to the throat of the obstruction grew most rapidly (with almost 30% of the patients experiencing a decrease of luminal area > 2.4 mm^2). Samady, et al. went one step further and correlated local WSS with plaque composition using IVUS-virtual histology (IVUS-VH) in 20 patients with CAD over 6 months [10]. They also found arterial segments with low WSS (< 1 Pa) developed greater plaque progression (0.12 ± 7.8 mm^2) and reduction in lumen area (by -0.9 ± 1.5 mm^2) as compared to higher WSS areas. Moreover low WSS regions experience an increase in fibrofatty area (0.01 ± 0.09 mm^2) compared to the high (> 5 Pa) WSS regions (-0.14 ± 0.44 mm^2) which actually experience regression of fibrofatty tissue. Smedby performed angiography on 237 patients over a span of 3 years to find that plaque growth was more rapid downstream of the stenosis, as

compared to upstream [110]. In agreement with these clinical observations, our model also shows a positive correlation between low WSS zones (< 1.2 Pa) and plaque progression. We observed increase leukocyte TEM in the region of low WSS i.e. in the downstream, or distal, shoulder region of the stenosis (**Figure 4.12**) followed by local plaque growth.

As a form of gross validation we simulated the same conditions as an experimental porcine model of atherogenesis. Our ABM-CFD mean lesion area predictions were similar to those quantified in the experimental model (**Figure 5.11**) at 2 and 4 months. However, at 4 months, the lesion area as predicted by the ABM-CFD model was in the lower range. This may be due, in part, to the fact that the plaque is comprised exclusively of leukocytes and ECM in the ABM, whereas in reality there may be migration and proliferation of smooth muscle cells and fibroblasts as well as production of additional ECM all of which could increase the lesion area. Yet, the ABM-CFD lesion area predictions highlight the influence of leukocyte accumulation on plaque development.

At the cellular-level, the ABMs spatial and temporal predictions on ratio of cell types within the artery wall corroborate with experimental and histological reports. We found the relative amount of neutrophils was the highest in the beginning (within ~ 2 months) and then again about a month after when the plaque started to grow inside the lumen (**Figure 5.8**). Mechanistically, neutrophil aggregation can be explained by the higher concentration of neutrophils in the blood and their increased adhesion rates in the presences of lower cytokine concentration and higher WSS conditions (Table 4.2, rules 1-3). A review by Soehnlein eloquently highlighted results on neutrophil involvement from animal studies. They showed significant neutrophil involvement during the initial progression of atherosclerosis as well as

during endothelial dysfunction as may be the case when the endothelium is disrupted by inward plaque growth [111]. Indeed the rapid influx of neutrophils, and then lymphocytes, after inward remodeling may explain the occurrence of plaque fissures in minimally stenotic plaques [40]. Spatially, after 7-months the model predicted neutrophils and monocytes coalesce towards the adventitia, cap, and shoulder regions of the plaque (**Figure 5.12**). Similarly, Rotzius et al. showed in mature lesions, neutrophils were abundant in the shoulder region of lesions, especially at the sites where the concentration of monocytes were also high. The ABM-CFD model can also be used to identify the global affect due to alteration of specific factors. For example, Stoneman et al. [112] depleted monocytes in ApoE knockout mice and showed a 50% reduction of plaque area after 10 weeks. Removing monocytes from the ABM resulted in around 80% reduction in plaque area by 10 weeks (data not shown). As expected, both models showed a reduction in plaque growth; the difference in magnitude may be due to genetic effects of the ApoE knockout, proliferation of the arterial cells and/or production of ECM.

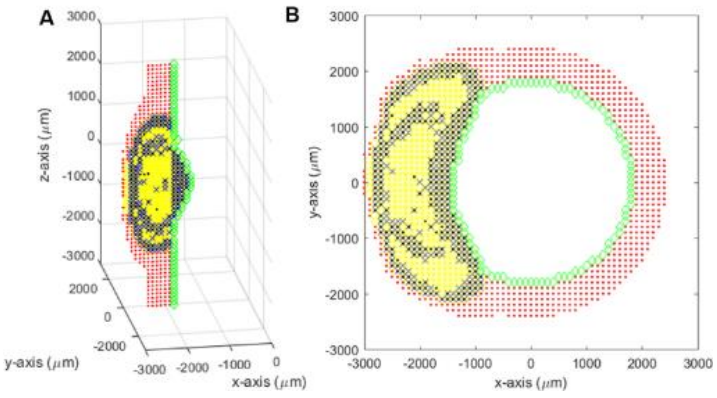

Figure 5.12 Spatial distribution of cells in the artery wall: Longitudinal (A) and corresponding transverse (B) cross sections in a 7-month simulation of atherosclerosis, where endothelial cells, arterial cells, neutrophils and monocytes are represented by green diamonds, red circles, blue crosses and black dots, respectively. All other cells in the wall (lymphocytes, M1, M2 and foam cell) are represented in yellow. Neutrophils and monocytes coalesce towards the cap, shoulder regions, and adventitia but to a lesser extent at the central region of plaque.

Conclusion

In conclusion, by considering key biological events such as diffusion of cytokines and LDL, chemically and hemodynamically-induced leukocyte adhesion, trans-endothelial migration, chemotaxis, cell apoptosis, monocyte differentiation, and foam cell formation, our ABM can capture and predict leukocyte TEM and thus plaque progression. Moreover coupling this ABM to a blood flow model allows for a better understanding of the spatiotemporal hemodynamic effects on plaque progression. Experimentally, the dependency of TEM on endothelial activation and WSS has been quantified [9-12, 16, 17, 87-89, 113, 114]. Clinically low WSS has been linked to areas of plaque growth and luminal constriction [115, 116]. Now, computationally we present a robust multiscale model to study the interdependency of leukocyte TEM, plaque growth and WSS with time. Together, it provides an accurate approach to predict atherosclerotic plaque dynamics and avoids the homogeneous idealizations or isolated correlations of existing approaches. Eventually, multi-scale modeling of plaque evolution will be insightful for individualized decision making (e.g. to treat or not to treat a lesion) and foundational for design changes in interventional approaches (e.g. hypothesizing how an artery will respond to a pharmaceutical candidate, stent design or graft).

Assumptions and limitations

Longitudinal human data during atherogenesis, where the severity of stenosis is < 10%, does not exist. We cannot directly compare our growth rate predictions, though the model's growth rate (i.e., going from 0 to 8% stenosis in 6 months) seems accelerated. One reason may

be due to fact that the rules on leukocyte adhesion and TEM are based on experiments conducted in-vitro. However, we have tried to minimize error within each rule by having them tested for robustness by blind researchers. Another reason may be spatial restrictions in the artery wall. As the primary focus was on spatiotemporal WSS-induced leukocyte transmigration we have fixed the ECM as 60% of each patch in the artery wall. In reality, matrix metalloproteinases, released by cells degrade the ECM and thus free up more space and slow the growth rate. Even so, the growth rate should not affect the dynamics observed on how plaque stenosis alters the hemodynamics and thus leukocyte transmigration. Moreover, comparing the model predictions on lesion area were similar to a pig model of atherogenesis.

As previously mentioned, each patch was a cube of length 100μm. Hence all the leukocytes present in same patch at a time experienced the same environment (i.e., cytokine concentration and WSS). Obviously smaller patch sizes would increase the resolution, but also the computational time. Spatial results confirmed that the cytokine concentration in one patch did not change much from the next patch even in the most concentrated zone (**Figure 5.13**). Likewise, Razavi et al. showed the WSS changes by less than 2% within 100 μm, even in the case of 60% stenosis [117]. Therefore, for a reasonable computational time, as well as capturing the variations of the parameters properly, the patch size was considered as 100μm.

A rigid wall assumption was imposed. Differences of WSS between compliant and rigid wall models depend on several factors (e.g., degree of compliance, geometry, curvature, and stenosis severity). Coronary arteries with mild stenosis, exhibit a change in diameter < 2% over a cardiac cycle, and peak WSS differences between compliant and rigid wall models is < 10% [98]. In arteries with severe stenosis the difference is around 30-40% [99]. Therefore, a rigid wall

assumption is a first approximation for the case of early atherosclerosis studied herein, but can be expanded upon in the future.

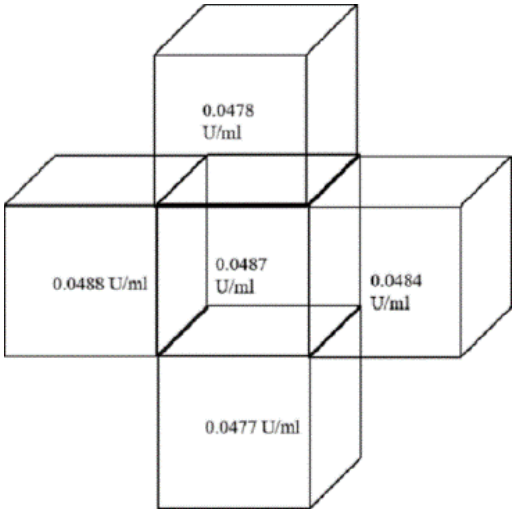

Figure 5.13 100µm patch size is reasonable given the sensitivity in change cytokine concentration does not change much: Schematic presentation of patches and the cytokine concentration on the corresponding patches. Obviously, there is not much change in the neighbor patches. So considering same cytokine concentration throughout a patch is reasonable.

CHAPTER 6

MECHANISTIC MODEL OF LEUKOCYTE TRANSMIGRATION

Overview

In the previously described model (in chapters 4 & 5), we quantified leukocyte adhesion as function of cytokine concentration. In reality, cytokines induce selectin and adhesion molecule upregulation on endothelial cells. The presences of these proteins increases the probability a leukocyte will adhere on the endothelial cell. In this chapter, we expand the ABM to include these mechanistic pathways of adhesion and others. Moreover, in the previous model we only considered the effect of one lipoprotein, low-density lipoprotein (LDL). In the current model, we have included the effects of tri-glyceride rich lipoprotein (TGRL), and high-density lipoprotein (HDL). HDL has atheroprotective properties, so by including HDL in the model, we are also considering its anti-inflammatory effect. In this chapter, we also take into account removal of LDL and ox-LDL, Together HDL and lipoprotein removal reduce the rate of plaque progression. By breaking down the cause-and-effect rules into their more mechanistic parts, we can produce a more accurate and robust model.

After performing a parameter sensitivity study, we saw that ICAM-1 and E-Selectin are more sensitive to changes in TNF-α compare to that of IL-1 β, whereas VCAM-1 is more sensitive to changes in IL-1β. VCAM-1 is also more sensitive changes in HDL compared to how ICAM-1 or E-Selectin are regulated by HDL. Overall, these sensitivity studies give insight into the role lipoproteins and cytokines play in plaque progression, and also suggest how pharmaceuticals that target those proteins my effect plaque growth.

Finally, we compared the current mechanistic model to our previous published model [86] and as expected the growth rate of plaque was much slower in the current model.

Events in our mechanistic ABM

Expression of adhesion molecules (AMs) on EC surface:

Early state of atherosclerosis involves recruitment of leukocytes to the endothelium and their transendothelial migration (TEM). This process is mainly mediated through adhesion molecules (AMs) which are expressed on the endothelial cell (EC) surface. Hence increasing levels of those molecules leads to increased leukocyte TEM, and thus plaque progression. In particular, E-selectin is involved in tethering and rolling of leukocytes on the EC surface, whereas Intercellular adhesion molecule (ICAM) and vascular cell adhesion molecule (VCAM-1) are involved in firmly adhering the leukocyte onto the endothelium.

The factors that affect selectin and adhesion molecule (AM) expression are as follows:

1. Cytokine concentration (TNF-α, IL-1β, IFN-γ)
2. Tri-glyceride rich lipoprotein (TGRL)
3. Wall shear stress (WSS)
4. Oxidized LDL (ox-LDL)

<u>Cytokine concentration dependence on expression of AMs and selectins</u>

Research in the last decade has shown that several pro-inflammatory cytokines, including TNF-α and IL-1β potently increase the expression of many AMs and thus increase the adhesiveness between leukocytes and the endothelium. IFN-γ, on the other hand acts both a pro-inflammatory and anti-inflammatory cytokine [118, 119]. However, AM expression due to IFN-γ very small compare to that of TNF-α and IL-1β [120]. Hence, the influence of IFN-γ is neglected

here. It is worthwhile to note, when multiple cytokines are present simultaneously, the resulting AM and selectin expressions are different only one cytokine is present and acting on the endothelial cell. This synergistic effect of the cytokines will be discussed later. **Figure 6.1** shows the dose dependence of TNF-α on AMs expression. Data were taken from Ting et al.[1].

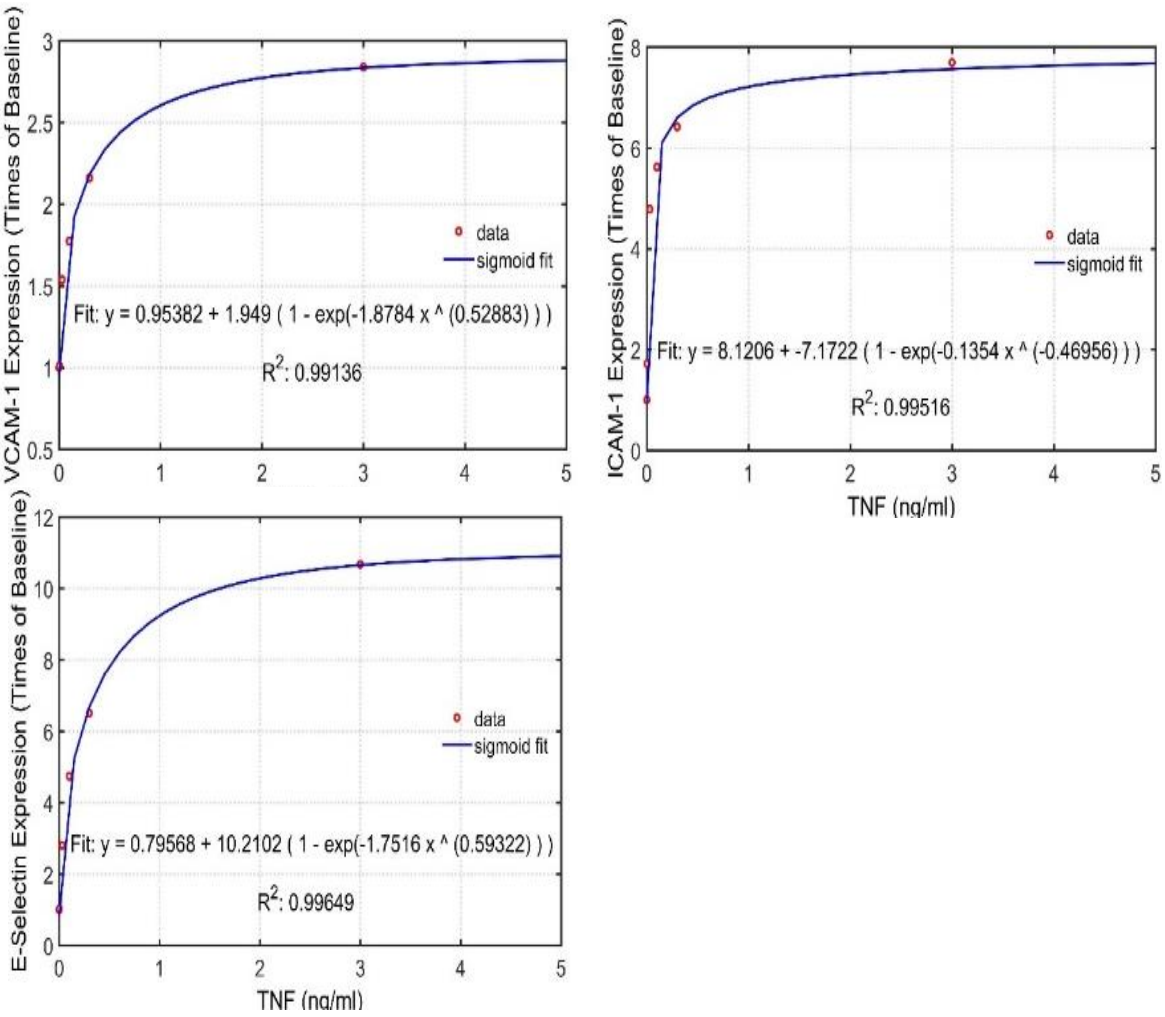

Figure 6.1 AM expression as function of TNF-α: Data (o) are collected from [1]. The best fit sigmoidal function is considered as the ABM rule for AM expression as function of TNF-α.

TriGlyceride-Rich Lipoprotein (TGRL) dependence

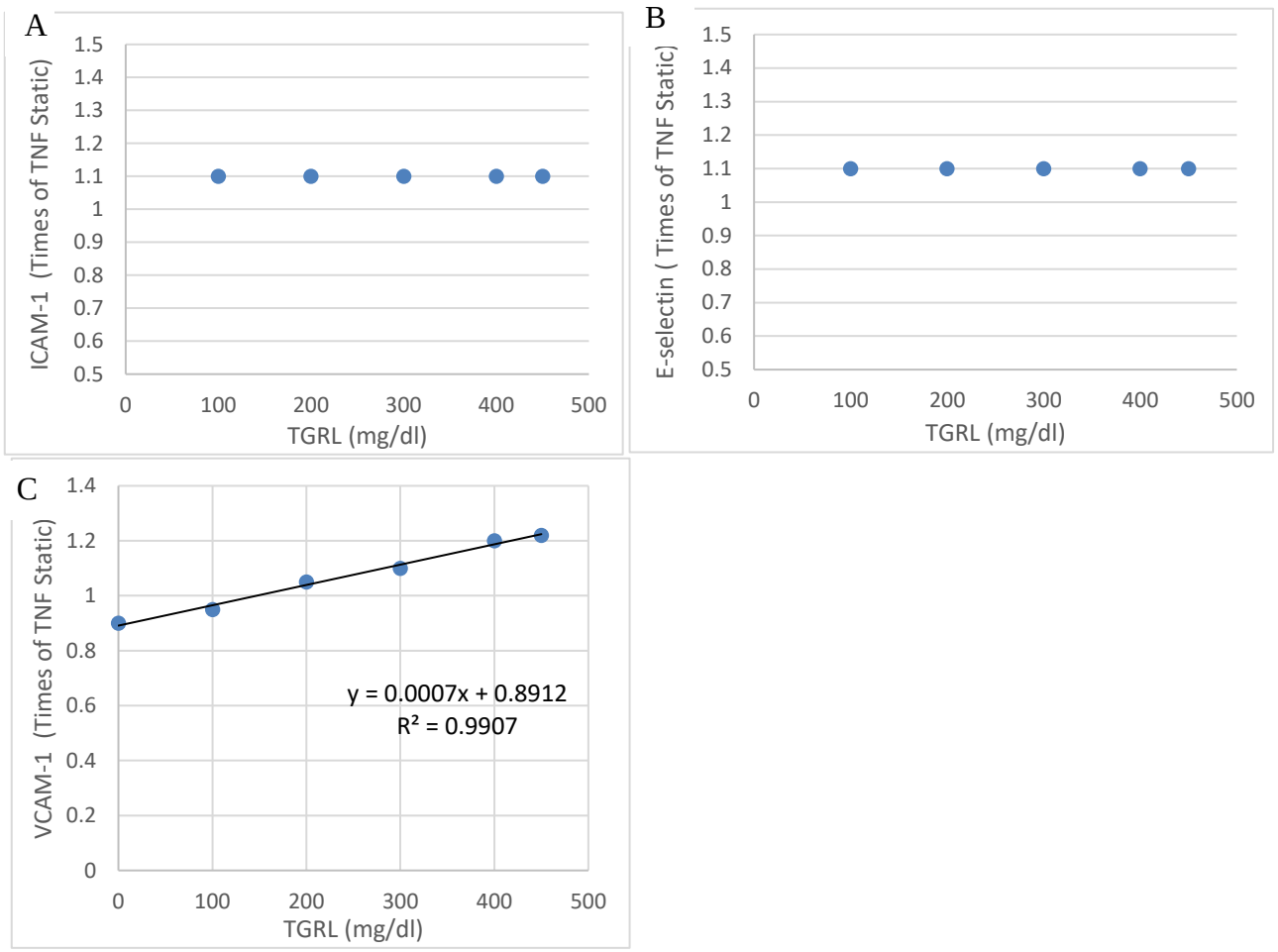

Figure 6.2 AM expression as function of TGRL: Data (o) are collected from previous literature [2] for (A) ICAM-1, (B) VCAM-1 and (C) E-Selectin expression as a function of TGRL. The ICAM-1 and E-Selectin do not change with TGRL whereas VCAM-1 does. The line plot is the best fit considered as rule of VCAM-1 expression with TGRL.

High levels of TGRLs in blood are a key factor in the development of atherosclerosis, yet the exact mechanism is still unclear. TGRL alone does not elicit the expression of AMs. However, in the presence of cytokine stimulation TGRL enhances VCAM-1 expression significantly [1, 2]. Interestingly, TGRL does not increase the expression of ICAM-1 and E-

Selectin over the entire dose range of TNF-α (0.003 – 3 ng/ml). **Figure 6.2** shows data derived from Wang et al. [2] and the resulting ABM mathematical expressions.

WSS dependence

It is well known that atherosclerosis develops preferentially at sites of low and oscillatory shear stress in arteries. Specifically, ECs sense a gradient of fluid shear stress and transduce signals that regulate AMs expression. **Figure 6.3** shows experimental relations correlating augmented expression of TNFα induced E-selectin, ICAM-1 and VCAM-1 in the presence of WSS [3].

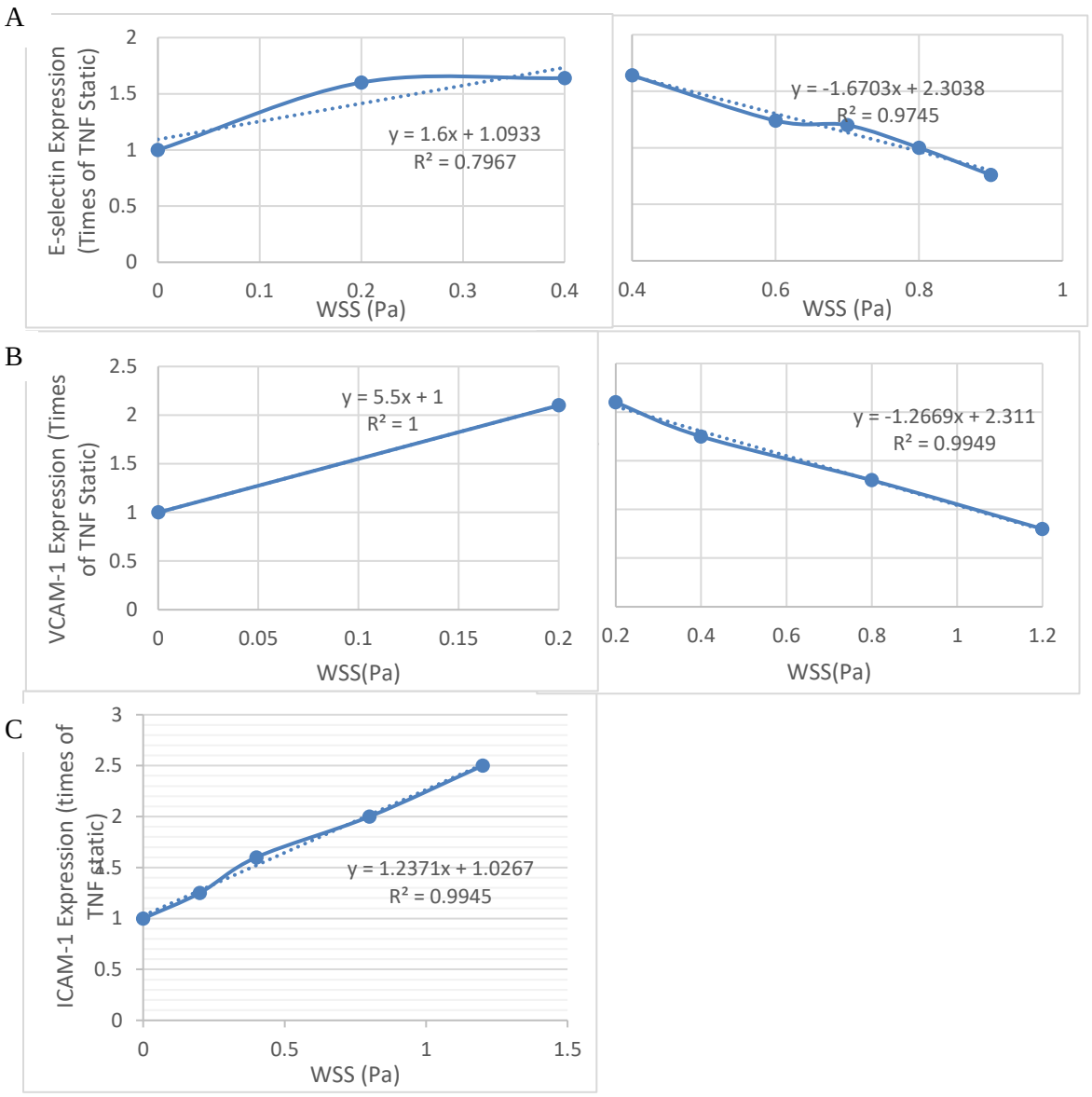

Figure 6.3 AM expression, above TNFα induced at static, as function of WSS: Data (o) are collected from [3] for (A) E-Selectin, (B) VCAM-1 and (C) ICAM-1 expression as function of WSS. The best fit linear function is considered as rule of selectin and AM expression with WSS.

We have separate functions for AMs and E-Selectin expression based on cytokine, TGRL concentration and WSS. **Figure 6.4** shows a color plot of AMs and E-Selectin expression in presence of TNF-α, TGRL and WSS together. Note that the contribution of ox-LDL and IL-1β are not plotted but contribute to AM and selectin expression are included in the ABM. . The color bar shows the AMs expression with respect to baseline expression.

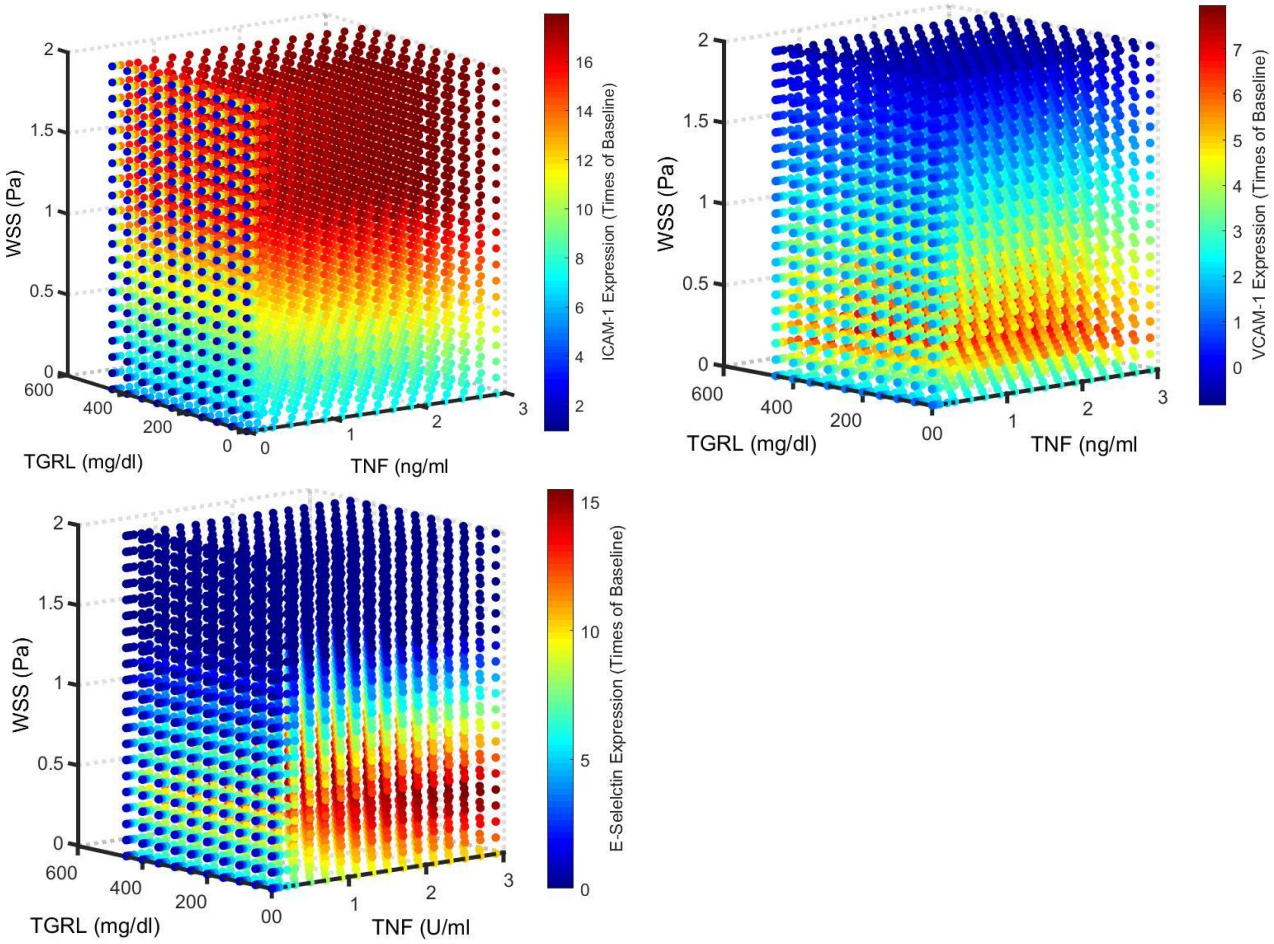

Figure 6.4 Multivariable dependence of AM expression: Color plot shows the gradual change of AM expression with change of TNF-α, TGRL, WSS together. Color bar represents the value of E-selectin and AM expression.

Ox-LDL dependence

Ox-LDL contributes to the development of atherosclerosis in several ways, one of which is the stimulation of endothelial cells (EC) to express selectins and AMs. We compared (**Figure 6.5** A) dependence of ICAM-1 expression with ox-LDL from different sources [6-8]. Cominacini

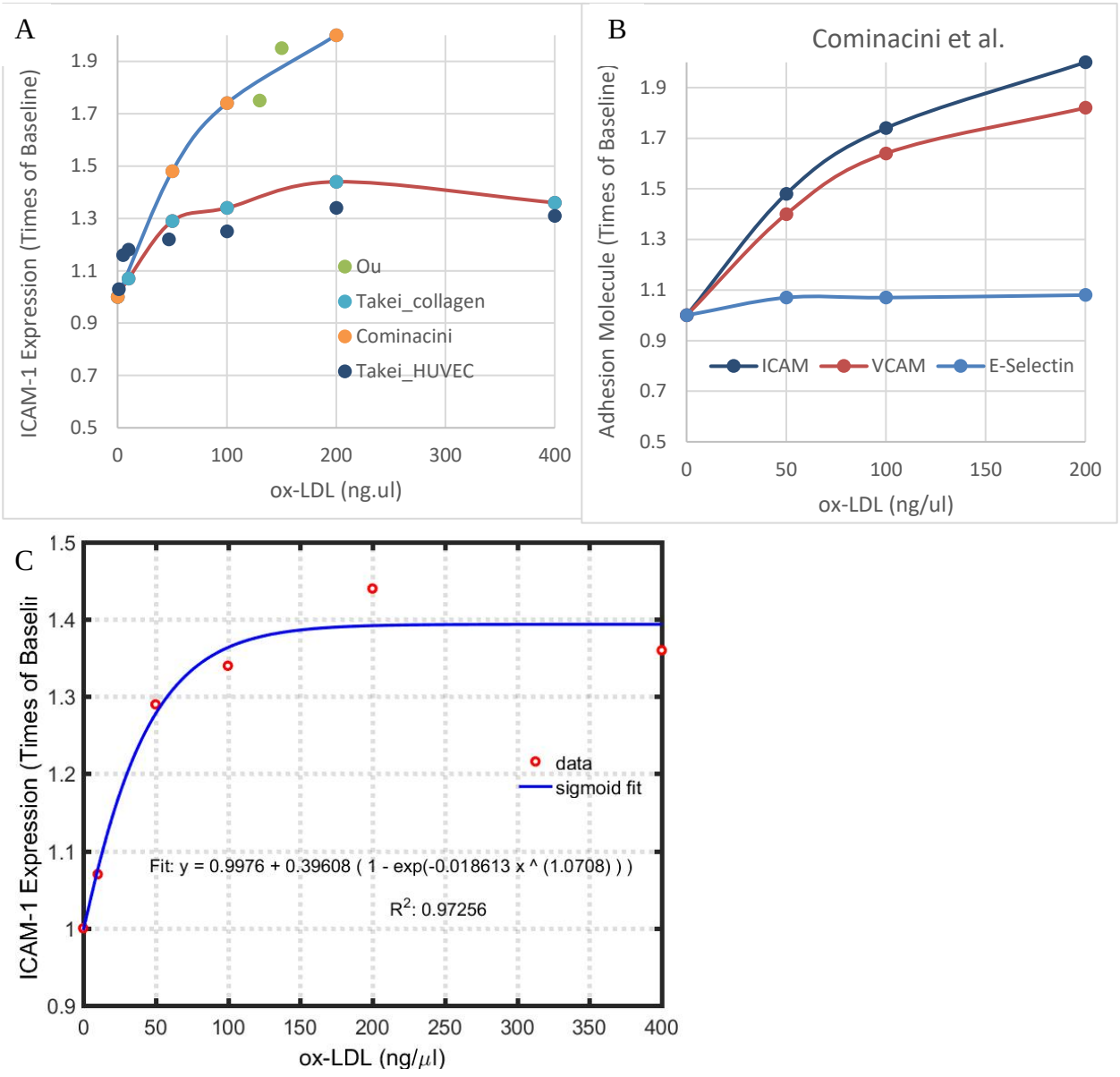

Figure 6.5 Dependence of AMs and E-Selectin expression as function of ox-LDL: (A) Comparison of ICAM-1 expression from different sources [6-8]. (B) Expression from Cominacini et al. (C) Data (o) of ICAM-1 expression from [8]. The line plot (sigmoid fit) is the derived rule.

et al. [6] showed that ICAM-1 and VCAM-1 increase significantly with ox-LDL but E-Selectin changes only about 7% for a wide range of ox-LDL(50-200 ng/μl) (**Figure 6.5**, B). On the contrary, Takei et al. [8] showed only a small amount of ICAM-1 is expressed in the presence of ox-LDL. Khan et al.[121] agreed with Takei et al., and also stated that ox-LDL does not affect VCAM-1 or E-Selectin expression. Takei et al. experiments were also more physiolgical. They platted the ECs on collagen substrates. In reality collagen is present in the artery wall and subendothelial matrix. Therefore, we considered the data from Takei et al. to derive the rule for AM and selectin expresion by ECs as a function of ox-LDL, as shown in **Figure 6.5**, C.

Synergistic effect

Individually, each pro-inflammatory cytokine, LDL or WSS increases expression of selectins and adhesion molecules on endothelial cells. However, in combination the cytokines, LDL and WSS can summate to produce an even greater expression of selectins and AMs. Both Dustin et al. [122] and Honghui et al.[123] showed that expression of AMs increases in presence of TNF-α and IL-1β together than when the EC was stimulated by only one. The combinatorial effect is different than simply an additive effect of these two cytokines. There is an increase of 40% and 35% from maximum in ICAM-1 and VCAM-1 expression respectively in presence of TNF-α and IL-1β together. For example, if ICAM-1 expression from some value of TNF-α and IL-1β separately are 3 and 4 times of baseline respectively, then when they act together the final value of ICAM-1 will be 40% more than maximum ICAM-1 (which was 4 times of baseline) i.e. final ICAM-1 will be 5.6 times of baseline. Similarly, Khan et al. showed that Ox-LDL enhances VCAM-1 expression induced by TNF-α by 45% in HUVECs [121]. But the AMs/ E-Selectin

expression from ox-LDL is so small compare to that of TNF-α and IL-1β that synergistic effect of ox-LDL, TNF-α and IL-1β is same as that of TNF-α and IL-1β . Now, ICAM-1 and VCAM-1 produced as a result of TNF-α alone is more than that of IL-1β alone. So as explained above, when both are present together after the synergistic effect thet ICAM-1 and VCAM-1 will be 40% and 35% more than TNF-α alone respectively.

Dependence of leukocyte adhesion on adhesion molecule and E-Selectin

Leukocyte adhesion on the EC surface depends on the concentration of selectins and AMs on the EC.

Adhesion of neutrophils

Several experiments, either non-blocking or blocking particular receptors, were used to tease out the contribution each endothelial surface molecule has on neutrophil adhesion. Using in-vitro vascular monolayers of HUVECs, Stroka et al. [17] showed that when the endothelium was incubated with 25 ng/ml TNF-α for 24 hours and on 3 kPa sub-endothelial stiffness under no-flow conditions, 76% of the neutrophils transmigrated through the EC surface. Assuming all the cells that adhered ended up transmigrating, the adhesion is also 76%. Stimulation of the EC surface with 25 ng/ml TNF-α (for 24 hours), results in expression 7.91, 2.9 and 11 times above the baseline (i.e., no stimulation) value of ICAM-1, VCAM-1 and E-Selectin, respectively. Using antibodies to block selectins and VCAM-1, Robinson et al. [124] showed that with 20 ng/ml TNF-α, which gives nearly same value of AMs expression as with 25 ng/ml, 67% of total adhesion is due to ICAM-1. Since the total adhesion is 76%, the adhesion due to 7.91 times of baseline value of ICAM-1 is 51% (i.e. 67% of the total 76%). Neutrophil adhesion does not

depend on VCAM-1 [125]. Therefore, the rest of adhesion with TNF-α stimulation, i.e., 25%, is due to the 11 times baseline value of E-Selectin (**Figure 6.6**). Neelamegham et al. [126] showed with 5ng/ml IL-1β, which gives 2.06, 3.77 and 17.05 times of baseline value of ICAM-1, VCAM-1 and E-Selectin respectively, the total adhesion is 44%. Using antibodies to block each integrin and/or selectin they found the breakdown of contribution of ICAM, VCAM and ES to

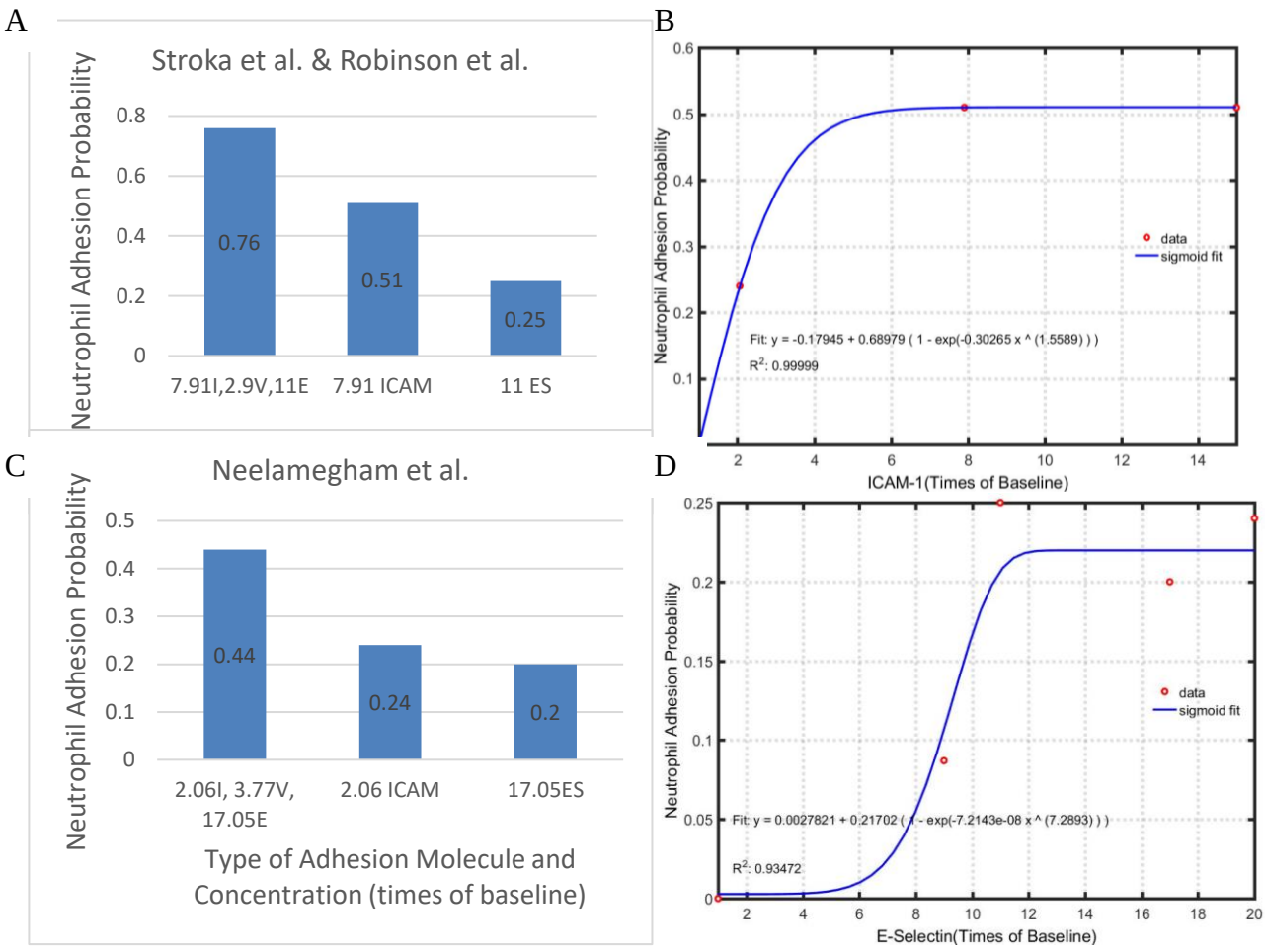

Figure 6.6 Neutrophil adhesion as function of AM: Left panel (A, C) shows the neutrophil adhesion probability from different sources and the relative contribution of different AMs. For example, Neelamegham et al. found 44% adhesion probability when EC expresses 2.06, 3.77 and 17.05 times of baseline value of ICAM, VCAM and E-Selectin respectively. Adhesion due to ICAM-1, VCAM-1 and E-Selectin alone are 24%, 0% and 20% respectively. Right panel (B, D): Rules derived from those sources. 'o' represents data and line plot is the fit representing rule of neutrophil adhesion as function of AMs.

adhesion is 24%, 0 and 20% respectively (**Figure 6.6**). Bahra et al. [9] showed that even when E-Selectin is 9 times it's baseline value the adhesion probability of neutrophils is very small (~8%), wheras it increases significantly (25%) when E-Selectin is 11 times it's baseline value. Based on all the findings mentioned above, rules for neutrophil adhesion probability as a function of either ICAM-1 or E-Selectin are shown in **Figure 6.6** (B, D).

Adhesion of monocytes

Unlike neutrophils, monocytes depend on the expression of VCAM-1, in addition to E-Selectin and ICAM-1. Using in-vitro vascular monolayers of HUVECs, Hayenga et al. showed that 44% of the monocytes adhered on the EC surface when the endothelium was preincubated with 25 ng/ml of TNF-α for 24 hours and grown into a monolayer on 3 kPa sub-endothelial stiffness hydrogels, under no-flow conditions [16]. Stimulating EC surface by the above condition gives rise to 7.91, 2.9 and 11 times of baseline value of ICAM-1, VCAM-1 and E-Selectin respectively. Kevin et al. activated the endothelium with 10 ng/ml TNF-α for 24 hours, which resulted same activation as above i.e. 7.8, 2.9 and 11 times of baseline value of ICAM-1, VCAM-1 and E-Selectin respectively [127]. Kevin et al. also showed that 14.41% of total adhesion is due to ICAM-1 (**Figure 6.7**, left) [127]. Rafii et al. [128] and Takahashi et al. [129] used 10 U/ml and 25 U/ml of IL-1β respectively to stimulate the EC surface; using blocking antibodies both groups showed the relative contributions of ICAM-1, VCAM-1 and E-Selectin

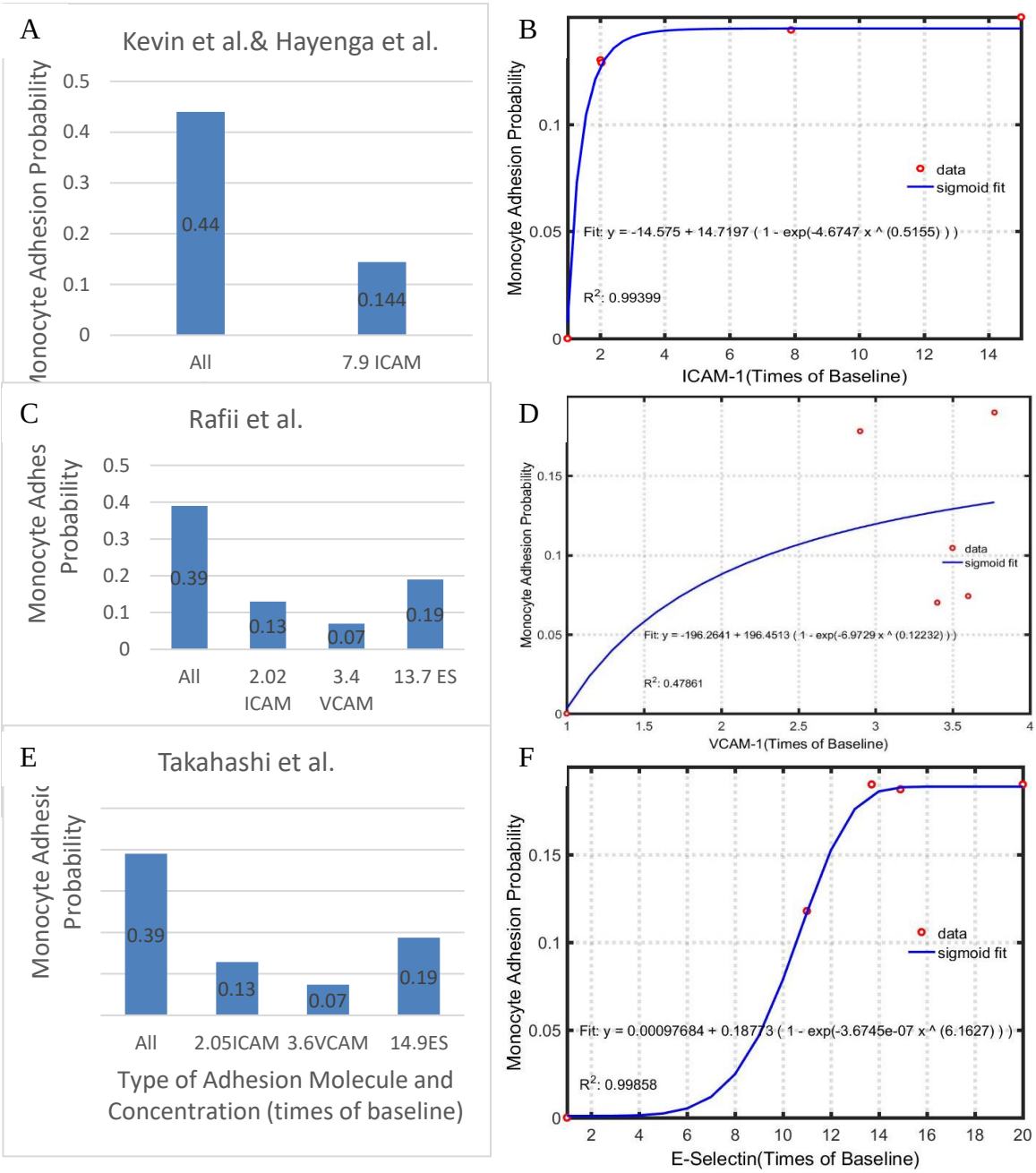

Figure 6.7 Monocyte adhesion as function of selectins: Left panel (A, C, E) shows the monocyte adhesion probability from different sources and the relative contribution of different AMs. For example, Takahashi et al. found 39% adhesion probability when EC expresses 2.05, 3.6 and 14.9 times of baseline value of ICAM-1, VCAM-1 and E-Selectin respectively. Adhesion due to ICAM-1, VCAM-1 and E-Selectin alone are 13%, 7% and 19% respectively. Right panel (B, D, F): Rules derived from those sources. 'o' represents data and sigmoid functions are fit and represent the rule for monocyte adhesion as function of AMs.

are13%, 7% and 19% respectively (see **Figure 6.7**, left). Giuffre et al. [130] used the same stimulation as Kevin et al. did and showed 40% of total adhesion is due to VCAM-1. Together,

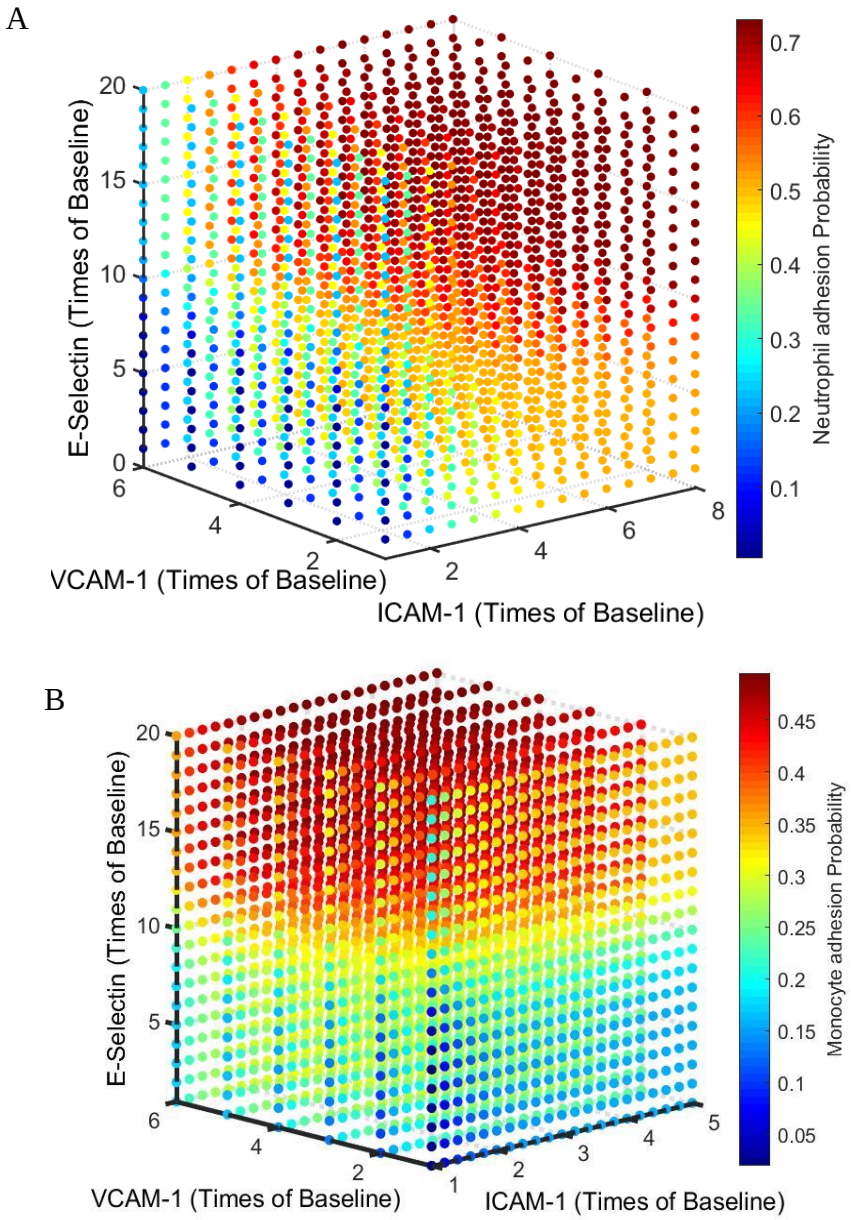

Figure 6.8 Leukocyte adhesion probability as function of AMs and E-Selectin: (A) Neutrophil adhesion probability (B) Monocyte adhesion probability. Color bar shows the magnitude of adhesion probability

with all these results we were able to make rules regarding monocyte adhesion as a function of integrins and selectins.

Figure 6.8 shows the leukocyte adhesion probability in presence of all the AMs and E-selectin.

Time required for leukocyte capture to TEM

After a leukocyte is captured to an activated endothelium, it spends some time migrating on the endothelium before transmigrating. Then the leukocyte transmigrates through the endothelium and the AMs used are recycled and expressed on the surface of the endothelium again. Therefore, if another leukocyte adheres at the same location AMs should be available. However, the time from capture to TEM is not immediate and depends on the type if leukocyte. For example, the average time taken by a neutrophil to transmigrate after capture is around 10 minutes [17]. Similarly, Hayenga et al. [16] showed that average time spent by each monocyte over endothelium after capture was around 15 minutes and average time taken for TEM was approximately 3 minutes. Hence, the probability of monocyte adhesion found before is over 18 minutes. The probability of adhesion per unit time for all cell types are shown in Table 6.1(rule numbers 24-29).

Now, to consider how TEM time effects the number of leukocytes that will adhere there can be two scenarios (high cytokine concentration and low cytokine concentration). First, the number of leukocytes present within 15 μm layer above the endothelium is much less as compared to the concentration of AMs and E-Selectin expression. When the cytokine concentration is very high (as is the case when the plaque is big), the AMs/ E-Selectin are highly

expressed. In that case, the leukocytes do not have to wait for the recycled AMs and E-Selectin, and so the above mention capture to TEM time does not really matter.

In case of the second scenario, when the cytokine concentration is very small (as in case of a fatty streak), the expression of AMs and E-Selectin are limited. Hence, the probability of leukocyte adhesion may depend on capture to TEM time, because the few integrins and selectins need to be recycled to the EC surface before another leukocyte can bind. In this scenario, the probability of leukocyte adhesion as function of concentration of AMs (see quantification above) would be executed every 10 or 18 minutes depending on cell type. For example, based on the concentration of neutrophils in the blood, let's say over 60 minutes 100 neutrophils come within 15 μm of the endothelium and have potential to get captured. Assume that the AMs and E-Selectin on EC surface are such that 76% of those captured neutrophils should adhere. Now if we take into account the time required from neutrophil capture to TEM is 10 minutes, then neutrophils can be captured and transmigrate 6 times in 1 hour. Within the 10 minutes of capture to TEM the AM and selectins may not be available for the next neutrophil to bind to. Therefore, to reduce the probability of neutrophil adhesion, we assume the number of neutrophils that would be captured in 1 hour is only 16.6 (i.e., 100 possible /6 ten min stents). Based on the adhesion rule, 76% of 16.6 captured neutrophils i.e. 12.6 neutrophils would then adhere on surface after 1 hour. For the ABM simulations shown below, we used this scenario. A mathematical expression of adhesion probability as function of AMs, E-selectin and time is given in 6.1.

Suppose:

N: Total number of leukocytes (neutrophils/ monocytes/lymphocytes) that come within the 15 μm layer above the endothelium over time interval t

f(A): Adhesion probability as function of ICAM-1/ VCAM-1 or E-Selectin

T: Time required for leukocytes to go from capture to TEM (mentioned above)

N_1: Number of leukocytes that get opportunity to get same value of AMs and E-Selectin available at same location = (N/ T)

N_a: Number of leukocytes that adhere

P: Probability of leukocytes adhesion (Total number present / Total number of adhered)

$$N_a = N_1 f(A) = \frac{N}{T} f(A)$$

$$P = \frac{N_a}{N} = \frac{1}{T} f(A) \tag{6.1}$$

NOTE: Although we used this scenario, in reality the concentration of AMs is typically not a rate limiting step, therefore in future ABMs (not show in this dissertation) we will not limit adhesion based on the time required for TEM.

Detachment of adhered cells in presence of flow

After attachment, the leukocytes may get detached from the EC surface if the drag force from the blood flow is higher than the adhesive strength between leukocytes and the integrin/ selectin. The bond strength between leukocyte receptors and selectin is weaker than the bond strength between leukocytes and integrin. Hence, higher WSS is required to break the receptor-integrin (ICAM-1/VCAM-1) bond and detach the leukocytes from the endothelial surface than through selectin bonds.

Lawrence et al. showed the detachment of adhered neutrophils from the surface after applying a range of WSS onto the surface [18]. They injected neutrophils through a port of the flow chamber and allowed them to settle onto artificial surface containing 200 sites / μm^2 of CD62 (receptor for selectins) or 250 sites / μm^2 of ICAM-1. After 6 min of contact, shear stress was applied in staggered increments and the final number of neutrophils bound were expressed as percentage of neutrophils compared to those adhered initially. They found that more than 90% of the neutrophils remain adhered when attached with integrin even with high WSS (2 Pa) (**Figure 6.9**), whereas adhesion significantly reduced with WSS if attached only through selectins (**Figure 6.9**).

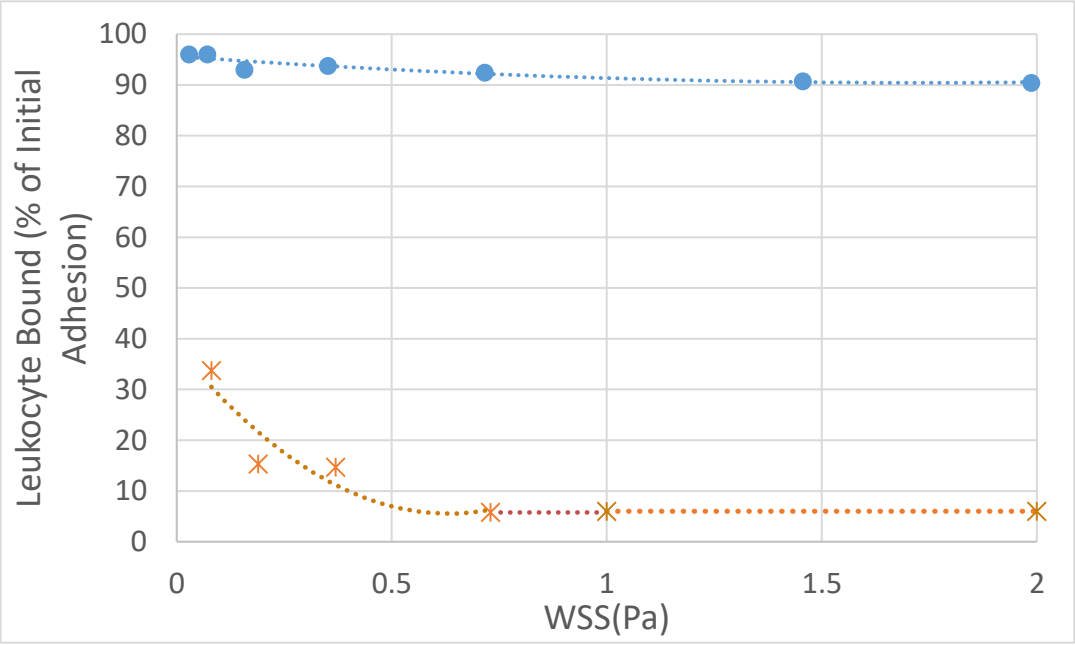

Figure 6.9 Detachment of adhered cells with flow: After initial attachment with selectin/ integrin, depending on WSS the leukocytes get detached from surface. As WSS increases, the number of leukocytes bound to surface decreases. The bond strength between leukocytes and selectin (orange,*) is weaker than that of with integrin (blue,circle). Hence, final adhesion is higher for integrin than selectin. Data were taken from [14, 18]

Although they used particular concentration of integrins and selectins and only looked at neutrophil detachment, we used their data to formulate our detachment rule for all leukocytes and ranges of AMs and E-Selectin concentration (see Table 6.1, rules 30-32).

Leukocyte transendothelial migration (TEM)

Once the leukocytes adhered to surface, and survived probability of detachment by the drag force from the flow, depending on the stiffness of artery wall, they transmigrate through wall. The rules for TEM as function of stiffness has been described in chapter 4. Once in the wall, leukocyte migration is directed by chemotaxis. A detailed explanation of leukocyte movement within the wall has been demonstrated in chapter 4.

HDL and atherosclerosis

Levels of HDL is inversely associated with the risk for the development of atherosclerosis [131-134]. HDL exhibits multiple physiologic effects that play a role in reducing risk for atherosclerosis. It can reduce the cytokine stimulated AMs expression [13, 135] and thus leukocyte adhesion in a concentration dependent manner. HDL decreases AMs and E-Selectin expression by inhibiting sphingosine-1 phosphate signaling and nuclear factor kappaB (NF-kB) [136-138]. Although we are not using the pathways here, it can be replaced eventually upon

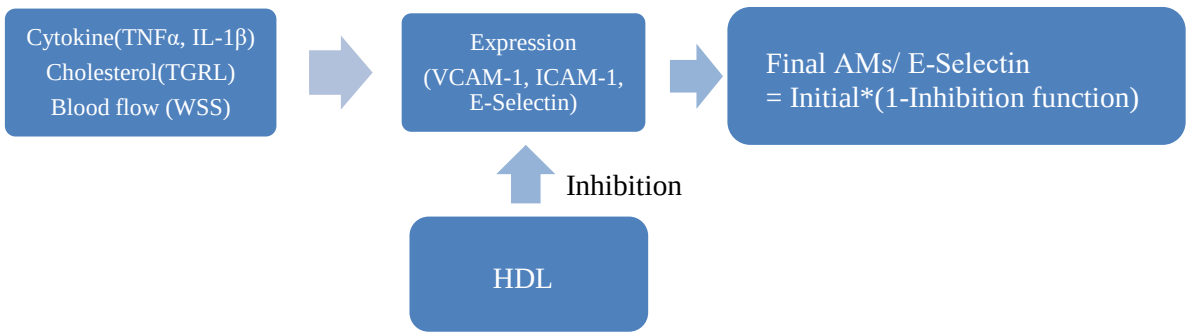

finding the quantitative relation for that pathways. Therefore, in our current model the final value of AMs and E-Selectin will be as in the flow chart.

Increased level of oxidized low density lipoprotein (ox-LDL) is a risk factor for atherosclerosis. HDL plays an important role in preventing atherosclerosis by inhibiting LDL oxidation in the artery wall. Mackness et al. showed in-vitro that inhibition of ox-LDL is dependent on HDL concentration and reached a maximum of 90% at 2000 ng/µl [14]. ABM rules detailing the effects of HDL are specified in **Figure 6.10**

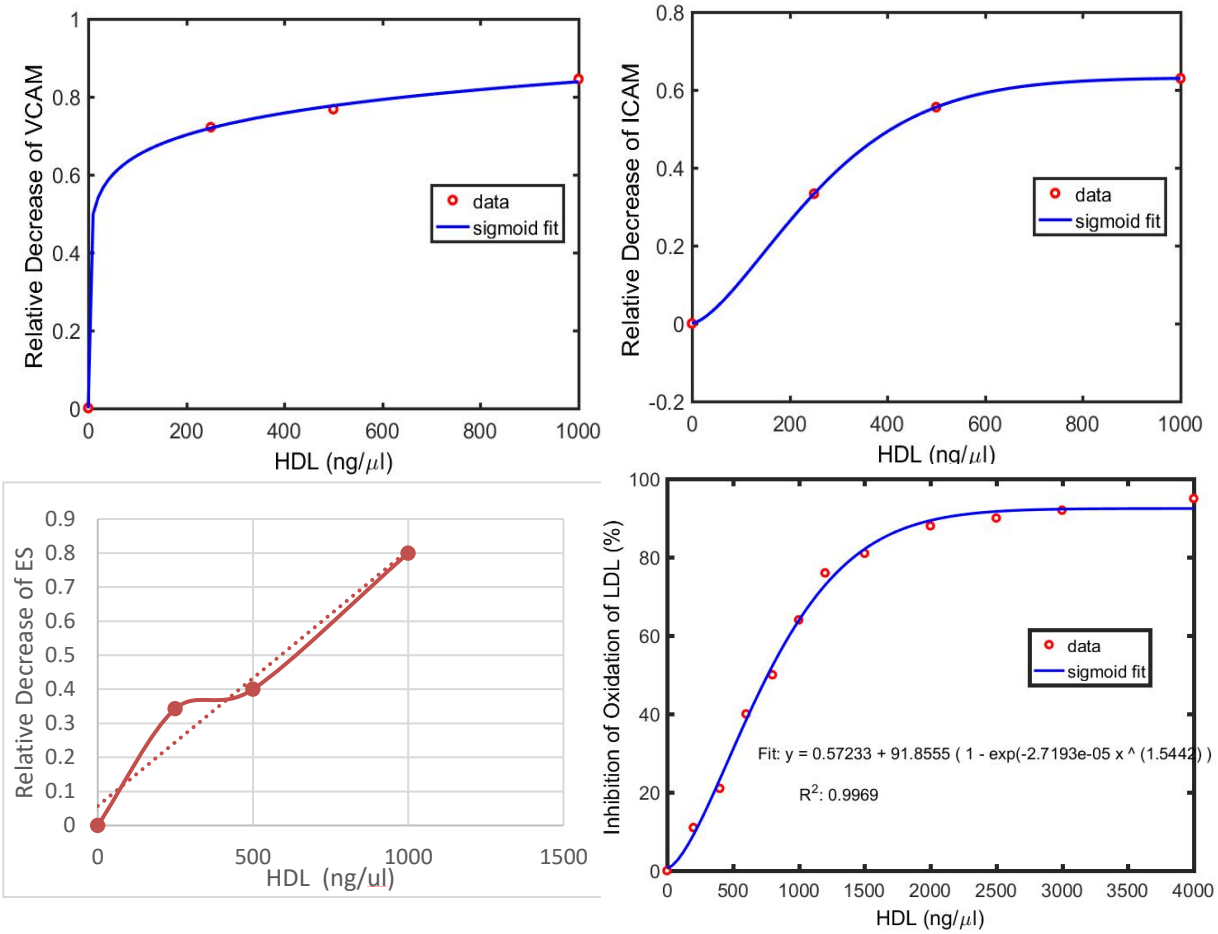

Figure 6.10 Atheroprotective effect of HDL on selectin and AM expression, and ox-LDL: HDL decrease the AM expression and reduce the effect of ox-LDL. As previous, 'o' represents data [13-15]and line plot represents the fit. These figures show relative decrease of the indicated proteins from initial (before applying HDL)

Consumption of LDL and ox-LDL by macrophages

As mentioned before, once LDL enters the artery wall, it gets oxidized forming ox-LDL. A monocyte derived macrophage consumes both LDL and ox-LDL and differentiates into a foam-cell. Leake et al showed degradation of LDL/ ox-LDL by macrophages [21]. They incubated iodine labelled LDL/ ox-LDL at indicated concentration in **Figure 6.11** with macrophages (10^6 cells) for 24 hours and then determined the amount of LDL/ox-LDL in the media. Subtracting this amount from the initial concentration gives the consumption of LDL/ ox-LDL by those (10^6 cells) macrophages. **Figure 6.11** shows the consumption rate of LDL and ox-LDL by macrophages.

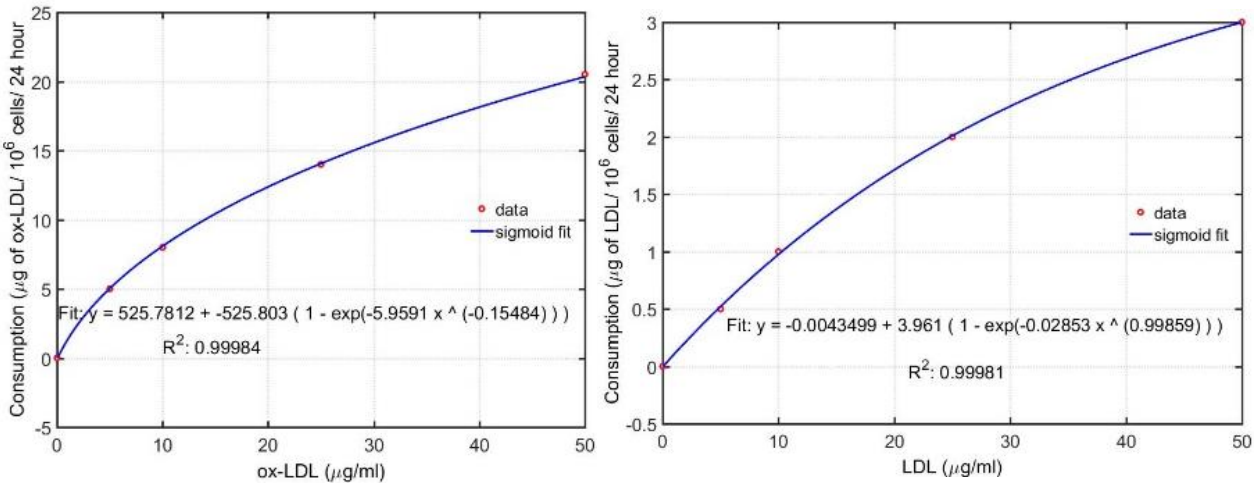

Figure 6.11 Consumption of LDL and ox-LDL by macrophages: Macrophage consumption rate of ox-LDL and LDL. Data were taken from Leake et al.[21]

All the rules were patch based i.e. applied in each patch. The rules are listed in table 6.1.

Table 6.1. Table of all rules in the mechanistic ABM

No.	**Behavior**	**ABM Rule**	**Ref:**
1.	EC expression of ICAM-1 based on TNF-α (no flow)	$ICAM = 8.121 - 7.172(1 - \exp(-0.135x^{-0.47}))$ $x: TNF\alpha[ng/ml]\,; ICAM[times\ of\ baseline]$	[1]
2.	EC expression of VCAM-1 based on TNF-α (no flow)	$VCAM = 0.954 + 1.949(1 - exp(-1.878\ x^{0.529}))$ $x: TNF\alpha\ [ng/ml]\,; VCAM[times\ of\ baseline]$	[1]
3.	EC expression of E-Selectin based on TNF-α (no flow)	$ESelectin = 0.796 + 10.21(1 - exp(-1.752\ x^{0.593}))$ $x: TNF\alpha[ng/ml]\,; ESelectin[times\ of\ baseline]$	[1]
4.	EC expression of ICAM-1 based on TGRL in presence of TNFa (no flow)	$ICAM = 1.1$ * *(ICAM expression with TNF-α)* $ICAM[times\ of\ baseline]$; TGRL > 0	[2]
5.	EC expression of VCAM-1 based on TGRL in presence of TNFa (no flow)	$VCAM = (0.0007x + 0.891)$ * *(VCAM expression with TNF-α)* $x: TGRL[mg/dl]; VCAM[times\ of\ baseline]$	[2]
6.	EC expression of E-Selectin based on TGRL in presence of TNFa (no flow)	*ESelectin =1.1 * (ES expression with TNF-α)* $ESelectin[times\ of\ baseline]$; TGRL > 0	[2]
7.	EC expression of ICAM-1 based on WSS	$ICAM(x) = (1.237x + 1.027) *$ $(ICAM\ expression\ with\ TNFa\ \&\ WSS = 0); x < 1.4$ $ICAM(x) = (1.237 * 1.4 + 1.027) *$ $(ICAM\ expression\ with\ TNFa\ \&\ WSS = 0); x \geq 1.4$ $x: WSS[Pa]; ICAM[times\ of\ baseline]$	[3]

8.	EC expression of VCAM-1 based on WSS	$VCAM(x) = (5.5x + 1) * (VCAM\ expression\ with\ TNFa\ for\ WSS = 0); x \leq 0.2$ VCAM(x) = (-1.267x+2.311) * *(VCAM expression with TNFa for WSS = 0)*; x>0.2 $x: WSS[Pa]; VCAM[times\ of\ baseline]$	[3]
9.	EC expression of E-Selectin based on WSS	$ESelectin(x) = (1.6x + 1.093) * (ES\ expression\ with\ TNFa\ for\ WSS = 0); x < 0.4$ *ESelectin(x) = (-1.6703x+2.304)* $(ES\ expression\ with\ TNFa\ for\ WSS = 0)$; $x \geq 0.4$ $x: WSS[Pa];\ ESelectin[times\ of\ baseline]$	[3]
10.	EC expression of ICAM-1 based on IL-1β (no flow)	$ICAM(x) = 1 + 1.056(1 - \exp(-11.718x^{0.790}))$ $x: \text{IL1}\beta[ng/ml]; ICAM[times\ of\ baseline]$	[123]
11.	EC expression of VCAM-1 based on IL-1β (no flow)	$VCAM(x) = 1 + 2.772(1 - \exp(-4.342x^{0.502})$ $x: \text{IL1}\beta[ng/ml]; VCAM[times\ of\ baseline]$	[123]
12.	EC expression of E-Selectin based on IL-1β (no flow)	$ESelectin(x) = 1 + 17.078\ (1 - exp(-1.3619\ x^{0.225}))$ $x: \text{IL1}\beta[ng/ml]; ESelectin[times\ of\ baseline]$	[139]
13.	EC expression of ICAM-1 based on ox-LDL	$ICAM(x) = 0.998 + 0.396(1 - \exp(-0.019x^{1.071}))$ $x: \text{oxLDL}[ng/ul]; ICAM[times\ of\ baseline]$	[8]
14.	EC expression of VCAM-1 based on ox-LDL	$VCAM = 1$ $VCAM[times\ of\ baseline]$	[8]
15.	EC expression of E-Selectin based on ox-LDL	$ESelectin = 1$ $ESelectin[times\ of\ baseline]$	[8]
16.	Synergistic effect of TNFα and IL-1β	ICAM= 1.4 times of ICAM due to TNF-α alone VCAM = 1.35 times of VCAM due to TNF-α alone E-Selectin does not change	[121]
17.	Inhibition of ICAM-1 by HDL	$Decrease = -5.0665e - 19 + 0.6312(1 - \exp(-0.0001918x^{1.4983}))$ $x: HDL[ng/ul]; Decrease[fractional\ decrease\ from\ initial]$	[13]

18.	Inhibition of VCAM-1 by HDL	Decrease $= -0.00086967 + 3.3756(1 - \exp(-0.11958x^{0.12618}))$ $x: HDL[ng/ul]; Decrease[fractional\ decrease\ from\ initial]$	[13]
19.	Inhibition of E-Selectin by HDL	$Decrease = 0.0008x + 0.0571; x<1000\ ng/ul$ $x: HDL[ng/ul]; Decrease[fractional\ decrease\ from\ initial]$	[13]
20.	Inhibition of ox-LDL by HDL	$Decrease(\%) = 0.57233 + 91.8555(1 - \exp(-2.7193e-05\ x^{1.5442}))$ $x: HDL[ng/ul] Decrease[\%decrease\ from\ initial]$	
21.	Downregulation of ICAM with time	% Decrease = 0	[140]
22.	Downregulation of VCAM with time	Decrease (% of total VCAM-1 per hour) = $-0.0288x^2 + 3.6275x - 12.387$ x: time [hour]	[140]
23.	Downregulation of ES with time	Decrease (% of total VCAM-1 per hour) = $-0.0288x^2 + 3.6275x - 12.387$ x: time [hour]	[140]
24.	Neutrophil adhesion prob. based on ICAM-1	$P(x) = \begin{cases} \frac{1}{T}\left[-0.179 + 0.690\ (1 - \exp(-0.303x^{1.559}))\right]; x < 7 \\ \left[-0.179 + 0.690\ (1 - \exp(-0.303x^{1.559}))\right]; x > 7 \end{cases}$ P: probability of adhesion per unit time [fraction/ s]; T: Capture to TEM time (600s); x: ICAM [times of baseline]	[9, 17, 124, 126]
25.	Neutrophil adhesion prob. based on VCAM-1	$P(x) = 0$ P: probability of adhesion per unit time[s]; x: VCAM [times of baseline]	[125]
26.	Neutrophil adhesion prob. based on ES	$P(x) = \begin{cases} \frac{1}{T}[0.278e^{-2} + 0.217(1 - \exp(-7.214e^{-8}x^{7.289}))]; x < 11 \\ [0.278e^{-2} + 0.217(1 - \exp(-7.214e^{-8}x^{7.289}))]; x > 11 \end{cases}$ P: probability of adhesion per unit time[s]; T: Capture to TEM time (600s); x: ES [times of baseline]	[9, 17, 124, 126]
27.	Monocyte/ lymphocyte adhesion prob. based on ICAM-1	$P(x) = \begin{cases} \frac{1}{T}\left[-14.58 + 14.72\ (1 - \exp(-4.675x^{0.516}))\right]; x < 7 \\ \left[-14.58 + 14.72\ (1 - \exp(-4.675x^{0.516}))\right]; x > 7 \end{cases}$ P: probability of adhesion per unit time[s]; T: Capture to TEM time (1080s); x: ICAM [times of baseline]	[16, 127-130]

28.	Monocyte/ lymphocyte adhesion prob. based on VCAM-1	$P(x) = \begin{cases} \frac{1}{T}[-196.3 + 196.5(1 - \exp(-6.973x^{0.122}))]; x < 2 \\ [-196.3 + 196.5(1 - \exp(-6.973x^{0.122}))]; x > 2 \end{cases}$ P: probability of adhesion per unit time[s]; T: Capture to TEM time (1080s); x: VCAM [times of baseline]	[16, 127 - 130]
29.	Monocyte/ lymphocyte adhesion prob. based on ES	$P(x) = \begin{cases} \frac{1}{T}[0.977e^{-3} + 0.188(1 - \exp(-3.675e^{-7}x^{6.163}))]; x < 11 \\ [0.977e^{-3} + 0.188(1 - \exp(-3.675e^{-7}x^{6.163}))]; x > 11 \end{cases}$ P: probability of adhesion per unit time[s]; T: Capture to TEM time (1000s); x: ES [times of baseline]	[16, 127 - 130]
30.	Detachment of leukocytes, adhered to ESelectin, based on WSS	$\%\ of\ Initial\ Adhesion\ due\ to\ selectin(x) = \begin{cases} 82.247x^2 - 103.84x + 38.329; x \leq 0.7 \\ 6; x > 0.7 \end{cases}$ $x: WSS[Pa]$	[18]
31.	Detachment of leukocytes, adhered to ICAM-1, based on WSS	$\%\ of\ Initial\ Adhesion\ due\ to\ ICAM(x) = \begin{cases} 1.740x^2 - 6.013x + 95.619; x \leq 2 \\ 90; x > 2 \end{cases}$ $x: WSS[Pa]$	[18]
32.	Detachment of leukocytes, adhered to VCAM-1, based on WSS	$\%\ of\ Initial\ Adhesion\ due\ to\ VCAM(x) = \begin{cases} 1.740x^2 - 6.013x + 95.619; x \leq 2 \\ 90; x > 2 \end{cases}$ $x: WSS[Pa]$	Considered same as ICAM
33.	Dependence of monocyte/ lymphocyte TEM on stiffness	$TEM = \begin{cases} 0.78x^2 + 4.8x + 51.06\ ; 1 < x < 5 \\ 95\ ; x > 5 \end{cases}$ $x: stiffness[kPa]; TEM[\%\ of\ adhered\ cells]$	[16]
34.	Dependence of neutrophil TEM on stiffness	$TEM = \begin{cases} 9.18x + 46.96\ ; 0.42 < x < 5 \\ 91\ ; x > 5 \end{cases}$ $x: stiffness[kPa]; TEM[\%\ of\ adhered\ cells]$	[17]
35.	Dependence of directional plaque growth on plaque to lumen area ratio at each z-plane	Plaque area < 40% lumen area = plaque grows outward Plaque area ≥ 40% lumen area = 65% inward and 35% outward	[84]

36.	Concentration of LDL at the EC wall based on WSS	$\frac{C_w}{t} = C_0(0.0048x^2 - 0.0419x + 1.1423); \text{x} \leq 5$ $= C_0(1.04); \text{x} > 5$ $x: WSS[Pa]; C_0: LDL\ concentration\ in\ lumen[ng/\mu l]; t = 3600s;\ C_w: LDL\ concentration\ at\ the\ wall\ [ng/\mu l]$	[20]
37.	Concentration of TGRL at the EC wall based on WSS	$\frac{C_w}{t} = C_0(0.0048x^2 - 0.0419x + 1.1423); \text{x} \leq 5$ $= C_0(1.04); \text{x} > 5$ $x: WSS[Pa]; C_0 = TGRL\ concentration\ in\ lumen[ng/\mu l]; t = 3600s$ $C_w: TGRL\ concentration\ at\ the\ wall\ [ng/\mu l]$	Considered same as LDL
38.	Concentration of HDL at the EC wall based on WSS	$\frac{C_w}{t} = C_0(0.1586x^2 - 0.5223x + 1.4403); \text{x} \leq 2$ $= C_0\ ; \text{x} > 2$ $x: WSS[Pa]; C_0 = HDL\ concentration\ in\ lumen[ng/\mu l]; t = 3600s;$ $C_w: HDL\ concentration\ at\ the\ wall\ [ng/\mu l]$	[141]
39.	LDL oxidation rate	0.75% of LDL / day	[142]
40.	Consumption rate of Ox-LDL by Macrophage	$Consumption = 0.042e^{-6}\ (525.8 - 525.8(1 - \exp(-5.959x^{-0.155}))\ )$ $x: oxLDL[ng/ul]\ ; Consumption[\mu g/cell/hour]$	[21]
41.	Consumption rate of LDL by Macrophage	$Consumption = 0.042e^{-6}\ (-0.004 + 3.961(1 - \exp(-0.029x^{0.999}))\ )$ $x: LDL[ng/ul]\ ; Consumption[\mu g/cell/hour]$	[21]
42.	Lifespan of leukocytes in wall	Neutrophils: 2 days, Monocytes: 7 days, Lymphocytes: 7 days, Macrophages: 100 days	[143]

43.	Monocyte to macrophage type ratio	Upon entering the artery wall a monocyte differentiates into macrophage accordingly: M1(pro-inflammatory): M2(anti-inflammatory) = 2:1	[83, 91-93]
44.	Foam cell formation	If oxLDL > 260 ng/µl and lifespan of M1 is over 100 days, M1 becomes foam cell	[94]
45.	TNF-α production	$2.2x10^{-2}$ ng/ml/1h/neutrophil; 3.7 ng/ml/1h/monocyte	[82]
46.	IL-1 production	$2.2x10^{-3}$ ng/ml/1h/neutrophil; 0.3 ng/ml/1h/monocyte	[82]
47.	IL-10 production	0.16 ng/ml/1h/lymphocyte	[90]
48.	Removal of IL1β by IL-10	$\frac{IL1\beta}{t} = \begin{cases} (-0.0096x + 1) \times IL1\beta \text{ ; x} < 7 \\ (-0.0096 * 7 + 1) \times IL1\beta \text{ ; x} \geq 7 \end{cases}$ $x: IL10[ng/ml]; t = 1h$	[4]
49.	Removal of TNFα by IL-10	$\frac{TNF\alpha}{t} = \begin{cases} (-0.0095x + 1) \times TNF\alpha; x < 7 \\ (-0.0095 * 7 + 1) \times TNF\alpha; x \geq 7 \end{cases}$ $x: IL10[ng/ml]; t = 1h$	[5]
50.	Initial patch composition (excluding leukocytes)	Healthy artery wall patch: SMC: Collagen: Elastin = 0.74: 0.20: 0.05 Atheroma wall patch: SMC: Collagen: Elastin = 0.32: 0.64:0.05	[144-146]
51.	SMC Content (% of wall)	FT: 22.4%; FF: 16% Normal: 44.4% NC/ Calcium: 0	
52.	Volume of one SMC	500 um^3 both for contractile and synthetic SMC	[147]
53.	Collagen production per SMC	150 ug / contractile SMC/ hour 310 ug / synthetic SMC/ hour	[148, 149]
54.	Collagen removal	Total collagen production by n number of plaque patches = total collagen removal by all plaque patches, where a patch is considered a plaque patch if it has any leukocytes	**

The grey part is the rule set, will be used in future (see chapter 7)
* Content of ECM is considered 70%, 50% and 60% of wall in FT, FF and normal areas respectively. Hence, the SMC content on those areas are as given
** Mass constraint balance (check chapter 7 for detail)

Analyzing the rules

1. Model sensitivity to various factors

Leukocyte adhesion, TEM and plaque progression depend on lot of factors. Cytokines and other factors enhance expression of selectins and AMs on the endothelial cell surface. Those AMs aid in leukocyte adhesion and TEM. Among all the factors, cytokines (TNF-α and IL-1β) and WSS are potent factors that increase AMs' expression and affect plaque progression. HDL, on the other hand reduces the AMs expression and thus slower the plaque growth. To quantify the relative effect of each factor, we performed a sensitivity study and observe how the model reacts with a small change of the factors.

Sensitivity of AM expression based on cytokine value

The ABM was setup such that the cytokine concentrations were either the same for both TNF-α and IL-1β or changed by an order of two. The relative change of AM expression was measured relative to the AMs expression on that value. **Figure 6.12** shows that relative change of ICAM-1 and E-Selectin expression as a function of cytokine concentration. ICAM-1 and E-Selectin are more sensitive to changes in TNF-α compare to that of IL-1 β, whereas VCAM-1 is more sensitive to changes in IL-1β.

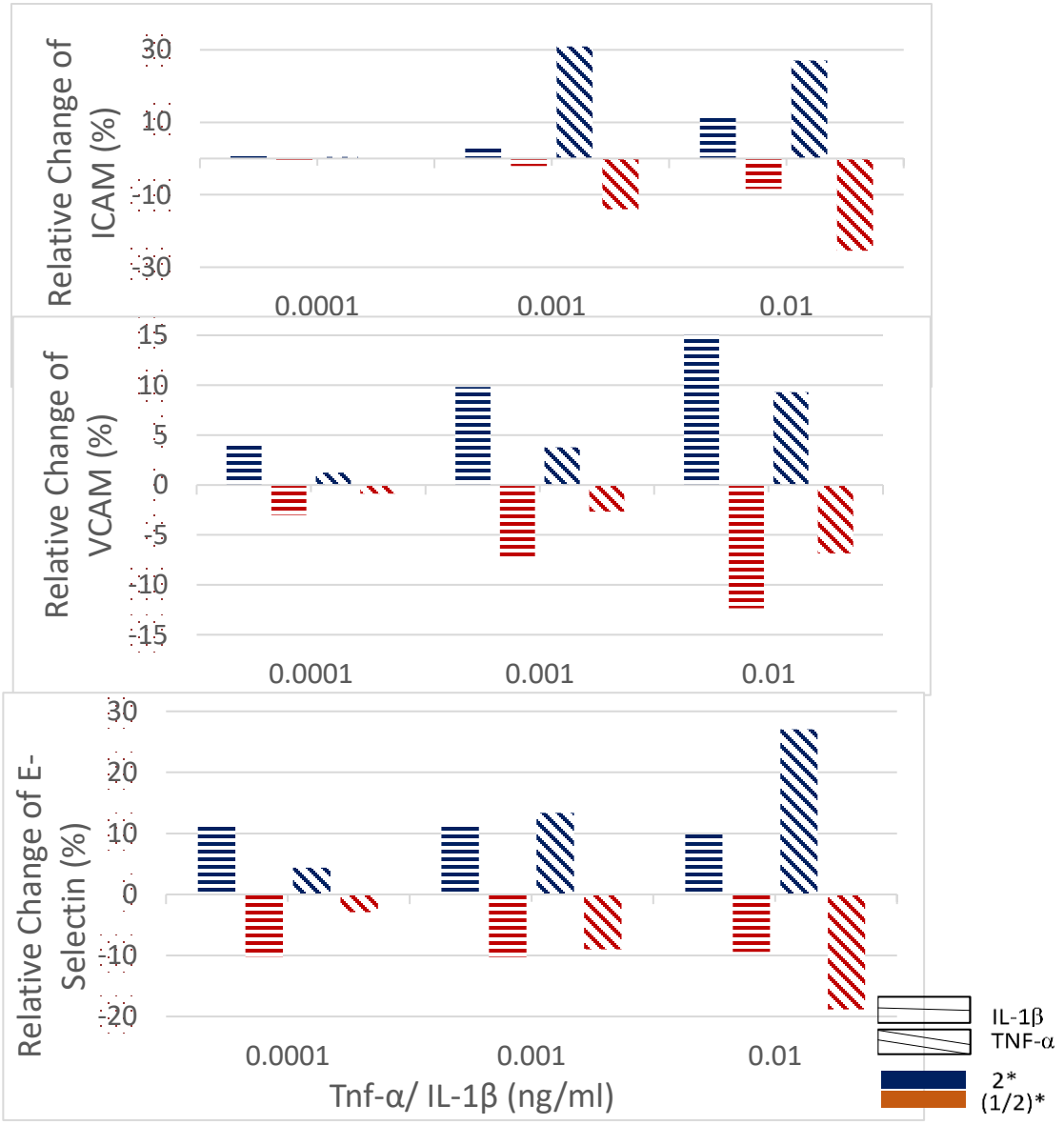

Figure 6.12 Sensitivity study of adhesion molecule for different cytokine concentration: TNF-α (inclined bar) and IL-1β (straight bar) are changed to 2 times (blue) and (1/2) times (orange) of the reference value. ICAM-1 and E-Selectin are sensitive more to change of TNF-α than to IL-1β whereas VCAM-1 to IL-1β.

Sensitivity of AM expression based on HDL

A very small value of HDL reduces VCAM-1 expression whereas to reduce ICAM-1 and E-Selectin at least 500 ng/µl HDL is needed (**Figure 6.13**).

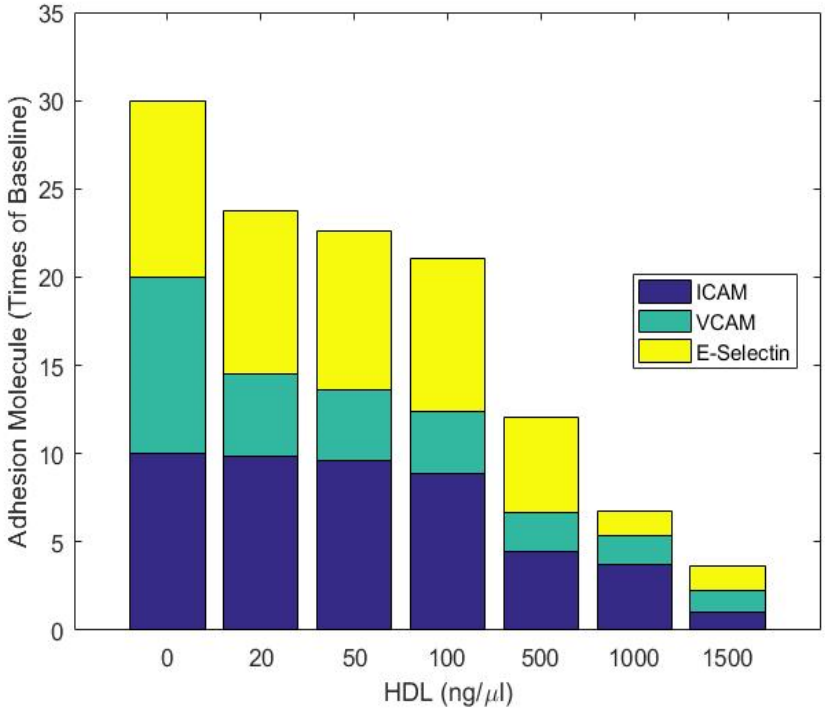

Figure 6.13 Sensitivity study of adhesion molecule expression based on HDL concentration: Initially ICAM-1, VCAM-1 and E-Selectin are all the same i.e. 10 times of baseline. HDL is then applied to the endothelial cells at different concentrations. It is obvious that even small amount of HDL, can decrease VCAM significantly, whereas ICAM and ES requires a higher concentration of HDL.

2. Adhesion Probability with Cytokine Concentration

Adhesion probability due to IL-1β

IL-1β increases the AMs and E-Selectin expression which, in turn increases leukocyte adhesion. Hence, IL-1β increases the leukocyte adhesion. **Figure 6.14** shows the neutrophil and monocyte adhesion with change of IL-1β. Although the dependence of adhesion on ICAM-1, VCAM-1 and E-Selectin (expressed only due to IL-1β) are different for different cell types, the total adhesion for monocyte and neutrophil are same.

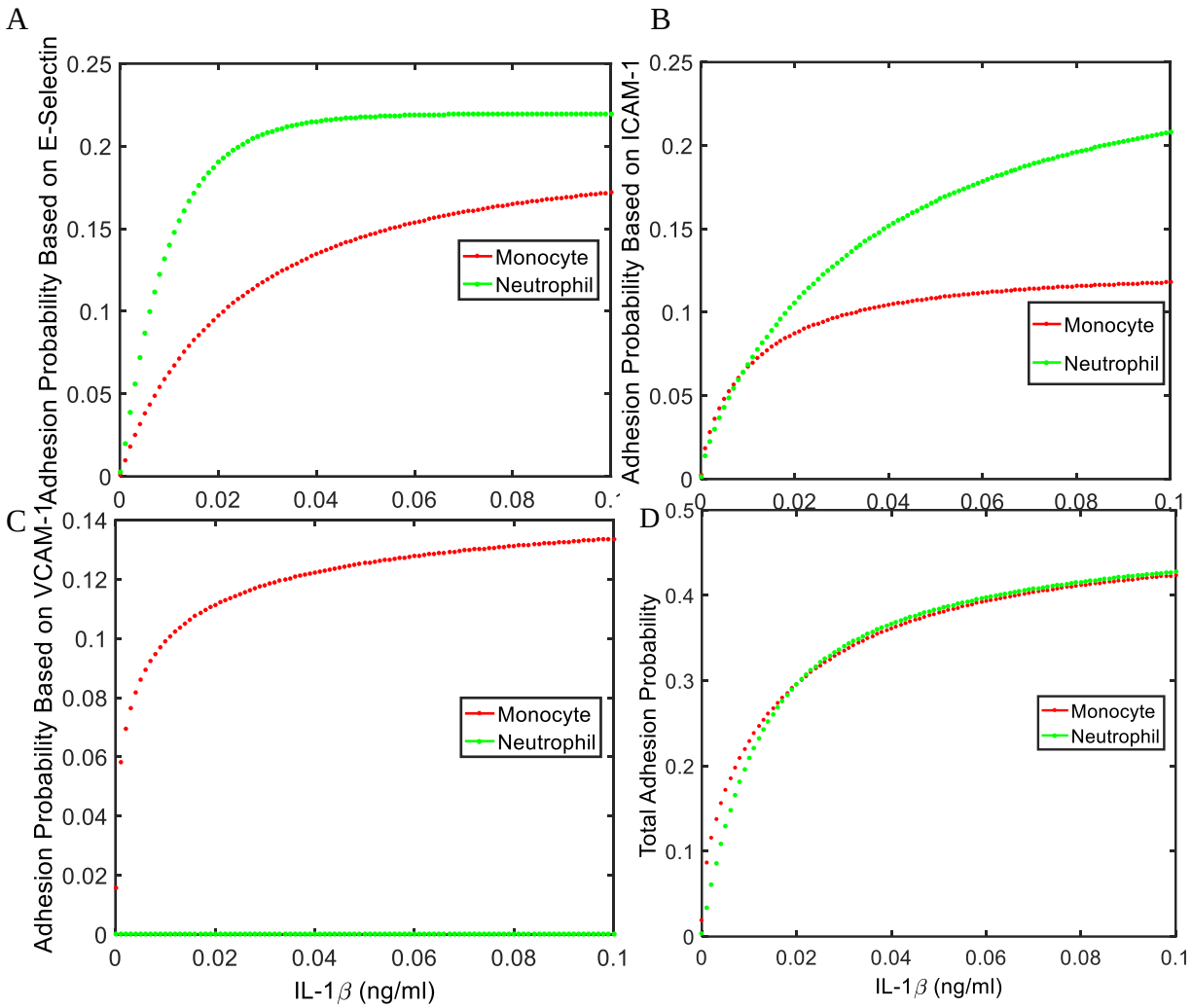

Figure 6.14 Adhesion probability as function of IL-1β: Adhesion probability of monocyte and neutrophil as function of (A) E-Selectin, (B) ICAM-1 and (C) E-Selectin. The AMs and E-Selectin are expressed only due to IL-1β. (D) Total adhesion probability due to all AMs and E-Seletin.

Adhesion probability due to TNF

The adhesion probability due to all the AMs and E-Selectin, is higher for neutrophils than for monocytes **Figure 6.15**.

With IL-1β, the adhesion probability is same for neutrophils and monocytes whereas with TNF-α, neutrophils adhesion is much higher than that of monocytes. Also the concentration of

neutrophils in higher than that of monocytes and they transmigrate from EC surface much faster than monocytes. Hence, overall the number of neutrophils that transmigrate over a certain time is higher than number of monocytes that transmigrate over that time.

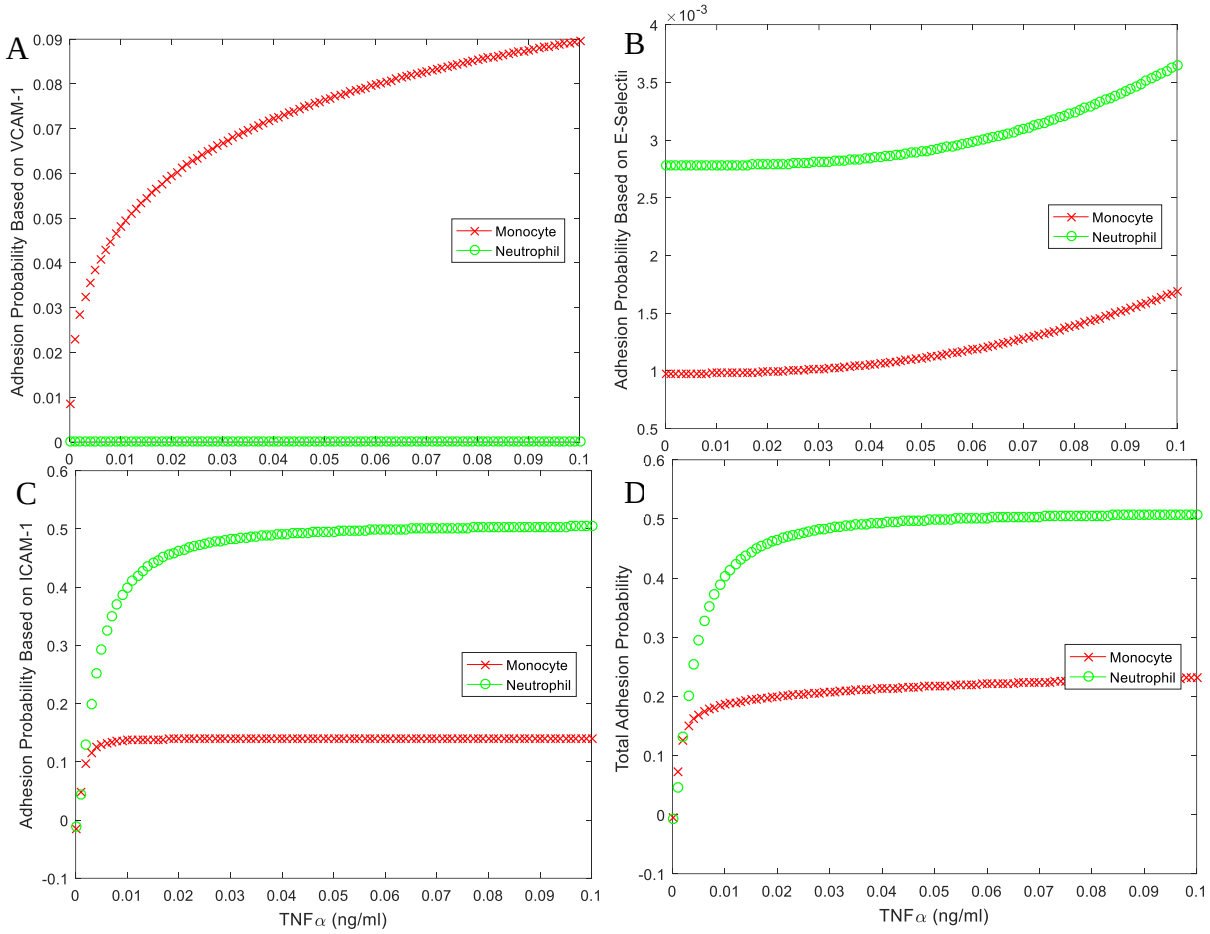

Figure 6.15 Adhesion probability with TNF-α: Adhesion probability of neutrophils and monocytes as function of (A) VCAM-1, (B) E-Selectin and (C) ICAM-1. All the AMs and E-Selection are expressed only due to TNFα. (D) is the total adhesion probability.

Results

We ran the simulation for 5 months and compared the results with previous (non-mechanistic) model. **Figure 6.16** shows the number of leukocytes present in the artery wall with time. **Figure**

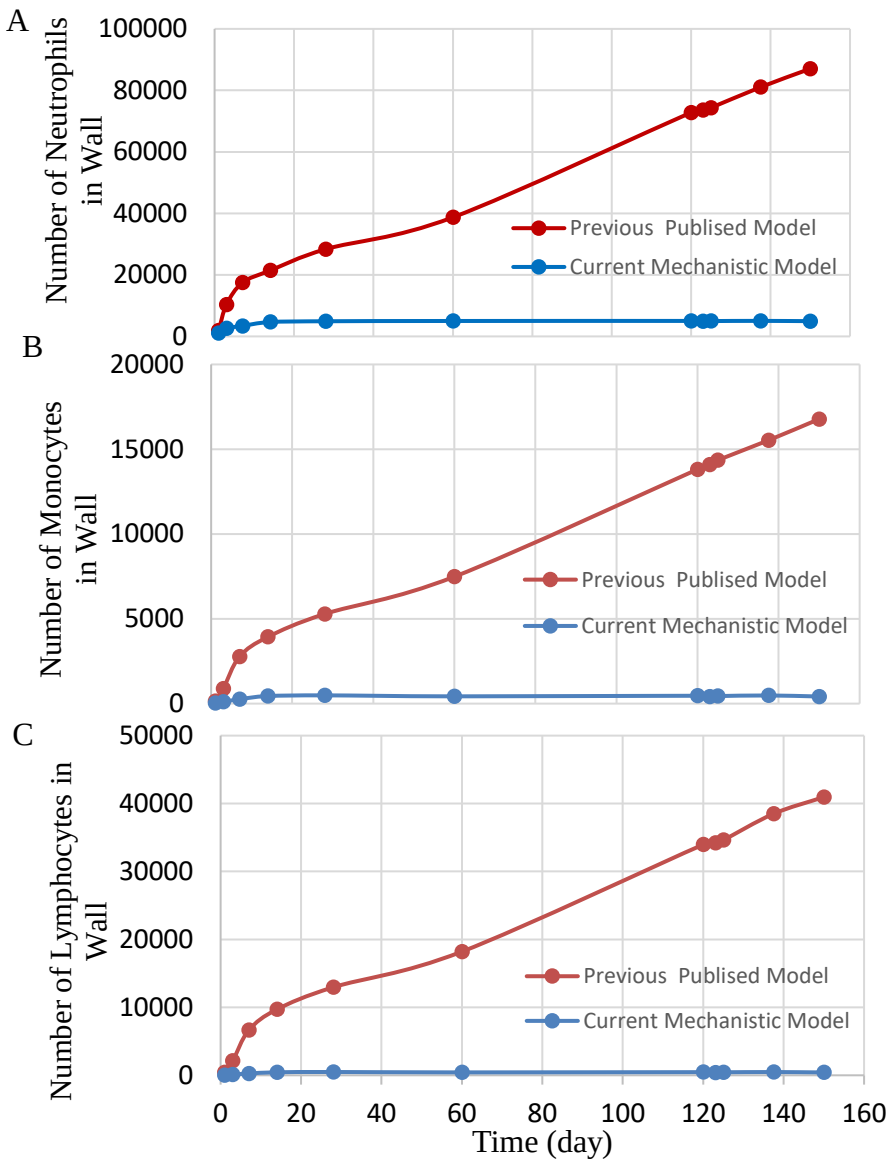

Figure 6.16 Comparison of leukocytes in wall between current and previous model: Number of neutrophils (A), monocytes (B) and lymphocytes (C) in the wall were measured with time. Red and blue data represent the previous and current model respectively.

6.17 shows the spatiotemporal growth of the artery. Both the results were compared to previous model.

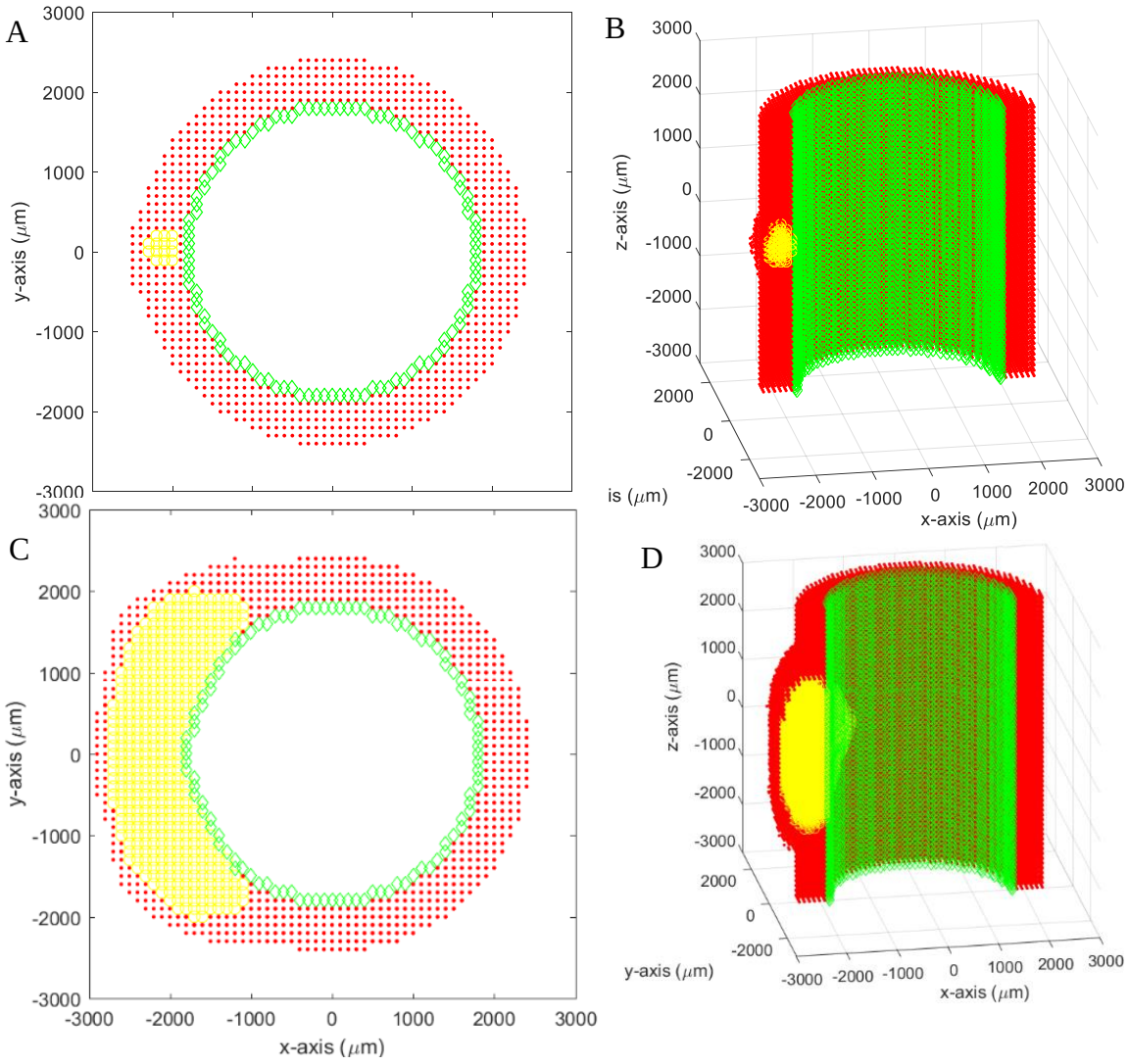

Figure 6.17 Comparison of 5 months plaque growth between current and previous model: Transverse cross section of artery from current (A, B) and previous (C, D) model. B, D represent the longitudinal cross sections.

Discussion

In this chapter we present a robust multiscale model. The ABM includes biological events, explained in chapter 4, as well as expands on events to include detailed steps. Each rule and the literary source used to derive the rule are described. Some rules only had a few data points. In this case we scoured the literature for more information to ultimately formulate a rule that represented the pathophysiological process (see rule for monocyte/ neutrophil adhesion). Several studies ([16, 17]) have shown that when ECs are stimulated with TNF-α or IL-1β, leukocytes adhere and then transmigrate within several minutes. This is probably due to the high concentration of AMs on EC surface. However, if the EC surface is stimulated with ox-LDL only, and thus AMs expression is less, then leukocytes take a longer time (approx. an hour) to adhere and transmigrate [150].

Finally, we compared the model with a previous published model [86]. As mentioned in chapter 5, the previous model seems accelerated since it only took 6 months for the lumen caliber to start to decrease. The acceleration was because the rules were derived from in-vitro experiments done with high concentrations of cytokines (pro-inflammatory), yet we did not consider concentration dependent effect is the ABM. Therefore, the leukocyte adhesion and TEM were very high from the beginning. However, in the current model we consider mechanistic pathways of adhesion, therefore we expect a more accurate and realistic growth rate of plaque. **Figure 6.17** shows a comparative result of plaque growth from these two models. As expected the growth rate was more realistic than previous model. The TEM time, mentioned before, significantly reduced the rate of leukocyte TEM in current model and thus plaque growth. However, in reality TEM time may not be the rate limiting step. Also in the current model the

leukocyte concentration in the lumen was considered homogeneous whereas in reality it is velocity dependent and thus spatially changes along the artery. In future we will have particle tracking and so the adhesion will be spatially dependent on cell concentration and AMs at particular location.

Some rules in the current model are still not mechanistic such as macrophage to FC formation (rule # 44) and anti-inflammatory effect of HDL (rule# 17-20). In future, we can extend our work by adding the pathways of those events. In addition, the current model considers uniform leukocyte concentration throughout the artery. In reality, the flow rate changes spatially specially for stenosed artery and so does the cell concentration. For example, the cell concentration abruptly decreases at the recirculation flow area. Depending on the cell concentration and AMs / E-Selectin expression, the adhesion rules change (as mentioned before also see rule 24-29). In future, we can use particle-tracing model and find spatial dependence of cell concentration.

Since the model seems to work physiologically, our next steps include incorporating patient data (blood profile and anatomy of artery) into the model and observing the plaque growth. That model will also include patient-specific compositions of artery wall and their contribution in plaque progression. This model will help clinicians in decision making about the treatment options to prevent plaque rupture. In chapter 7, we discussed how we are implementing patient data into the ABM and how we are considering the activity of a new cell type, smooth muscle cells.

CHAPTER 7

FUTURE WORK

MODEL SETUP WITH PATIENT SPECIFIC DATA

Overview

The eventual goal of the vascular mechanobiology laboratory is to create a patient-specific model capable of predicting disease evolution and suggesting treatment options. The first step towards this goal is to create a comprehensive multiscale model of leukocyte extravasation and the following growth and remodeling process (as presented in chapters 1 through 6). The next step, towards the eventual goal is to pass patient-specific imaging into our ABM. After setting up our ABM to mimic the patients' conditions we can validate out predicted remodeling using longitudinal data from patients. In this chapter I present our initial efforts towards this goal.

Background

Gray-scale intravascular ultrasound (IVUS) is a catheter based in-vivo imaging modality used for quantitative assessment of coronary artery disease. This imaging method helps to evaluate the patient's need to treat their coronary artery disease with either a stent, bypass, vascular graft, etc. In the case the patient doesn't receive treatment, IVUS can be used to track the progression-regression of the atherosclerotic lesion (typically for clinical trials of a new pharmaceutical claiming to reduce atherosclerotic plaques). However, IVUS alone only provides information about the inner and outer dimension of the artery. This limitation has been partially overcome by Volcano sponsored software that can post-processes the IVUS-based images to estimate the spatial

composition of the artery. The processed images are termed virtual histology IVUS (VH-IVUS). VH-IVUS specifically provides the geometry of the artery as well as 5 compositions: fibrous tissue, fibrofatty, necrotic core, calcified, and healthy (or normal wall). **Figure 7.1** illustrate the different tissue types in one axial slice of VH-IVUS.

Wall Compositions:

- **Fibrous tissue (FT)** is identified as a dark green group of pixels on the VH IVUS screen. This tissue is characterized by bundles of collagen fibers with little or no lipid accumulation in the fibrous [151, 152].
- **Fibrofatty (FF) tissue** is identified as a light green group of pixels on the VH IVUS screen. This tissue is characterized by loosely packed collagen fibers with lipid accumulation. There is no necrotic tissue and no or few cholesterol clefts [151, 152].
- **Necrotic core (NC) tissue** is identified as a red group of pixels on the VH IVUS screen. A high level of lipid with many necrotic cells and remnants of dead lymphocytes and foam cells characterize this tissue. There are few or no collagen fibers. The extracellular matrix (ECM) is not well organized and has poor mechanical stability [151, 152].
- **Dense calcium** is identified as a white pixel group on the VH IVUS screen. This tissue is characterized by compact calcium crystals [151, 152].
- **Normal wall** is identified as a gray pixel group on the VH IVUS image**.** It is composed of contractile SMC, collagen, elastin.

Different phenotypes of smooth muscle cells (SMC):

Previously, our ABM has not included the behavior of normal arterial cells, like smooth muscle cells (SMC). SMC are the predominate cell type in the arterial media and give the artery

the ability to contract (contractile type) or if needed synthesize proteins (synthetic type). SMC phenotypic modulation plays a key role in atherosclerosis by changing their phenotype from contractile to synthetic, which are characterized by changes in morphology and migration rates. Different mechanical and biological factors affect this conversion. Initially, the artery wall is comprised of contractile SMC. Once inflammatory cells transmigrate into the wall they release cytokines. Cytokines stimulate SMC growth and proliferation and hence the SMC differentiates into a synthetic phenotype [153, 154].

Overall, importing the geometry and the compositions of an artery, based on VH-IVUS, as well as behavior of SMCs into ABM can allow us to predict plaque progression for patient specific cases.

Methods

VH-IVUS data processing

A MATLAB code was developed to process the VH-IVUS images into their spatial tissue types and then produce the input file of this information for the ABM. In VH-IVUS each dataset color represents a different composition of artery. MATLAB recognizes each color and produces a corresponding table of positions (x, y and z) of those colors. **Figure 7.1** shows an example slice of VH-IVUS image and a binary image representing each composition.

Importing VH-IVUS data into ABM:

The text files containing the positions of the compositions, mentioned above, are called upon by the ABM. The ABM then defines each spatial patch according to the corresponding composition. The element size of ABM is chosen to be equal to the pixel size of VH-IVUS. The grid size of ABM is 20μm radially and 450μm axially; since each pixel is 20 x 20 μm and each

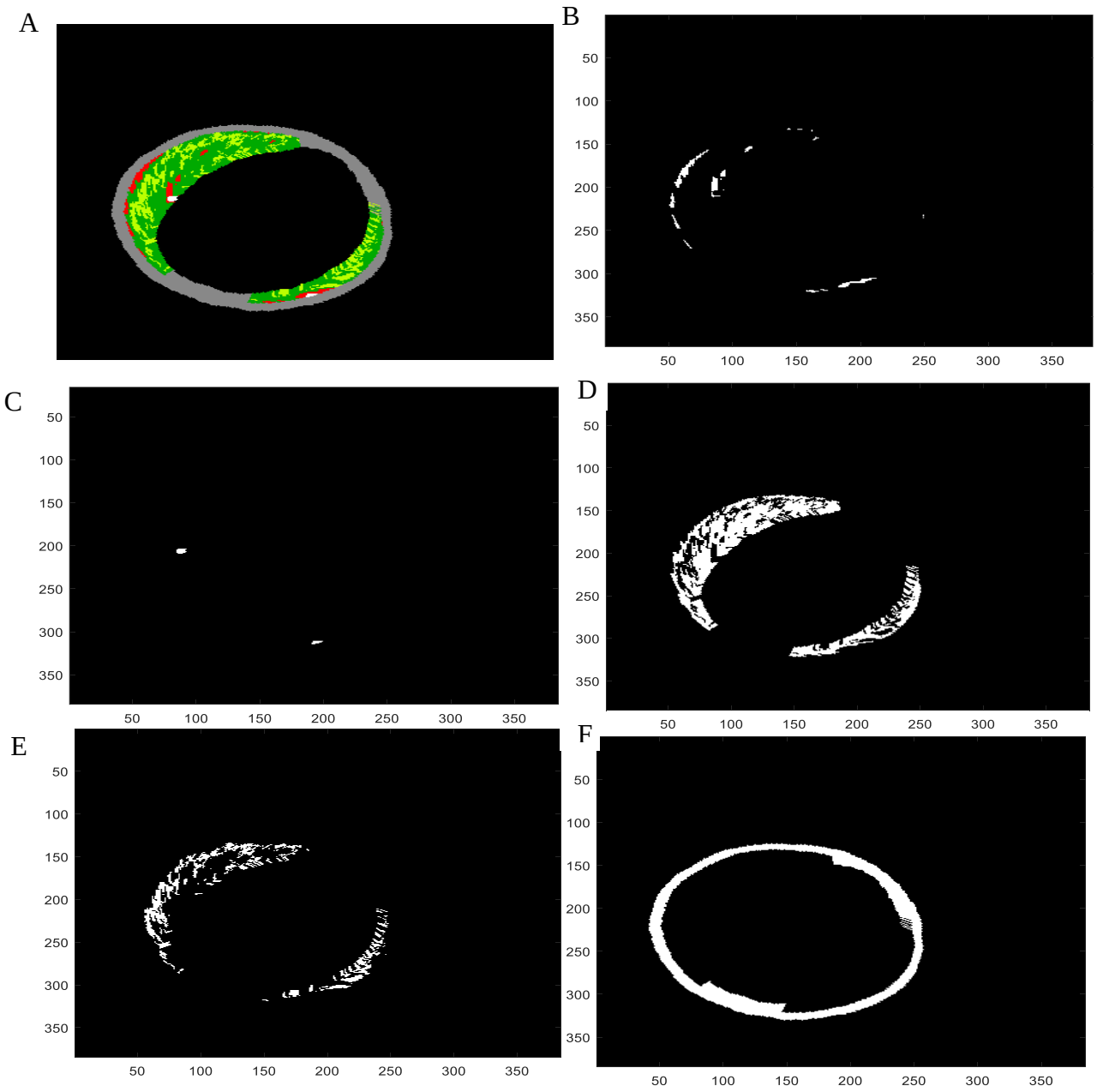

Figure 7.1 VH-IVUS data processing in Matlab: (A) VH-IVUS image of one axial segment of the LAD. It has 5 colors representing 5 different compositions. Binary image were created to isolate the (B) red channel which represents the NC, (C) white channel which represents calcium, (D) dark green channel which represents FT, (E) light green channel which represents FF, and (F) grey channel which represents the normal artery wall.

axial slice is 450 μm. All the patches inside the donut (**Figure 7.1**, A) are considered as luminal

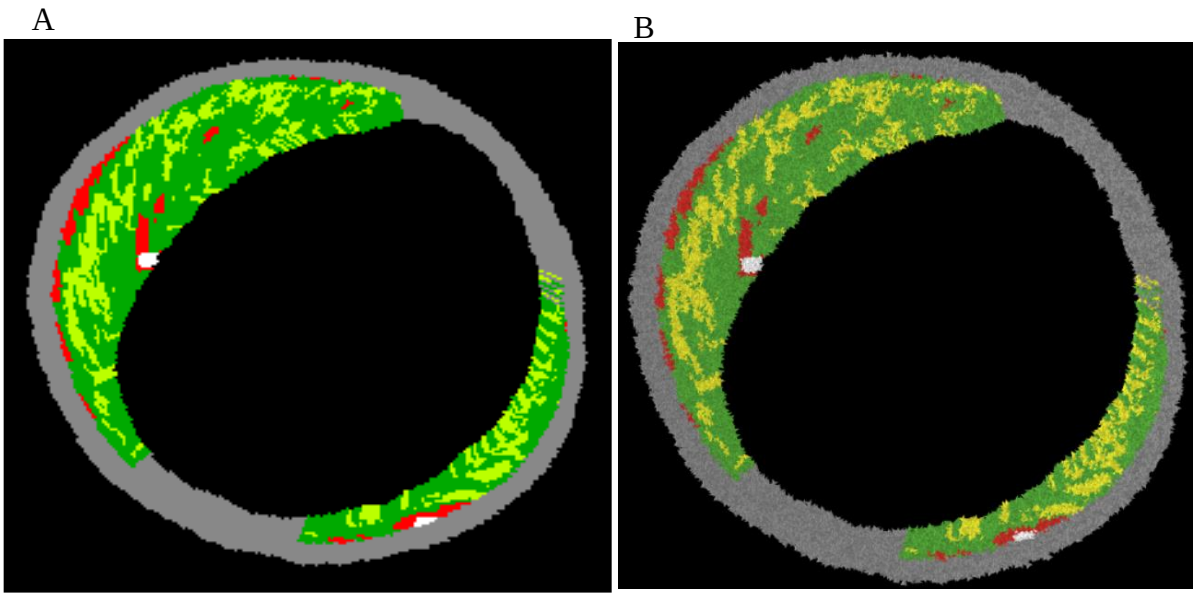

Figure 7.2 Set up of ABM with VH-IVUS data: A slice of VH-IVUS image with compositions (A), mentioned above, and corresponding cross section of ABM (B) with all those compositions.

patches. **Figure 7.2** shows a slice of ABM where all the compostions were imported from VH-IVUS.

Initial setup

Classification of VH IVUS into cells and matrix

In the normal artery patches (gray by VH IVUS), the SMCs are contractile while in the plaque patches they are synthetic in nature. In the normal artery patches the distribution is as, SMC: Collagen: Elastin = 0.74: 0.20: 0.05, whereas for the plaque patches (both FT and FF) the distribution is 0.32: 0.64: 0.05 [144]. The calcium and necrotic core patches do not have any SMCs or collagen. Table 7.1 shows the initial spatial distribution of SMC, collagen, elastin and leukocytes.

Table 7.1 Initial setup of patient specific IVUS-ABM model and assumptions considered

FT	FF	Normal artery	NC	Calcified	Leukocyte concentration
70% normal wall and 30% leukocytes (i.e. 22.4% SMC, 44.8% Collagen, 3.5% Elastin and 30% leukocytes)	50% normal wall and 50% FCs & leukocytes (i.e. 16% SMC, 32% Collagen, 2.5% elastin, 35% FC and 15% leukocytes)	60% normal wall and 40% leukocytes [80, 155, 156] (i.e. 44.4% SMC, 12% collagen, 3% elastin and 40% leukocytes)	100% FCs & leukocytes (i.e., 70% FC and 30% leukocytes), no ECM	100% calcium i.e. no ECM or no cells	$6x10^9$/L
Assumptions	1. The volume of contractile SMCs and synthetic SMCs are same 2. The collagen production per SMC is same for the fibrous tissue (FT) and fibrofatty (FF) plaque as they are both synthetic type SMCs 3. Mass balance constraint: The total collagen production from SMCs in the plaque patches is almost same as total collagen removal from all those patches. 4. Collagen in normal artery patches (gray on VH IVUS) the collagen production equals collagen removal.				

Collagen production and removal:

Production:

Collagen is produced both from contractile and synthetic SMCs. The total collagen production at one tick is sum of the collagen production from individual SMCs in plaque type patches (i.e., any patch with a leukocyte in it).

So, M_i = Total collagen production from i^{th} patch $=\sum_s M_s \; or \; \sum_c M_c$, where s and c represent synthetic and contractile SMCs respectively on that patch. A patch can only have either synthetic or contractile SMCs (depending on the presences of leukocytes).

So if,

M = Total collagen production from all the patches having SMCs and at least 1 leukocyte

B = Total number of patches having SMCs and at least 1 leukocyte

Then, $M = \sum_{i=1}^{B} M_i$

Removal:

Total collagen production and total collagen removal should be balanced so that there is not a net collagen production. Since we are not considering removal of collagen by metalloproteinases (MMPs), because production of MMPs depends on arterial stress, for now we are assuming

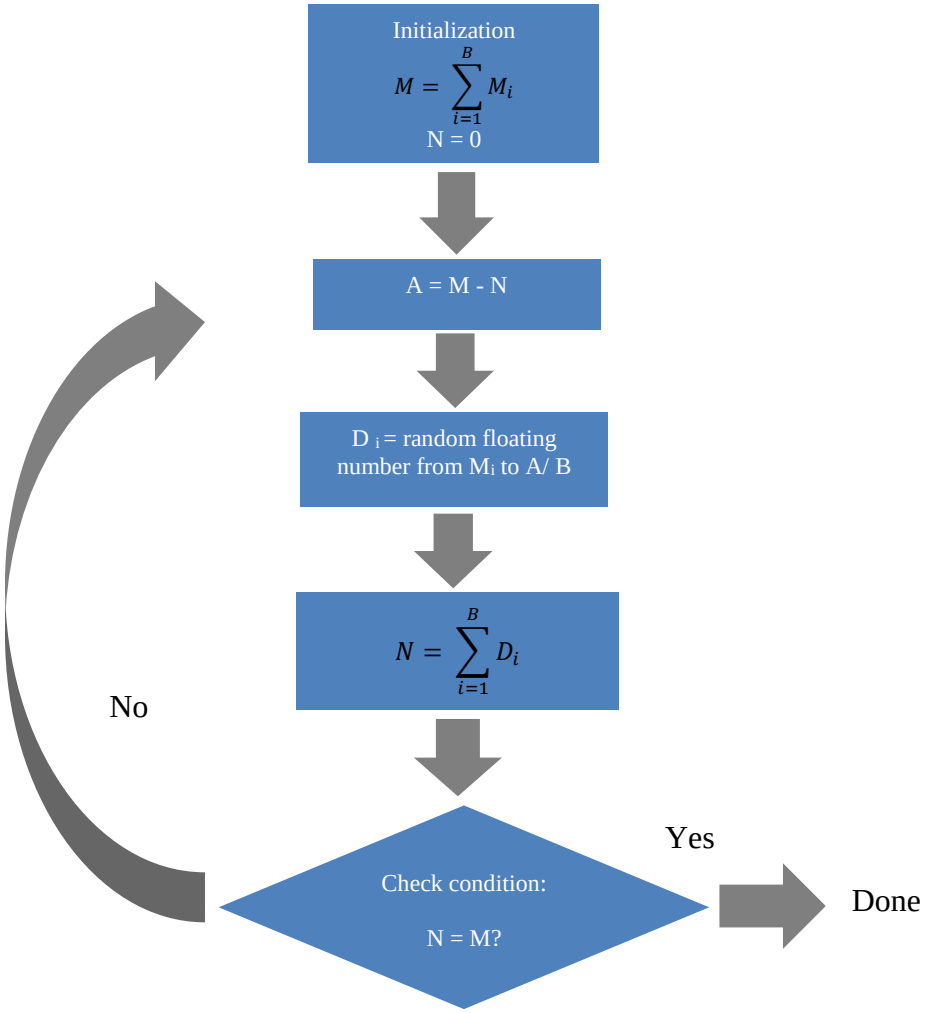

Figure 7.3 Flow chart of collagen balance: The total collagen production in the artery is balanced by removal of the collagen.

about equal removal of collagen. However, due to the randomness, some patches may have more collagen removal than others. This rule will be replaced in the eventual model. Suppose,

N = Total collagen removal (see in the flow chart)

A = M - N

C = Average collagen removal per plaque = A/B

D_i = random floating number from M_i to C (generated by B plaque patches having collagen)

Figure 7.3 shows a flow chart of collagen turnover.

Discussion

Here we reported the initial setup of our ABM using patient specific data. The geometry and composition of artery are imported from IVUS-VH data. In future, we will run the model and compare the plaque progression with 6 month patient-specific followup data. Specifically, we will quantify the plaque area, and the change of area of different compositions.

One of the goals of our lab is to develop of a complete model of leukocyte transmigration and thus atherosclerosis. **Figure 7.4** shows a basic flow diagram and the interaction of the tools required to achieve this goal. A model of the artery developed using ABM is the primary driver which simulates all the biological events associated with atherogenesis, including leukocyte transmigration. It also provides the change in the geometry of artery due to accumulation of an atherosclerotic plaque. After determining the geometry of an artery, and its constituents, a finite element analysis (FEA) program then calculates the maximum principle stresses throughout the arterial wall. The stresses then serve as input into the ABM, which in turn may cause a change in the geometry of artery (remodeling) to maintain the homeostasic condition. As mentioned earlier,

the remodeled geometry is then used to compute the wall shear stress (CFD) resulting from the blood-flow. Like the stress in the wall, the shear stress on the endothelium is then used by the atherogenesis model (ABM) to determine leukocyte transmigration, diffusion, and endothelial cell behavior. Combining these flexible tools, we will be able to capture the biological complexity and mechanical heterogeneity that exists in atherosclerosis.

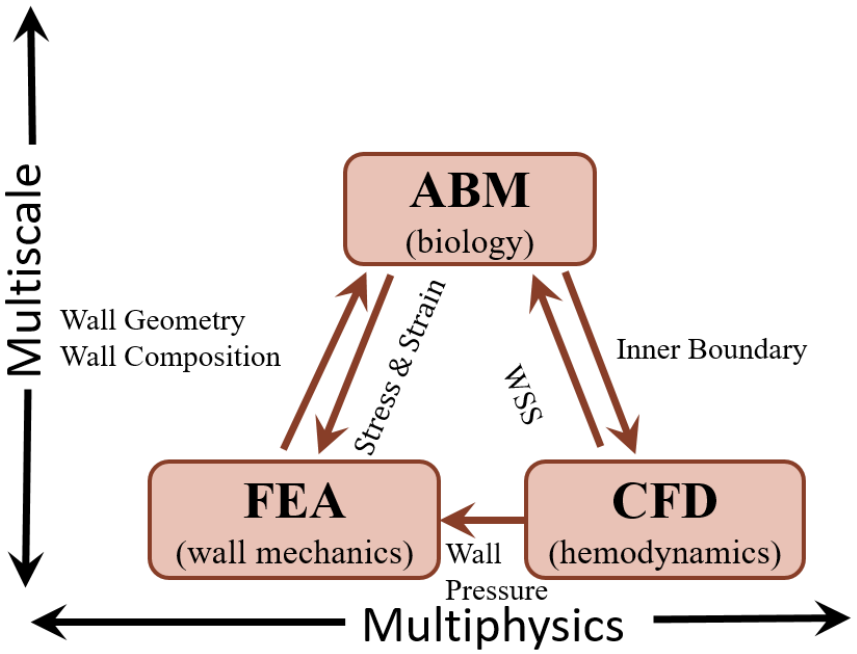

Figure 7.4 Flow chart of complete model of atherogenesis. To make an integrated model of atherogenesis, modeling of biology, hemodynamics and wall mechanics are needed. This figure shows the tools for each model and the corresponding input and output

REFERENCES

1. Ting, H.J., et al., *Triglyceride-rich lipoproteins prime aortic endothelium for an enhanced inflammatory response to tumor necrosis factor-alpha.* Circ Res, 2007. **100**(3): p. 381-90.

2. Wang, Y.I., et al., *Endothelial inflammation correlates with subject triglycerides and waist size after a high-fat meal.* Am J Physiol Heart Circ Physiol, 2011. **300**(3): p. H784-91.

3. Tsou, J.K., et al., *Spatial regulation of inflammation by human aortic endothelial cells in a linear gradient of shear stress.* Microcirculation, 2008. **15**(4): p. 311-23.

4. Cassatella, M.A., et al., *Interleukin 10 (IL-10) inhibits the release of proinflammatory cytokines from human polymorphonuclear leukocytes. Evidence for an autocrine role of tumor necrosis factor and IL-1 beta in mediating the production of IL-8 triggered by lipopolysaccharide.* J Exp Med, 1993. **178**(6): p. 2207-11.

5. Oswald, I.P., et al., *Interleukin 10 inhibits macrophage microbicidal activity by blocking the endogenous production of tumor necrosis factor alpha required as a costimulatory factor for interferon gamma-induced activation.* Proc Natl Acad Sci U S A, 1992. **89**(18): p. 8676-80.

6. Cominacini, L., et al., *Antioxidants inhibit the expression of intercellular cell adhesion molecule-1 and vascular cell adhesion molecule-1 induced by oxidized LDL on human umbilical vein endothelial cells.* Free Radic Biol Med, 1997. **22**(1-2): p. 117-27.

7. Lee, W.-J., et al., *Ellagic acid inhibits oxidized LDL-mediated LOX-1 expression, ROS generation, and inflammation in human endothelial cells*. Vol. 52. 2010. 1290-300.

8. Takei, A., Y. Huang, and M.F. Lopes-Virella, *Expression of adhesion molecules by human endothelial cells exposed to oxidized low density lipoprotein. Influences of degree of oxidation and location of oxidized LDL.* Atherosclerosis, 2001. **154**(1): p. 79-86.

9. Bahra, P., et al., *Each step during transendothelial migration of flowing neutrophils is regulated by the stimulatory concentration of tumour necrosis factor-alpha.* Cell Adhes Commun, 1998. **6**(6): p. 491-501.

10. Bevilacqua, M.P., et al., *Interleukin 1 acts on cultured human vascular endothelium to increase the adhesion of polymorphonuclear leukocytes, monocytes, and related leukocyte cell lines.* J Clin Invest, 1985. **76**(5): p. 2003-11.

11. Melder, R.J., et al., *Selectin- and integrin-mediated T-lymphocyte rolling and arrest on TNF-alpha-activated endothelium: augmentation by erythrocytes.* Biophys J, 1995. **69**(5): p. 2131-8.

12. Munn, L.L., R.J. Melder, and R.K. Jain, *Analysis of cell flux in the parallel plate flow chamber: implications for cell capture studies.* Biophys J, 1994. **67**(2): p. 889-95.

13. Cockerill, G.W., et al., *High-Density Lipoproteins Inhibit Cytokine-Induced Expression of Endothelial Cell Adhesion Molecules.* Arteriosclerosis, Thrombosis, and Vascular Biology, 1995. **15**(11): p. 1987.

14. Mackness, M.I., et al., *The role of high-density lipoprotein and lipid-soluble antioxidant vitamins in inhibiting low-density lipoprotein oxidation.* Biochemical Journal, 1993. **294**(Pt 3): p. 829-834.

15. Cockerill, 1995 #135;Mackness, 1993 #218;Cockerill, 1995 #135//
.

16. Hayenga, H.N. and H. Aranda-Espinoza, *Stiffness Increases Mononuclear Cell Transendothelial Migration.* Cellular and Molecular Bioengineering, 2013. **6**(3): p. 253-265.

17. Stroka, K.M. and H. Aranda-Espinoza, *Endothelial cell substrate stiffness influences neutrophil transmigration via myosin light chain kinase-dependent cell contraction.* Blood, 2011. **118**(6): p. 1632-40.

18. Lawrence, M.B. and T.A. Springer, *Leukocytes roll on a selectin at physiologic flow rates: distinction from and prerequisite for adhesion through integrins.* Cell, 1991. **65**(5): p. 859-73.

19. He, X. and D.N. Ku, *Pulsatile flow in the human left coronary artery bifurcation: average conditions.* J Biomech Eng, 1996. **118**(1): p. 74-82.

20. Deng, X., et al., *Luminal surface concentration of lipoprotein (LDL) and its effect on the wall uptake of cholesterol by canine carotid arteries.* J Vasc Surg, 1995. **21**(1): p. 135-45.

21. Leake, D.S. and S.M. Rankin, *The oxidative modification of low-density lipoproteins by macrophages.* Biochem J, 1990. **270**(3): p. 741-8.

22. Willerson, J.T. and P.M. Ridker, *Inflammation as a cardiovascular risk factor.* Circulation, 2004. **109**(21 Suppl 1): p. Ii2-10.

23. Ross, R., *Atherosclerosis — An Inflammatory Disease.* New England Journal of Medicine, 1999. **340**(2): p. 115-126.

24. Luscinskas, F.W., et al., *Leukocyte transendothelial migration: a junctional affair.* Semin Immunol, 2002. **14**(2): p. 105-13.

25. Muller, W.A., *Mechanisms of leukocyte transendothelial migration.* Annu Rev Pathol, 2011. **6**: p. 323-44.

26. van Buul, J.D. and P.L. Hordijk, *Signaling in leukocyte transendothelial migration.* Arterioscler Thromb Vasc Biol, 2004. **24**(5): p. 824-33.

27. Timmins, L.H., et al., *Focal association between wall shear stress and clinical coronary artery disease progression.* Ann Biomed Eng, 2015. **43**(1): p. 94-106.

28. Timmins, L.H., et al., *Colocalization of low and oscillatory coronary wall shear stress with subsequent culprit lesion resulting in myocardial infarction in an orthotopic heart transplant patient.* JACC Cardiovasc Interv, 2013. **6**(11): p. 1210-1.

29. Timmins, L.H., et al., *Framework to co-register longitudinal virtual histology-intravascular ultrasound data in the circumferential direction.* IEEE Trans Med Imaging, 2013. **32**(11): p. 1989-96.

30. Samady, H., et al., *Coronary artery wall shear stress is associated with progression and transformation of atherosclerotic plaque and arterial remodeling in patients with coronary artery disease.* Circulation, 2011. **124**(7): p. 779-88.

31. Levesque, M.J. and R.M. Nerem, *The elongation and orientation of cultured endothelial cells in response to shear stress.* J Biomech Eng, 1985. **107**(4): p. 341-7.

32. Malek, A.M., S.L. Alper, and S. Izumo, *Hemodynamic shear stress and its role in atherosclerosis.* Jama, 1999. **282**(21): p. 2035-42.

33. Traub, O. and B.C. Berk, *Laminar shear stress: mechanisms by which endothelial cells transduce an atheroprotective force.* Arterioscler Thromb Vasc Biol, 1998. **18**(5): p. 677-85.

34. Estrada, R., et al., *Microfluidic endothelial cell culture model to replicate disturbed flow conditions seen in atherosclerosis susceptible regions.* Biomicrofluidics, 2011. **5**(3): p. 32006-3200611.

35. Warboys, C.M., et al., *The role of blood flow in determining the sites of atherosclerotic plaques.* F1000 Medicine Reports, 2011. **3**: p. 5.

36. Wasilewski, J., et al., *Predominant location of coronary artery atherosclerosis in the left anterior descending artery. The impact of septal perforators and the myocardial bridging effect.* Kardiochirurgia i Torakochirurgia Polska = Polish Journal of Cardio-Thoracic Surgery, 2015. **12**(4): p. 379-385.

37. Thorne, B.C., et al., *Toward a multi-scale computational model of arterial adaptation in hypertension: verification of a multi-cell agent based model.* Front Physiol, 2011. **2**: p. 20.

38. Gradus-Pizlo, I., et al., *Left anterior descending coronary artery wall thickness measured by high-frequency transthoracic and epicardial echocardiography includes adventitia.* Am J Cardiol, 2003. **91**(1): p. 27-32.

39. Waller, B.F., et al., *Anatomy, histology, and pathology of coronary arteries: a review relevant to new interventional and imaging techniques--Part IV.* Clin Cardiol, 1992. **15**(9): p. 675-87.

40. Libby, P., *The Vascuar Biology of Atherosclerosis*, in *Heart Disease. A Textbook of Cardiovascular Medicine*, E. Braunwald, D.P. Zipes, and P. Libby, Editors. 2001, W.B. Sauders Company: Philadelphia. p. 995-1009.

41. Soulis, J.V., M. Dimitrakopoulou, and G.D. Giannoglou, *Low Density Lipoprotein transport in the normal human aortic arch.* Hippokratia, 2014. **18**(3): p. 221-225.

42. Aviram, M. and B. Fuhrman, *LDL oxidation by arterial wall macrophages depends on the oxidative status in the lipoprotein and in the cells: role of prooxidants vs. antioxidants.* Mol Cell Biochem, 1998. **188**(1-2): p. 149-59.

43. Asakura, T. and T. Karino, *Flow patterns and spatial distribution of atherosclerotic lesions in human coronary arteries.* Circulation Research, 1990. **66**(4): p. 1045.

44. Park, S.T., et al., *Atherosclerotic carotid stenoses of apical versus body lesions in high-risk carotid stenting patients.* Am J Neuroradiol, 2010. **31**(6): p. 1106-12.

45. Roach, M.R., *Biophysical analyses of blood vessel walls and blood flow.* Annu Rev Physiol, 1977. **39**: p. 51-71.

46. Asakura, T. and T. Karino, *Flow patterns and spatial distribution of atherosclerotic lesions in human coronary arteries.* Circ Res, 1990. **66**(4): p. 1045-66.

47. Zarins, C.K., et al., *Carotid bifurcation atherosclerosis. Quantitative correlation of plaque localization with flow velocity profiles and wall shear stress.* Circ Res, 1983. **53**(4): p. 502-14.

48. Svindland, A., *The localization of sudanophilic and fibrous plaques in the main left coronary bifurcation.* Atherosclerosis, 1983. **48**(2): p. 139-45.

49. Caro, C.G., *Discovery of the role of wall shear in atherosclerosis.* Arterioscler Thromb Vasc Biol, 2009. **29**(2): p. 158-61.

50. Truskey, G.A., et al., *Characterization of a sudden expansion flow chamber to study the response of endothelium to flow recirculation.* J Biomech Eng, 1995. **117**(2): p. 203-10.

51. McKinney, V.Z., K.D. Rinker, and G.A. Truskey, *Normal and shear stresses influence the spatial distribution of intracellular adhesion molecule-1 expression in human umbilical vein endothelial cells exposed to sudden expansion flow.* J Biomech, 2006. **39**(5): p. 806-17.

52. Barber, K.M., A. Pinero, and G.A. Truskey, *Effects of recirculating flow on U-937 cell adhesion to human umbilical vein endothelial cells.* Am J Physiol, 1998. **275**(2 Pt 2): p. H591-9.

53. Chiu, J.J., et al., *Analysis of the effect of disturbed flow on monocytic adhesion to endothelial cells.* J Biomech, 2003. **36**(12): p. 1883-95.

54. Milner, J.S., et al., *Hemodynamics of human carotid artery bifurcations: computational studies with models reconstructed from magnetic resonance imaging of normal subjects.* J Vasc Surg, 1998. **28**(1): p. 143-56.

55. Papaharilaou, Y., D.J. Doorly, and S.J. Sherwin, *The influence of out-of-plane geometry on pulsatile flow within a distal end-to-side anastomosis.* J Biomech, 2002. **35**(9): p. 1225-39.

56. Zhao, S.Z., et al., *Blood flow and vessel mechanics in a physiologically realistic model of a human carotid arterial bifurcation.* J Biomech, 2000. **33**(8): p. 975-84.

57. Long, Q., et al., *Reconstruction of blood flow patterns in a human carotid bifurcation: a combined CFD and MRI study.* J Magn Reson Imaging, 2000. **11**(3): p. 299-311.

58. Pedersen, E.M., A.P. Yoganathan, and X.P. Lefebvre, *Pulsatile Flow Visualization in a Model of the Human Abdominal-Aorta and Aortic Bifurcation.* J Biomech, 1992. **25**(8): p. 935-944.

59. Ku, D.N. and D.P. Giddens, *Pulsatile flow in a model carotid bifurcation.* Arteriosclerosis, 1983. **3**(1): p. 31-9.

60. Chen, J., X.Y. Lu, and W. Wang, *Non-Newtonian effects of blood flow on hemodynamics in distal vascular graft anastomoses.* J Biomech, 2006. **39**(11): p. 1983-95.

61. Keynton, R.S., S.E. Rittgers, and M.C. Shu, *The effect of angle and flow rate upon hemodynamics in distal vascular graft anastomoses: an in vitro model study.* J Biomech Eng, 1991. **113**(4): p. 458-63.

62. Jannat, R.A., et al., *Neutrophil adhesion and chemotaxis depend on substrate mechanics*, in *J Phys Condens Matter*. 2010. p. 194117.

63. Schaff, U.Y., et al., *Vascular mimetics based on microfluidics for imaging the leukocyte--endothelial inflammatory response.* Lab Chip, 2007. **7**(4): p. 448-56.

64. Schaff, U.Y., et al., *Calcium flux in neutrophils synchronizes beta2 integrin adhesive and signaling events that guide inflammatory recruitment.* Ann Biomed Eng, 2008. **36**(4): p. 632-46.

65. Gutierrez, E. and A. Groisman, *Quantitative measurements of the strength of adhesion of human neutrophils to a substratum in a microfluidic device.* Anal Chem, 2007. **79**(6): p. 2249-2258.

66. Rouleau, L., et al., *Neutrophil adhesion on endothelial cells in a novel asymmetric stenosis model: effect of wall shear stress gradients.* Ann Biomed Eng, 2010. **38**(9): p. 2791-804.

67. Yang, X., et al., *Traffic of leukocytes in microfluidic channels with rectangular and rounded cross-sections.* Lab Chip, 2011. **11**(19): p. 3231-40.

68. Prabhakarpandian, B., et al., *Synthetic microvascular networks for quantitative analysis of particle adhesion.* Biomed Microdev, 2008. **10**(4): p. 585-95.

69. Prabhakarpandian, B., et al., *Microfluidic devices for modeling cell-cell and particle-cell interactions in the microvasculature.* Microvasc Res, 2011. **82**(3): p. 210-20.

70. Urschel, K., et al., *Role of shear stress patterns in the TNF-alpha-induced atherogenic protein expression and monocytic cell adhesion to endothelium.* Clin Hemorheol Microcirc, 2010. **46**(2-3): p. 203-10.

71. Dodge, J.T., Jr., et al., *Lumen diameter of normal human coronary arteries. Influence of age, sex, anatomic variation, and left ventricular hypertrophy or dilation.* Circulation, 1992. **86**(1): p. 232-46.

72. Rioufol, G., et al., *Adventitia measurement in coronary artery: an in vivo intravascular ultrasound study.* Heart, 2006. **92**(7): p. 985-986.

73. Blumenreich, M.S., *The White Blood Cell and Differential Count*, in *Clinical Methods: The History, Physical, and Laboratory Examinations*, H.K. Walker, W.D. Hall, and J.W. Hurst, Editors. 1990: Boston.

74. Pappalardo, F., S. Musumeci, and S. Motta, *Modeling immune system control of atherogenesis.* Bioinformatics, 2008. **24**(15): p. 1715-21.

75. Goodhill, G.J., *Diffusion in axon guidance.* Eur J Neurosci, 1997. **9**(7): p. 1414-21.

76. Dabagh, M., P. Jalali, and J.M. Tarbell, *The transport of LDL across the deformable arterial wall: the effect of endothelial cell turnover and intimal deformation under hypertension.* Am J Physiol Heart Circ Physiol, 2009. **297**(3): p. H983-96.

77. Wheater, P.R., *Functional histology : a text and colour atlas*. 1994: Edinburgh : C. Livingstone.

78. Zulliger, M.A., et al., *A strain energy function for arteries accounting for wall composition and structure.* J Biomech, 2004. **37**(7): p. 989-1000.

79. Chen, H., et al., *The layered structure of coronary adventitia under mechanical load.* Biophys J, 2011. **101**(11): p. 2555-62.

80. Hayenga, H.N., et al., *Differential progressive remodeling of coronary and cerebral arteries and arterioles in an aortic coarctation model of hypertension.* Front Physiol, 2012. **3**: p. 420.

81. Cullen, P., et al., *Rupture of the atherosclerotic plaque: does a good animal model exist?* Arterioscler Thromb Vasc Biol, 2003. **23**(4): p. 535-42.

82. Hatanaka, E., et al., *Neutrophils and monocytes as potentially important sources of proinflammatory cytokines in diabetes.* Clin Exp Immunol, 2006. **146**(3): p. 443-7.

83. Adamson, S. and N. Leitinger, *Phenotypic modulation of macrophages in response to plaque lipids.* Curr Opin Lipidol, 2011. **22**(5): p. 335-42.

84. Glagov, S., et al., *Compensatory enlargement of human atherosclerotic coronary arteries.* N Engl J Med, 1987. **316**(22): p. 1371-5.

85. Korshunov, V.A., S.M. Schwartz, and B.C. Berk, *Vascular remodeling: hemodynamic and biochemical mechanisms underlying Glagov's phenomenon.* Arterioscler Thromb Vasc Biol, 2007. **27**(8): p. 1722-8.

86. Bhui, R. and H.N. Hayenga, *An agent-based model of leukocyte transendothelial migration during atherogenesis.* PLoS Comput Biol, 2017. **13**(5): p. e1005523.

87. Breviario, F., et al., *IL-1-induced adhesion of polymorphonuclear leukocytes to cultured human endothelial cells. Role of platelet-activating factor.* J Immunol, 1988. **141**(10): p. 3391-7.

88. Sheikh, S., et al., *Exposure to fluid shear stress modulates the ability of endothelial cells to recruit neutrophils in response to tumor necrosis factor-alpha: a basis for local variations in vascular sensitivity to inflammation.* Blood, 2003. **102**(8): p. 2828-34.

89. Gonzales, R.S. and T.M. Wick, *Hemodynamic modulation of monocytic cell adherence to vascular endothelium.* Ann Biomed Eng, 1996. **24**(3): p. 382-93.

90. Rafiq, K., et al., *Regulation of the IL-10 production by human T cells.* Scand J Immunol, 2001. **53**(2): p. 139-47.

91. Colin, S., G. Chinetti-Gbaguidi, and B. Staels, *Macrophage phenotypes in atherosclerosis.* Immunol Rev, 2014. **262**(1): p. 153-66.

92. Kadl, A., et al., *Identification of a novel macrophage phenotype that develops in response to atherogenic phospholipids via Nrf2.* Circ Res, 2010. **107**(6): p. 737-46.

93. Ley, K., Y.I. Miller, and C.C. Hedrick, *Monocyte and macrophage dynamics during atherogenesis.* Arterioscler Thromb Vasc Biol, 2011. **31**(7): p. 1506-16.

94. Dubland, J.A. and G.A. Francis, *Lysosomal acid lipase: at the crossroads of normal and atherogenic cholesterol metabolism.* Frontiers in Cell and Developmental Biology, 2015. **3**: p. 3.

95. Johnston, B.M., et al., *Non-Newtonian blood flow in human right coronary arteries: Transient simulations.* Journal of Biomechanics. **39**(6): p. 1116-1128.

96. Chaichana, T., Z. Sun, and J. Jewkes, *Computational fluid dynamics analysis of the effect of plaques in the left coronary artery.* Comput Math Methods Med, 2012. **2012**: p. 504367.

97. Nosovitsky, V.A., et al., *Effects of curvature and stenosis-like narrowing on wall shear stress in a coronary artery model with phasic flow.* Comput Biomed Res, 1997. **30**(1): p. 61-82.

98. Liu, B. and D. Tang, *Computer simulations of atherosclerotic plaque growth in coronary arteries.* Mol Cell Biomech, 2010. **7**(4): p. 193-202.

99. Yang, C., et al., *In Vivo/Ex Vivo MRI-Based 3D Non-Newtonian FSI Models for Human Atherosclerotic Plaques Compared with Fluid/Wall-Only Models.* Comput Model Eng Sci, 2007. **19**(3): p. 233-246.

100. Lelovas, P.P., N.G. Kostomitsopoulos, and T.T. Xanthos, *A comparative anatomic and physiologic overview of the porcine heart.* J Am Assoc Lab Anim Sci, 2014. **53**(5): p. 432-8.

101. Millon, A., et al., *Animal models of atherosclerosis and magnetic resonance imaging for monitoring plaque progression.* Vascular, 2013.

102. Zaragoza, C., et al., *Animal Models of Cardiovascular Diseases.* Journal of Biomedicine and Biotechnology, 2011. **2011**: p. 13.

103. Pelosi, G., et al., *Inflammation blood and tissue factors of plaque growth in an experimental model evidenced by a systems approach.* Front Genet, 2014. **5**: p. 70.

104. Hwang, M., et al., *Rule-based model of vein graft remodeling.* PLoS One, 2013. **8**(3): p. e57822.

105. Olivares, A.L., M.A. Gonzalez Ballester, and J. Noailly, *Virtual exploration of early stage atherosclerosis.* Bioinformatics, 2016.

106. Bailey, A.M., B.C. Thorne, and S.M. Peirce, *Multi-cell agent-based simulation of the microvasculature to study the dynamics of circulating inflammatory cell trafficking.* Ann Biomed Eng, 2007. **35**(6): p. 916-36.

107. Sakellarios, A., et al., *Prediction of Atherosclerotic Plaque Development in an in Vivo Coronary Arterial Segment Based on a Multi-level Modeling Approach.* IEEE Trans Biomed Eng, 2016.

108. Misra, J.C., M.K. Patra, and S.C. Misra, *A non-Newtonian fluid model for blood flow through arteries under stenotic conditions.* J Biomech, 1993. **26**(9): p. 1129-41.

109. Stone, P.H., et al., *Prediction of progression of coronary artery disease and clinical outcomes using vascular profiling of endothelial shear stress and arterial plaque characteristics: the PREDICTION Study.* Circulation, 2012. **126**(2): p. 172-81.

110. Smedby, O., *Do plaques grow upstream or downstream?: an angiographic study in the femoral artery.* Arterioscler Thromb Vasc Biol, 1997. **17**(5): p. 912-8.

111. Soehnlein, O., *Multiple roles for neutrophils in atherosclerosis.* Circ Res, 2012. **110**(6): p. 875-88.

112. Stoneman, V., et al., *Monocyte/macrophage suppression in CD11b diphtheria toxin receptor transgenic mice differentially affects atherogenesis and established plaques.* Circ Res, 2007. **100**(6): p. 884-93.

113. Yang, L., et al., *ICAM-1 regulates neutrophil adhesion and transcellular migration of TNF-α-activated vascular endothelium under flow.* Blood, 2005. **106**(2): p. 584.

114. Muller, W.A., et al., *PECAM-1 is required for transendothelial migration of leukocytes.* The Journal of Experimental Medicine, 1993. **178**(2): p. 449.

115. Schrauwen, J.T.C., et al., *Influence of the Accuracy of Angiography-Based Reconstructions on Velocity and Wall Shear Stress Computations in Coronary Bifurcations: A Phantom Study.* PLoS ONE, 2015. **10**(12): p. e0145114.

116. Brown, A.J., et al., *Role of biomechanical forces in the natural history of coronary atherosclerosis.* Nat Rev Cardiol, 2016. **13**(4): p. 210-220.

117. Razavi, A., E. Shirani, and M.R. Sadeghi, *Numerical simulation of blood pulsatile flow in a stenosed carotid artery using different rheological models.* J Biomech, 2011. **44**(11): p. 2021-30.

118. McLaren, J.E. and D.P. Ramji, *Interferon gamma: a master regulator of atherosclerosis.* Cytokine Growth Factor Rev, 2009. **20**(2): p. 125-35.

119. Muhl, H. and J. Pfeilschifter, *Anti-inflammatory properties of pro-inflammatory interferon-gamma.* Int Immunopharmacol, 2003. **3**(9): p. 1247-55.

120. Dustin, M.L. and T.A. Springer, *Lymphocyte function-associated antigen-1 (LFA-1) interaction with intercellular adhesion molecule-1 (ICAM-1) is one of at least three mechanisms for lymphocyte adhesion to cultured endothelial cells.* J Cell Biol, 1988. **107**(1): p. 321-31.

121. Khan, B.V., et al., *Modified low density lipoprotein and its constituents augment cytokine-activated vascular cell adhesion molecule-1 gene expression in human vascular endothelial cells.* J Clin Invest, 1995. **95**(3): p. 1262-70.

122. Dustin, M.L., et al., *Induction by IL 1 and interferon-gamma: tissue distribution, biochemistry, and function of a natural adherence molecule (ICAM-1). J. Immunol. 1986. 137: 245-254.* J Immunol, 2011. **186**(9): p. 5024-33.

123. Chen, H., et al., *Cytokine-induced cell surface expression of adhesion molecules in vascular endothelial cells in vitro.* J Tongji Med Univ, 2001. **21**(1): p. 68-71.

124. Robinson, L.A., et al., *The Role of Adhesion Molecules in Human Leukocyte Attachment to Porcine Vascular Endothelium: Implications for Xenotransplantation.* The Journal of Immunology, 1998. **161**(12): p. 6931-6938.

125. Bochner, B.S., et al., *Adhesion of human basophils, eosinophils, and neutrophils to interleukin 1-activated human vascular endothelial cells: contributions of endothelial cell adhesion molecules.* J Exp Med, 1991. **173**(6): p. 1553-7.

126. Neelamegham, S., et al., *Hydrodynamic Shear Shows Distinct Roles for LFA-1 and Mac-1 in Neutrophil Adhesion to Intercellular Adhesion Molecule-1.* Blood, 1998. **92**(5): p. 1626-1638.

127. Kevil, C.G., R.P. Patel, and D.C. Bullard, *Essential role of ICAM-1 in mediating monocyte adhesion to aortic endothelial cells.* American Journal of Physiology-Cell Physiology, 2001. **281**(5): p. C1442-C1447.

128. Rafii, S., et al., *Infection of Endothelium With E1[−]E4⁺, but Not E1[−]E4[−], Adenovirus Gene Transfer Vectors Enhances Leukocyte Adhesion and Migration by Modulation of ICAM-1, VCAM-1, CD34, and Chemokine Expression.* Circulation Research, 2001. **88**(9): p. 903-910.

129. Takahashi, M., et al., *Involvement of adhesion molecules in human monocyte adhesion to and transmigration through endothelial cells in vitro.* Atherosclerosis, 1994. **108**(1): p. 73-81.

130. Giuffre, L., et al., *Monocyte adhesion to activated aortic endothelium: role of L-selectin and heparan sulfate proteoglycans.* J Cell Biol, 1997. **136**(4): p. 945-56.

131. Bandeali, S. and J. Farmer, *High-density lipoprotein and atherosclerosis: the role of antioxidant activity.* Curr Atheroscler Rep, 2012. **14**(2): p. 101-7.

132. Barter, P., *The role of HDL-cholesterol in preventing atherosclerotic disease.* European Heart Journal Supplements, 2005. **7**(suppl_F): p. F4-F8.

133. Barter, P.J., et al., *Antiinflammatory Properties of HDL.* Circulation Research, 2004. **95**(8): p. 764-772.

134. Libby, P., P.M. Ridker, and A. Maseri, *Inflammation and Atherosclerosis.* Circulation, 2002. **105**(9): p. 1135-1143.

135. Cockerill, G.W., et al., *High-density lipoproteins inhibit cytokine-induced expression of endothelial cell adhesion molecules.* Arterioscler Thromb Vasc Biol, 1995. **15**(11): p. 1987-94.

136. Cameron, S., et al., *A Novel Anti-Inflammatory Effect for High Density Lipoprotein*. Vol. 10. 2015.

137. Cockerill, G.W., et al., *High-Density Lipoproteins Differentially Modulate Cytokine-Induced Expression of E-Selectin and Cyclooxygenase-2.* Arteriosclerosis, Thrombosis, and Vascular Biology, 1999. **19**(4): p. 910.

138. Tedgui, A. and Z. Mallat, *Anti-Inflammatory Mechanisms in the Vascular Wall.* Circulation Research, 2001. **88**(9): p. 877.

139. Melrose, J., et al., *IFN-gamma inhibits activation-induced expression of E- and P-selectin on endothelial cells.* J Immunol, 1998. **161**(5): p. 2457-64.

140. Scholz, D., et al., *Expression of adhesion molecules is specific and time-dependent in cytokine-stimulated endothelial cells in culture.* Cell and Tissue Research, 1996. **284**(3): p. 415-423.

141. Meng, W., et al., *Concentration polarization of high-density lipoprotein and its relation with shear stress in an in vitro model.* J Biomed Biotechnol, 2009. **2009**: p. 695838.

142. Olivares, A.L., M.A. Gonzalez Ballester, and J. Noailly, *Virtual exploration of early stage atherosclerosis.* Bioinformatics, 2016. **32**(24): p. 3798-3806.

143. Segovia-Juarez, J.L., S. Ganguli, and D. Kirschner, *Identifying control mechanisms of granuloma formation during M. tuberculosis infection using an agent-based model.* Journal of Theoretical Biology, 2004. **231**(3): p. 357-376.

144. Chen, H. and G.S. Kassab, *Microstructure-Based Biomechanics of Coronary Arteries in Health and Disease.* Journal of biomechanics, 2016. **49**(12): p. 2548-2559.

145. Edlin, R.S., et al., *Characterization of primary and restenotic atherosclerotic plaque from the superficial femoral artery: Potential role of Smad3 in regulation of SMC proliferation.* J Vasc Surg, 2009. **49**(5): p. 1289-95.

146. Torzewski, M., et al., *Reduced in vivo aortic uptake of radiolabeled oxidation-specific antibodies reflects changes in plaque composition consistent with plaque stabilization.* Arterioscler Thromb Vasc Biol, 2004. **24**(12): p. 2307-12.

147. E Todd, M. and B. Gowen, *Arterial wall and smooth muscle cell development in young Wistar rats and the effects of surgical denervation*. Vol. 69. 1991. 438-46.

148. Strauss, B.H., et al., *Extracellular matrix remodeling after balloon angioplasty injury in a rabbit model of restenosis.* Circ Res, 1994. **75**(4): p. 650-8.

149. Okada, Y., et al., *Collagen Synthesis by Cultured Arterial Smooth Muscle Cells during Spontaneous Phenotypic Modulation.* Pathology International, 1990. **40**(3): p. 157-164.

150. Klouche, M., et al., *Enzymatically modified, nonoxidized LDL induces selective adhesion and transmigration of monocytes and T-lymphocytes through human endothelial cell monolayers.* Arterioscler Thromb Vasc Biol, 1999. **19**(3): p. 784-93.

151. Nasu, K., et al., *Accuracy of In Vivo Coronary Plaque Morphology Assessment: A Validation Study of In Vivo Virtual Histology Compared With In Vitro Histopathology.* Journal of the American College of Cardiology, 2006. **47**(12): p. 2405-2412.

152. Nair, A., et al., *Coronary plaque classification with intravascular ultrasound radiofrequency data analysis.* Circulation, 2002. **106**(17): p. 2200-6.

153. Beamish, J.A., et al., *Molecular Regulation of Contractile Smooth Muscle Cell Phenotype: Implications for Vascular Tissue Engineering.* Tissue Engineering. Part B, Reviews, 2010. **16**(5): p. 467-491.

154. Rensen, S.S.M., P. Doevendans, and G. van Eys, *Regulation and characteristics of vascular smooth muscle cell phenotypic diversity.* Netherlands Heart Journal, 2007. **15**(3): p. 100-108.

155. Carew, T.E., R.N. Vaishnav, and D.J. Patel, *Compressibility of the arterial wall.* Circ Res, 1968. **23**(1): p. 61-8.

156. Kochova, P., et al., *The contribution of vascular smooth muscle, elastin and collagen on the passive mechanics of porcine carotid arteries.* Physiol Meas, 2012. **33**(8): p. 1335-51.

BIOGRAPHICAL SKETCH

Rita Bhui was born in West Bengal (W.B.), India. After completing her schoolwork, she entered Durgapur Govt. College, W.B. for undergraduate study. She received a Bachelor of Science (B.Sc.) with a major in Physics in 2003. She then attended the University of Burdwan as a graduate student and received her Master of Science (M.Sc.) in Physics with specialization in Electronics in 2005. During the following two years (March 2006-March 2008), she was employed as assistant teacher of Physics and Mathematics in a senior high school in W.B. after qualifying the entrance examination held by School Service Commission (SSC). During those years she was also qualified some competitive entrance examination (GATE, SLET, BARC entrance)* for Ph.D. (Physics) in India. In January 2010, she enrolled in graduate school of the University of Texas at Dallas (UTD) and received her M.S. (Master of Science) in Physics in 2013 and Ph.D. (Physics) degree in 2018.

* GATE: Graduate Aptitude Test in Engineering
SLET: State Level Eligibility Test
BARC: Bhabha Atomic Research Center

CURRICULUM VITAE

Rita Bhui

Department of Physics
Natural Science and Mathematics
The University of Texas at Dallas

800 W. Campbell Rd., BSB11, Richardson, TX 75080, USA
(+1) 404 285 4497, rxb091000@utdallas.edu

EDUCATION

Doctor of Philosophy, ***May 2018***
Physics, University of Texas at Dallas, TX, USA
Title: Multiscale Modeling of Leukocyte Transmigration during Atherosclerosis
Advisor: Heather N. Hayenga, Ph.D.
GPA: 3.8/4.0

Master of Science, Physics, ***2013***
University of Texas at Dallas, TX, USA
GPA: 3.7/4.0

Master of Science, Physics (specialization in Electronics), ***2005***
University of Burdwan, West Bengal, India
Equivalent GPA: 4.0/4.0

Bachelor of Science, Physics (Hons.), ***2003***
Physics Department, University of Burdwan, West Bengal, India
Equivalent GPA: 3.7/4.0

RESEARCH EXPERIENCE

Electrochemical Optoelectronics and Biosensors Laboratory, UT Dallas (2012- 2013)

- Investigated the effect of an Abasic site (a location in DNA that has neither a purine nor a pyrimidine base, either spontaneously or due to DNA damage) on the rate and yield of charge transport through temperature-controlled analysis of DNA duplex monolayers on multiplexed devices. This investigation elucidated the electrical impact of biologically spontaneous defects and aided development of biological sensors. [Pub.# 4]
- Studied DNA repair by glycosylase and DNA damage by H_2O_2/Fe through Fenton reaction.

Vascular Mechanobiology Laboratory, UT Dallas (Ph.D.) (2013- 2018)

- Developed a **multi-scale model** of plaque growth of a coronary artery during atherosclerosis. The model integrated cellular behaviors via **agent-based modeling** and hemodynamic effects via **computational fluid dynamics**. This approach captured and integrated the spatio-temporal events occurring at the cellular level in order to predict leukocyte transmigration and plaque evolution. [Pub. # 3]
- Coupled an agent-based model of the leukocyte transmigration with a direct numerical simulation (DNS) of the pulsatile flow in a stenotic coronary artery to compare the total leukocyte transmigration with time averaged and instantaneous flow. [Pub. # 1]
- Investigated the effect of wall shear stress on cell adhesion at bifurcated artery by performing computational fluid dynamics and comparing the results with in-vitro microfluidic experiments. [Pub. # 2]

COMPUTER SKILLS

Programming Language

MATLAB, C, Python

Software

COMSOL, NetLogo, Simvascular, Solidworks

COURSES

- Electromagnetics – I & II
- Mathematical Methods – I, II, & III
- Quantum Mechanics – I and II
- Statistical Physics
- Classical Mechanics
- Scientific Computing
- Relativity I
- Optical Properties of Solids
- Mechanobiology for Engineers

TEACHING EXPERIENCE

Graduate Teaching Assistantship, UTD

Fall 2014	College Physics (Mechanics, Thermodynamics, Heat)
Spring 2013	Mathematical Methods
Fall, Spring 2012	Physics Laboratory of Electricity and Magnetism course
Fall 2011	Mathematical Methods
Spring 2011	Mathematical Methods & Electromagnetism

Teaching experience at high school, India

2006- 2008	Mathematics and Physics (BhalkiPati Ashutosh High School, West Bengal)

PROFESSIONAL MEMBERSHIPS

- **American Heart Association (AHA)** *(2016 – Present)*
- **Biomedical Engineering Society (BMES)** *(2013 – Present)*

HONORS AND OTHER RECOGNITIONS

- National Scholarship (1999) for performance at High School Test
- National Scholarship (2003) for performance in B. Sc. by Govt. of India, Ministry of Human resources
- Performance in competitive entrance examinations for Ph. D. (Physics) in India
  - Ranked 6 (state) in SLET (State Level Eligibility Test), conducted by University Grant Commission (UGC), India, in 2006
  - Ranked 267 out of 4944 (all India, 94.6 percentile) in GATE (Graduate Aptitude Test in Engineering), conducted by Indian Institute of Technology (IIT) in 2006

MENTORING STUDENTS AND SERVICES

Mentoring Undergraduate Students

1. Kevin Gonzalez, B.S. Student in Physics at UT Dallas (Summer 2017 – ***Present***)
2. Victoria Koshevarova, B.S. Student in Biomedical Engineering (Fall 2016 – Summer 2017)
3. Caleb Cyrill, B.S. Student in Biomedical Engineering (Summer 2016 – Fall 2016)
4. Claudia Gabrielle Truong, B.S. Student in Biomedical Engineering (Summer 2016)

5. Jayant V Kurvari, B.S. Student in Biomedical Engineering (Summer 2016 – Fall 2016)
6. Roja Todigala, B.S. Student in Biomedical Engineering (Summer 2016)
7. Sahiti Yarakala, B.S. Student in Biomedical Engineering (Summer 2016)
8. Sarah A Shahub, B.S. Student in Biomedical Engineering (Summer 2016)
9. Andrew Paul Nguyenba, B.S. Student in Biomedical Engineering (Summer 2016)

Judging Undergraduate Research Grant Poster Contest (*April 2014)*
UT Dallas Undergraduate research awardee posters

PEER-REVIEWED PUBICATIONS

1. Umberto Ciri, ***Rita Bhui***, Jorge Bailon-Cuba, Heather N. Hayenga, and Stefano Leonardi "Direct numerical simulation of a pulsatile flow in a stenotic coronary artery." *Submitted in J. Biomechanics*

2. "Shear stress at bifurcations and its effect on neutrophil adhesion." *In progress*

3. ***Rita Bhui***, Heather N. Hayenga "An agent-based model of leukocyte transendothelial migration during atherogenesis." PLoS Comput Biology 2017

4. Marc A. McWilliams, ***Rita Bhui***, David W. Taylor, and Jason D. Slinker "The Electronic Influence of Abasic Sites in DNA." J. Am. Chem. Soc., 2015

PRESENTATIONS *(* indicates presenting author)*

1. ***Bhui R****, Hayenga H. A Multiscale Model of Leukocyte Transendothelial Migration. BMES Conference, Phoneix, AZ, October 11-14, 2017.

2. ***Bhui R****, Meyer C, Leonardi S, Hayenga H. A Multiscale Model of Leukocyte Transmigration. BMES Conference, Tampa, FL, October 7-10, 2015.

3. ***Bhui R****, Hayenga H. A Feasible Multiscale Model to Capture the Main Events during Atherogenesis. Sy-Bio Conference, UT Dallas, March 3, 2015.